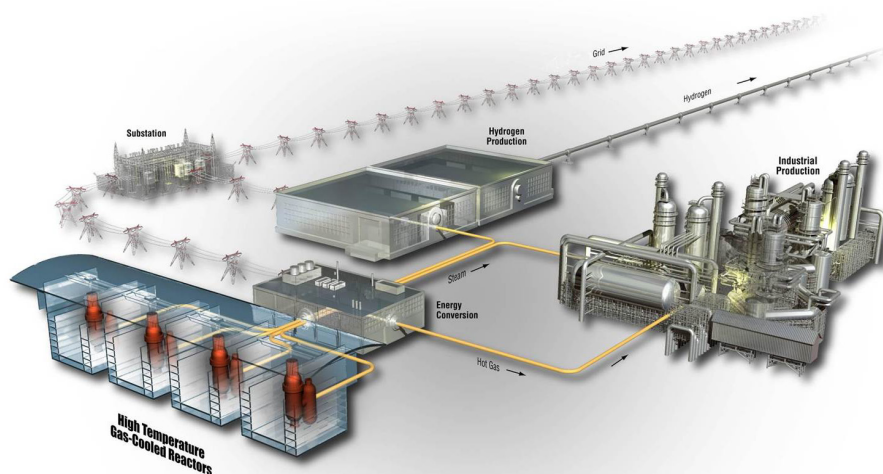


AGC-2 Irradiated Material Properties Analysis

William E. Windes
David T. Rohrbaugh
W. David Swank

May 2017

The INL is a
U.S. Department of Energy
National Laboratory
operated by
Battelle Energy Alliance



DISCLAIMER

This information was prepared as an account of work sponsored by an agency of the U.S. Government. Neither the U.S. Government nor any agency thereof, nor any of their employees, makes any warranty, expressed or implied, or assumes any legal liability or responsibility for the accuracy, completeness, or usefulness, of any information, apparatus, product, or process disclosed, or represents that its use would not infringe privately owned rights. References herein to any specific commercial product, process, or service by trade name, trade mark, manufacturer, or otherwise, does not necessarily constitute or imply its endorsement, recommendation, or favoring by the U.S. Government or any agency thereof. The views and opinions of authors expressed herein do not necessarily state or reflect those of the U.S. Government or any agency thereof.

AGC-2 Irradiated Material Properties Analysis

**William E. Windes
David T. Rohrbaugh
W. David Swank**

May 2017

**Idaho National Laboratory
INL ART TDO Program
Idaho Falls, Idaho 83415**

<http://www.inl.gov>

**Prepared for the
U.S. Department of Energy
Office of Nuclear Energy
Under DOE Idaho Operations Office
Contract DE-AC07-05ID14517**

INL ART TDO Program

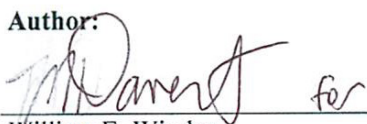
AGC-2 Irradiated Material Properties Analysis

INL/EXT-17-41165

Revision 0

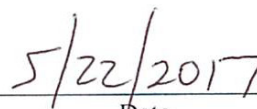
May 2017

Author:



William E. Windes

INL ART TDO Graphite R&D Technical Lead



Date

Technical Reviewer: (Confirmation of mathematical accuracy, correctness of data, and appropriateness of assumptions)



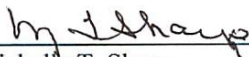
Timothy D. Burchell

ORNL Graphite Technical Peer Reviewer



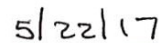
Date

Approved by:

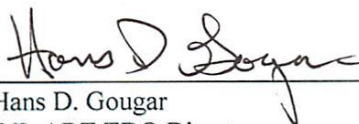


Michelle T. Sharp

INL Quality Engineer

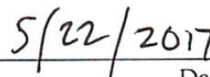


Date



Hans D. Gougar

INL ART TDO Director



Date

SUMMARY

This report documents analysis of irradiated property data from the Advanced Graphite Creep (AGC)-2 graphite specimens. The AGC-2 is the second of a series of six irradiation test trains planned as part of the AGC experiment to fully characterize neutron irradiation, temperature, and radiation creep behavior of various current nuclear graphite grades. The AGC-2 capsule was irradiated in the Idaho National Laboratory Advanced Test Reactor at a nominal temperature of 600°C, beginning with irradiation Cycle 149A on April 12, 2011, and ending with Cycle 151B on May 5, 2012, with a total received dose range of 1.3 to 4.7 dpa.

AGC-2 was designed to provide irradiation conditions similar to the first capsule, AGC-1 (i.e., the same graphite grades, a nominal irradiation temperature of 600°C, and the same applied mechanical stress levels), but was irradiated for a shorter period of time to provide material property values for the graphite samples at lower dose range than achieved in AGC-1. Material property and dimensional strain measurements were conducted on specimens from 15 nuclear graphite grades using a similar specimen assembly configuration as AGC-1 to provide a more direct comparison between the two capsules. However, AGC-2 contained an increased number of specimens (i.e., 487 total AGC-2 specimens versus 387 total AGC-1 specimens) and replaced specimens of the minor grade 2020 with the newer grade 2114.

Modifications to the AGC-2 capsule design were made to help maintain a narrow range of specimen temperatures. Optimally, specimens would be irradiated as close to 600°C as possible. The AGC-2 creep and control specimen temperatures ranged from 541 to 681°C.^{1,2} This was markedly better than the AGC-1 specimen temperature range of 468 to 716°C.^{22,3,4} Dose range received by the creep and control specimens ranged from 2.0 to 4.7 dpa. Dose range for the piggyback (button) specimens ranged from 1.3 to 4.7 dpa, because some of these specimens were physically located farther away from the peak centerline region.

Data covered in this report include specimen resistivity, elastic modulus (both by sonic resonance method and sonic velocity method), shear modulus, coefficient of thermal expansion, and thermal diffusivity. Experimental variables of irradiation dose, temperature, stress, and graphite grade that affect these property changes are presented with the observations.

CONTENTS

SUMMARY	v
ABBREVIATIONS AND ACRONYMS	xiii
1. INTRODUCTION	1
2. ADVANCED GRAPHITE CREEP EXPERIMENT	2
2.1 Design Parameters of Advanced Graphite Creep Experiment	2
2.2 Advanced Graphite Creep Graphite Grades and Specimen Dimensions	4
2.3 General Advanced Graphite Creep Test Train Design.....	5
2.4 Establishing Specimen Dose and Temperature.....	7
2.5 Physical Positions of Creep Specimens in the Stacks	8
3. AGC-2 TEST TRAIN CAPSULE	9
3.1 Design Parameters of AGC-2 Test Train	10
3.2 AGC-2 Graphite Grades.....	10
3.3 AGC-2 Specimen Stack Positions.....	11
4. AGC-2 AS-RUN IRRADIATION CONDITIONS	12
5. MATERIAL PROPERTY DATA	13
5.1 Density	15
5.2 Resistivity.....	23
5.3 Elastic Modulus by Sonic Velocity Method	31
5.4 Elastic Modulus by Sonic Resonance Method.....	40
5.5 Shear Modulus	41
5.6 Coefficient of Thermal Expansion	49
5.7 Thermal Diffusivity.....	60
6. CONCLUSIONS	67
6.1 General Comments.....	67
6.2 Specific Comments	68
6.2.1 Density	68
6.2.2 Electrical Resistivity	69
6.2.3 Elastic Modulus	69
6.2.4 Shear Modulus	70
6.2.5 Coefficient of Thermal Expansion	70
6.2.6 Thermal Diffusivity.....	71
7. REFERENCES	71

FIGURES

Figure 1. Irradiation dose and temperature parameters for the AGC experiment (HTV = high-temperature vessel, MSR = molten salt reactor, PB = Pebble Bed).	3
Figure 2. The AGC-2 creep capsule.....	6
Figure 3. Elevation sketch of the AGC experiment capsule.	7
Figure 4. A typical dose profile for creep graphite specimens using similar applied stress levels in matched stacks.	9
Figure 5. AGC-2 specimen irradiation temperature versus dose plot.	15
Figure 6. Percentage change of density for all AGC-2 graphite specimens.	16
Figure 7. Percent density change versus dose by graphite grade for all unstressed specimens only (no applied mechanical loads).	17
Figure 8. Percent density change versus dose of control (unstressed) major graphite grades only.	17
Figure 9. Average percent density change by graphite grade and applied load. The error bars represent ± 1 standard deviation from the mean and the numbers in the bars represent the sample size.	18
Figure 10. Percent density change versus specimen strain by graphite grade for creep, control, and unstressed piggyback specimens. Note negative strain increases from right to left (from 0.0 to -4.0%)	19
Figure 11. Percent density change versus dose by graphite grade for control and creep specimens.	19
Figure 12. Percent density change versus dose by fabrication process for creep and control specimens.....	20
Figure 13. Average percent density change by grain orientation and graphite grade for control and creep specimens.	20
Figure 14. Percent density change versus dose by grade and specimen grain orientation.....	21
Figure 15. Percent density change in unstressed specimens versus specimen irradiation temperature for a narrow dose range of 4.0 ± 0.5 dpa for different graphite grades.	22
Figure 16. Percent change in resistivity as a function of fast neutron dose for AGC-2 resistivity measurement specimens.	23
Figure 17. Percent resistivity change versus dose by graphite grade for control specimens.	24
Figure 18. Average percent resistivity change by graphite grade and applied stress. The error bars represent ± 1 standard deviation from the mean and numbers in the bars represent the sample size.....	25
Figure 19. Percent resistivity change versus dose by graphite grade for both control and creep specimens.....	25
Figure 20. Percent resistivity change versus dose for similar graphite fabrication processes for creep (—) and control (---) specimens. Solid lines represent linear fits of the creep specimens, while the dotted lines represent linear fits of the control specimens.....	26
Figure 21. Average percent resistivity change by grain orientation and graphite grade.....	27
Figure 22. Percent resistivity change versus dose by grade and specimen grain orientation.....	27

Figure 23. Percent resistivity change post irradiation versus specimen pre-irradiation density for control and creep specimens.	28
Figure 24. Percent resistivity change versus specimen strain by graphite grade for both control and creep specimens. Note negative strain increases from right to left (from 0.0 to -4.0%)	29
Figure 25. Percent resistivity change versus specimen irradiation temperature for a narrow dose range of 4.0 ± 0.5 dpa for different graphite grades.	30
Figure 26. Scatter plot of the percentage of modulus change from all AGC-2 graphite grades, stress conditions, and irradiation temperatures.	31
Figure 27. Percent modulus change versus dose by graphite grade for control specimens only.	32
Figure 28. Average percent modulus change by graphite grade and applied stress. The error bars represent ± 1 standard deviation from the mean and the numbers in the bars represent the sample size.	33
Figure 29. Percent modulus change versus dose by graphite grade for control and creep specimens.	34
Figure 30. Percent modulus change versus dose by fabrication process for creep (—) and control (- - -) specimens.	35
Figure 31. Average percent modulus change by grain orientation and graphite grade.	36
Figure 32. Percent modulus change versus dose by graphite grade and specimen grain orientation.	36
Figure 33. Percent modulus change versus specimen pre-irradiation density by graphite grade for control and creep specimens.	37
Figure 34. Percent modulus change versus specimen strain by graphite grade for control and creep specimens. Note negative strain increases from right to left (from 0.0 to -4.0%)	38
Figure 35. Percent change in Young's modulus versus specimen irradiation temperature for a narrow dose range of 4.0 ± 0.5 dpa for different graphite grades.	39
Figure 36. Scatter plot of the percentage of modulus change from all graphite grades, irradiation temperatures, and stresses.	41
Figure 37. Scatter plot of the percentage of shear modulus change from all graphite grades.	42
Figure 38. Percent shear modulus change versus dose by graphite grade for control specimens only.	43
Figure 39. Average percent shear modulus change by graphite grade and applied load. The error bars represent ± 1 standard deviation from the mean and numbers in the bars represent sample size.	43
Figure 40. Percent shear modulus change versus dose by graphite grade for control and creep specimens.	44
Figure 41. Percent shear modulus change versus dose by graphite fabrication process for control and creep specimens.	45
Figure 42. Average percent shear modulus change by grain orientation and graphite grade.	45
Figure 43. Percent shear modulus change versus dose by graphite grade and specimen orientation.	46
Figure 44. Percent shear modulus change versus specimen pre-irradiation density by graphite grade for control and creep specimens.	46

Figure 45. Percent shear modulus change versus specimen strain by graphite grade for control and creep specimens. Note negative strain increases from right to left (from 0.0 to -4.0%)	47
Figure 46. Percent change in shear modulus versus specimen irradiation temperature for a narrow dose range of 4.0 ± 0.5 dpa for the AGC-2 major graphite grades.....	48
Figure 47. Typical mean CTE measurement plot of nuclear grades over a range of temperatures (note: the graphite CTE data at each temperature are for illustration purposes only). It is observed that the CTE increases as temperature increases and the rate of increase also increases with increasing temperature.	50
Figure 48. Percent change of CTE for all graphite specimens at all test temperatures (100, 200, 300, 400, and 500°C).....	51
Figure 49. Percentage change of CTE at a single test temperature of 500°C for all tested specimens.....	52
Figure 50. Percent change in mean CTE at 500°C versus dose by graphite grade for control specimens only.	53
Figure 51. Average percent CTE change by graphite grade and applied load for measurement temperatures 100 to 500°C.	53
Figure 52. Percent CTE change by graphite grade and applied stress. The error bars represent ± 1 standard deviation from the mean and numbers in the bars represent sample size.	54
Figure 53. Percent CTE change at 500°C by graphite grade for stress levels of 0, 13.8, 17.2, and 20.7 MPa.....	55
Figure 54. Percent change of post irradiation CTE measurements at 500°C versus dose by fabrication process for creep (—) and control (- - -) specimens.	55
Figure 55. Average percent change CTE at 500°C by graphite grade, applied stress, and grain orientation for measurement temperatures at 500°C.	56
Figure 56. Percent change CTE at 500°C versus dose by graphite grade and specimen orientation.....	57
Figure 57. Percent CTE at 500°C change versus specimen pre-irradiation density by graphite grade for control and creep specimens.	57
Figure 58. Percent CTE change at 500°C versus specimen strain by graphite grade for control and creep specimens. Note negative strain increases from right to left (from 0.0 to -4.0%)	58
Figure 59. Percent change in CTE for unstressed specimens at 500°C versus specimen irradiation temperature for a narrow dose range of 4.0 ± 0.5 dpa for different graphite grades.	59
Figure 60. Specimen diffusivity versus measurement temperature for all AGC-2 piggyback specimens.....	61
Figure 61. Average percent diffusivity change by graphite grade for measurement temperatures 100 to 500°C. Note the Y-axis is inverted.....	62
Figure 62. Average percent diffusivity change by graphite grade (major grades only) for measurement temperatures 100 to 500°C. Note the Y-axis is inverted. The error bars represent ± 1 standard deviation from the mean.....	62
Figure 63. Percent change in diffusivity at 500°C as a function of irradiation dose. Note the Y-axis is inverted.	63
Figure 64. Average percent diffusivity change by graphite grade and grain orientation. Note the Y-axis is inverted.....	64

Figure 65. Percent diffusivity change versus specimen pre-irradiation density by graphite grade. Note the Y-axis is inverted.	64
Figure 66. Percent diffusivity change at 500°C versus specimen strain by graphite grade. Note the Y-axis is inverted and negative strain increases from right to left (from 0.0 to -4.0%)	65
Figure 67. Percent change in thermal diffusivity (at a measurement temperature of 500°C) for unstressed specimens versus specimen irradiation temperature for a narrow dose range of 4.0 ± 0.5 dpa for different graphite grades. Note the Y-axis is inverted.	66
Figure A-1. Percent modulus change versus dose by graphite grade for control specimens only.	74
Figure A-2. Average percent modulus change by graphite grade and applied load. The error bars represent ± 1 standard deviation from the mean and the numbers in the bars represent the sample size.	74
Figure A-3. Percent modulus change versus dose by graphite grade for control and creep specimens.	75
Figure A-4. Percent modulus change versus dose by fabrication process for control and creep specimens.	75
Figure A-5. Average percent modulus change by load and graphite forming process. The error bars represent ± 1 standard deviation from the mean.	76
Figure A-6. Average percent modulus change by grain orientation and graphite grade.	76
Figure A-7. Percent modulus change versus dose by graphite grade and specimen grain orientation.	77
Figure A-8. Percent modulus change versus specimen pre-irradiation density by graphite grade for control and creep specimens.	77
Figure A-9. Percent modulus change versus specimen post-irradiation density by graphite grade for stressed and unstressed specimens.	78
Figure A-10. Percent change in Young's modulus versus specimen irradiation temperature for a narrow dose range of 4.0 ± 0.5 dpa for different graphite grades.	79
Figure A-11. Percent modulus change versus specimen strain by graphite grade for both control and creep specimens. Note negative strain increases from right to left (from 0.0 to -4.0%).	80

TABLES

Table 1. Major, minor, alternate, and experimental graphite grades within the AGC-2 capsule.	11
Table 2. Total number of irradiated-creep specimens in the AGC-2 test series capsule.	12
Table 3. Number of with-grain, against-grain, creep, and piggyback specimens for the major graphite grades in the AGC-2 capsule.	13
Table 4. ASTM standards used for AGC-2 property measurements.	14

ABBREVIATIONS AND ACRONYMS

AG	against-grain
AGC	advanced graphite creep
ATR	Advanced Test Reactor
CCL	Carbon Characterization Laboratory
CTE	Coefficient of Thermal Expansion
HOPG	highly ordered pyrolytic graphite
HTR	high temperature reactor
INL	Idaho National Laboratory
PB	Piggyback “button” samples
PIE	post-irradiation examination
WG	with-grain

AGC-2 Irradiated Material Properties Analysis

1. INTRODUCTION

The Advanced Reactor Technologies Graphite Research and Development Program is conducting an extensive graphite irradiation experiment to provide data for licensing of a high-temperature reactor (HTR) design. In past applications, graphite has been used effectively as a structural and moderator material in both research and commercial high-temperature gas-cooled reactor designs.^{5,6} Nuclear graphite H-451, used previously in the United States for nuclear reactor graphite components, is no longer available. New nuclear graphite grades have been developed and are considered suitable candidates for new HTR reactor designs. To support the design and licensing of HTR core components within a commercial reactor, a complete properties database must be developed for these current grades of graphite. Quantitative data on in-service material performance are required for the physical, mechanical, and thermal properties of each graphite grade, with a specific emphasis on data accounting for the life-limiting effects of irradiation creep on key physical properties of the HTR candidate graphite grades. Further details on research and development activities and associated rationale required to qualify nuclear-grade graphite for use within an HTR are documented in the graphite technology research and development plan.⁷

The advanced graphite creep (AGC) experiment is currently underway to determine the in-service behavior of new graphite grades for HTR. This test series will examine the properties and behaviors of nuclear-grade graphite over a large spectrum of temperatures, irradiation fluence, and applied stress levels that are expected to induce irradiation creep strains within an HTR graphite component. Irradiation data are provided through the AGC experiment test series, which comprises six planned capsules irradiated in the Advanced Test Reactor (ATR) in a large flux trap at Idaho National Laboratory (INL). The AGC irradiation conditions are similar to the anticipated environment within a high-temperature core design. Each irradiation capsule is composed of more than 400 graphite specimens that are characterized before and after irradiation to determine the irradiation, temperature, and stressed induced changes in material properties and the rate of life-limiting irradiation creep for each graphite grade.

While creep rate calculations and analysis are documented in INL/EXT-16-39682, *AGC-2 Irradiation Creep Strain Data Analysis*,⁸ this report provides a post-irradiation examination (PIE) analysis of the irradiation-induced material property changes within AGC-2. Data and information produced in this document and the referenced documents within were generated under the approved quality assurance programs for the respective organizations, including INL and Oak Ridge National Laboratory in compliance with the appropriate NQA-1 requirements. It is anticipated that all qualified data will be robust enough to stand up to a review by the Nuclear Regulatory Commission as support for a graphite reactor design selection.

Results from this analysis will attempt to discern the effects from irradiation in-crystal damage and the effects resulting from microstructural evolution (i.e., changes in microstructure). It is anticipated that in-crystal irradiation defects will immediately affect the material property changes by providing atomic scattering centers interrupting electron and phonon transport, pinning sites affecting dislocation movement, and initial closure of microcracks (i.e., Mrozowski cracks) in the crystallites. With further irradiation the anisotropic crystallite response will begin to create significant microstructural changes by closing all Mrozowski cracks, alteration of large pore structures, realigning cracks, and significant volumetric dimensional change which can affect the material density, stiffness, and thermal expansion. Finally, irradiation induced creep strain can accelerate the microstructural changes exacerbating the material property changes sensitive to these mechanisms.

2. ADVANCED GRAPHITE CREEP EXPERIMENT

The AGC experiment test series is designed to establish data necessary to determine the safe operating envelope of graphite core components for an HTR by measuring the irradiated material property changes and the behavior of several new nuclear graphite grades over a large range of temperatures, neutron fluence, and mechanical compressive loads. The experiment consists of three interrelated stages: (1) pre-irradiation characterization of the graphite specimens, (2) the irradiation test series (designated as six separate irradiation test train capsules), and (3) PIE and analysis of the graphite specimens after irradiation. Separate reports for each distinct stage are prepared after each individual activity is completed.

Data within the separate reports detail the following information:

- a) **Pre-irradiation data reports:** The pre-irradiation data reports detail the total number of graphite grades and individual specimens, the specimen loading configuration designed to expose all specimens to the entire range of irradiation conditions, and the pre-irradiation material property testing data and results.
- b) **As-run irradiation reports:** The as-run irradiation reports detail the irradiation history of each capsule while in the reactor, noting any changes from the technical and functional specifications for each specific test series capsule and identifying possible improvements to the next test series capsule design.
- c) **Disassembly reports:** The disassembly reports detail specimen recovery from the irradiation capsule, noting any damage to the specimens and providing an inventory of recovered specimens for PIE testing.
- d) **PIE data reports:** The PIE data reports detail the changes in specimen dimensional measurements and irradiated material properties upon exposure to neutron irradiation.
- e) **PIE analysis reports:** The irradiation-induced analysis reports analyze the irradiation results reported within the data package reports, using the irradiation conditions recorded within the as-run irradiation report. The PIE analysis reports can be presented as two separate reports with irradiation creep analysis reported separately from material property changes. However, both PIE analyses interpret the irradiation behavior of the graphite grades to assist in determining a credible, safe operating envelope for graphite core components in an HTR design and licensing application.

This report is a PIE analysis report on irradiation-induced material property changes within the second AGC experiment capsule (AGC-2). A previous PIE analysis report on irradiation-induced creep in AGC-2 was published as “AGC-2 Irradiation Creep Strain Data Analysis.”⁸ Data from the “AGC-2 Specimen Post-Irradiation Data Package Report,”⁹ was used to analyze the electrical resistivity, elastic moduli, thermal expansion, and thermal diffusivity for each graphite grade.

2.1 Design Parameters of Advanced Graphite Creep Experiment

The AGC experiment test series is designed to measure changes in key thermal, physical, and mechanical material properties over the anticipated range of HTR operating conditions. By comparing the material properties of each specimen before and after irradiation, the experiment generates quantitative material property change data and irradiation creep data that will be used to predict the in-service behavior and operating performance of the current nuclear graphite grades for HTR designs. Specific emphasis is placed on the irradiation creep rate for the major graphite grades and the effect creep may have on key irradiated material properties of several candidate graphite grades for use in an HTR design.

The critical component of the experiment is the irradiation test series, which irradiates the graphite specimens after pre-irradiation examination characterization has been completed. The AGC experiment test series is composed of six planned irradiation test trains that are irradiated in ATR in a large flux trap, as described in the “Graphite Technology Development Plan.”⁷ The test series exposes test specimens of select nuclear graphite grades to high operating temperatures and only moderate irradiation dose range (generally, to dose levels well before Turnaround is achieved). Specifically, graphite specimens will be exposed to a fast neutron dose ranging from 1 to 7 dpa and nominal temperatures of 600, 800, and 1100°C (see Figure 1). The first and second AGC capsules, AGC-1 and AGC-2, were designed to be irradiated in ATR’s south flux trap.¹⁰ All other AGC capsules will be irradiated in ATR’s east flux trap. Generally, irradiations in the south flux trap require approximately 175 effective full-power days to provide a nominal fast neutron dose range (in graphite) of approximately 0.5 to 3.5 dpa. For capsules requiring a large dose range of approximately 3.5 to 7.0 dpa, the irradiation capsule (containing the graphite specimens) is irradiated for twice as long inside ATR (i.e., approximately 350 effective full-power days).

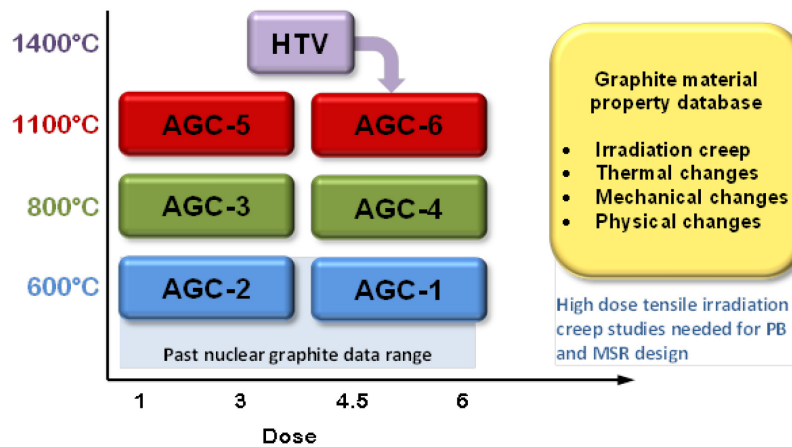


Figure 1. Irradiation dose and temperature parameters for the AGC experiment (HTV = high-temperature vessel, MSR = molten salt reactor, PB = Pebble Bed).

In addition to determining the irradiation-induced changes to material properties of selected nuclear graphite grades, the AGC experiment dedicates a significant amount of work scope to determining the rates of irradiation-induced creep for different nuclear graphite grades. The traditional method for measuring irradiation-induced creep is to apply a significant mechanical load (inducing a mechanical stress within the graphite) to half the specimens during irradiation, while leaving the remaining half of specimens unloaded (unstressed). Mechanically loaded (stressed) specimens are traditionally designated as creep specimens and unloaded (unstressed) specimens are designated as control specimens. The resulting difference in dimensional change between the loaded and unloaded specimens in the same capsule (assuming that temperature and dose are the same) provides the amount of irradiation-induced strain for each “matched pair” of graphite specimens. From this strain level, a creep rate for each graphite grade can be calculated as a function of dose, if both specimens were irradiated at the same constant temperature and dose. Thus, each capsule is designed to be irradiated at a constant temperature, allowing only the dose and applied mechanical load to vary within the test train of each test series capsule. With all graphite specimens at a constant temperature, only the applied stress level and dose will affect the calculated creep rate of each graphite grade within a test series capsule.

The AGC experiment is designed to measure constant creep strain behavior (secondary creep) of the various graphite grades. The experiment assumes that induced creep strain for all specimens is within the secondary creep regime and, therefore, behaves linearly with respect to received neutron dose.⁷ This assumption is valid provided the specimens do not go beyond their turnaround dose, where creep strain

can no longer be expected to be linear with irradiation dose (the onset of tertiary creep). Once the specimens begin to reach turnaround, the creep strain response becomes nonlinear with received dose. To ensure specimens exposed to the highest temperature and dose range (i.e., AGC-5 and AGC-6) will remain within the constant linear creep strain regime, a high-temperature irradiation vessel will be used to measure the dimensional changes of the graphite grades at a high temperature (1,400°C) and moderate dose (4.5 dpa). Results from this high-temperature dimensional change study will be used in the AGC-5 and AGC-6 designs, which constitute the upper temperature bounds of the AGC experiment (Figure 1). In addition, if any graphite grade achieves turnaround within the high-temperature irradiation vessel, the graphite grade will be considered to be outside the upper bounds of the AGC experiment and will be eliminated from the AGC-6 test train.

While the effects from applied mechanical stresses and neutron dose can be determined for each irradiation capsule, the temperature dependency of any irradiation-induced material property changes within the graphite grades is achieved by comparing the measured values of the specimens between irradiation capsules. Because each test train is irradiated at a constant temperature (600, 800, or 1100°C), the temperature-induced/enhanced material property changes must be determined by comparing specimens in different capsules exposed to similar doses and applied mechanical load levels. All AGC capsules are designed to have the same specimen stacking patterns. Thus, if specimens of identical graphite grades are located in similar positions within each capsule, a similar dose and load level will be imposed on the same grade of graphite. Maintaining consistent specimen positions for each grade within the six different capsules will allow determination of temperature-induced changes for irradiation creep and material properties across the AGC experiment.

2.2 Advanced Graphite Creep Graphite Grades and Specimen Dimensions

The AGC experiment is designed to ascertain the irradiation behavior of currently available nuclear graphite grades within the anticipated operating parameters of an HTR design. By exposing a variety of nuclear graphite grades that represent the range of fabrication parameters (i.e., grain size, fabrication processes, and raw source material) to the expected operating conditions for an HTR design (600 to 1,100°C and 0.5 to 7 dpa dose), a general comprehensive understanding of the irradiation response and behavior of graphite components can be achieved. This will limit the need for additional research in the future if the current graphite grades are altered (i.e., new raw material sources are used) or new grades are used in future reactors.

To provide all necessary material property tests in the AGC experiment, each test series capsule contains two primary specimen sizes: (1) larger “creep” and “control” specimens, providing irradiation creep-rate behavior as well as mechanical property behavior and (2) smaller “piggyback” (PB) specimens, providing thermal material property behavior for the major graphite grades as well as dimensional change for experimental, alternate, and minor grades. Creep/control specimens are fabricated only from major grade graphite types^{6,11,12} with the creep specimens subjected to an applied mechanical stress and control specimens are left unstressed. Piggyback specimens are fabricated from major, minor, and experimental grade graphite. The piggyback specimens are not mechanically loaded and are subjected only to neutron irradiation at high operating temperatures to assess the effects of a reactor environment on the specific graphite grade.

All specimens are 12.7 mm (0.5 in.) in diameter, with the larger creep/control specimens being 25.4 mm (1.0 in.) long and the piggyback specimens being 6 mm (0.25 in.) long. The large creep/control specimens provide accurate dimensional change, elastic modulus, thermal expansion, electrical resistivity, and mechanical strength measurements. However, the longer creep/control specimens make them unsuitable for thermal diffusivity measurements. The small “button-sized” piggyback specimens

permitted only dimensional measurements, density, and thermal-diffusivity testing to be performed. Together, both types of specimens provide the changes in material properties for stressed (creep) and unstressed (control) graphite grades.¹² Finally, small graphite containers that are 12.7 mm in diameter by 6 mm long contain thin wafers of highly oriented pyrolytic graphite (HOPG) specimens to assess fundamental irradiation damage in graphite crystal structures.

The AGC experiment uses a variety of current graphite grades to envelope the major fabrication parameters believed to be responsible for irradiation behavior of nuclear graphite.⁵ This range of fabrication parameters is represented by AGC experiment major grades, which were deemed to be production-ready grades that could be used in current or future HTR designs. Major graphite grades are one type of sample within an AGC irradiation capsule. In addition, four other sample types are designated within the AGC experiment. The five AGC sample types are categorized as follows:¹³

1. Major Grades (Irradiation Creep and Control Specimens)

These graphite grades are current reactor candidates for the core structures of an HTR design as well as legacy samples from historical (reference) grades to ensure the irradiation response is similar to previous studies. These major grades have an established fabrication maturity with good consistency and are the most likely to be used as high dose HTR core components. Only major grade specimens are used to determine the critical irradiation-induced creep strain rate.

2. Minor Grades (Piggyback “Button” Specimens)

These grades are HTR-relevant grades that are not yet production ready or are most likely to be used in the low neutron dose regions of the core (e.g., the permanent structure of the prismatic block HTR design).

3. Alternate Grades (Piggyback “Button” Specimens)

These are grades that current HTR vendors have identified as being of interest as alternate graphite grades for certain components within the reactor.

4. Experimental Grades (Piggyback “Button” Specimens)

Experimental graphite grades are included in the AGC experiment to assess the viability of new graphite grades whose manufacturing processes and raw materials are such that they may offer superior irradiation stability. Additionally, other carbonaceous materials (such as fuel compact matrix materials, carbon-carbon composites, silicon-carbide composites, or other experimental materials that could offer superior performance within the extreme environment of an HTR core) are included.

5. Single Crystal Graphite (Graphite containers)

Samples of highly ordered pyrolytic graphite in the form of thin wafers are included in AGC experiment to assess the fundamental irradiation response of single crystal graphite. These specimens offer specific dimensional change behavior of graphite, which is particularly significant to the behavior of polycrystalline (polygranular) graphite grades.

2.3 General Advanced Graphite Creep Test Train Design

All AGC experiment test trains have the same general physical configuration to provide similar dose and applied mechanical stresses on specimens of the same graphite grades. While there are some key machining and structural differences between the AGC capsule designs in order to change and control irradiation temperature in the different capsules, the majority of the capsule design is identical. A schematic of the AGC-2 test train and location of graphite specimens within the test train is shown in Figure 2.¹⁴

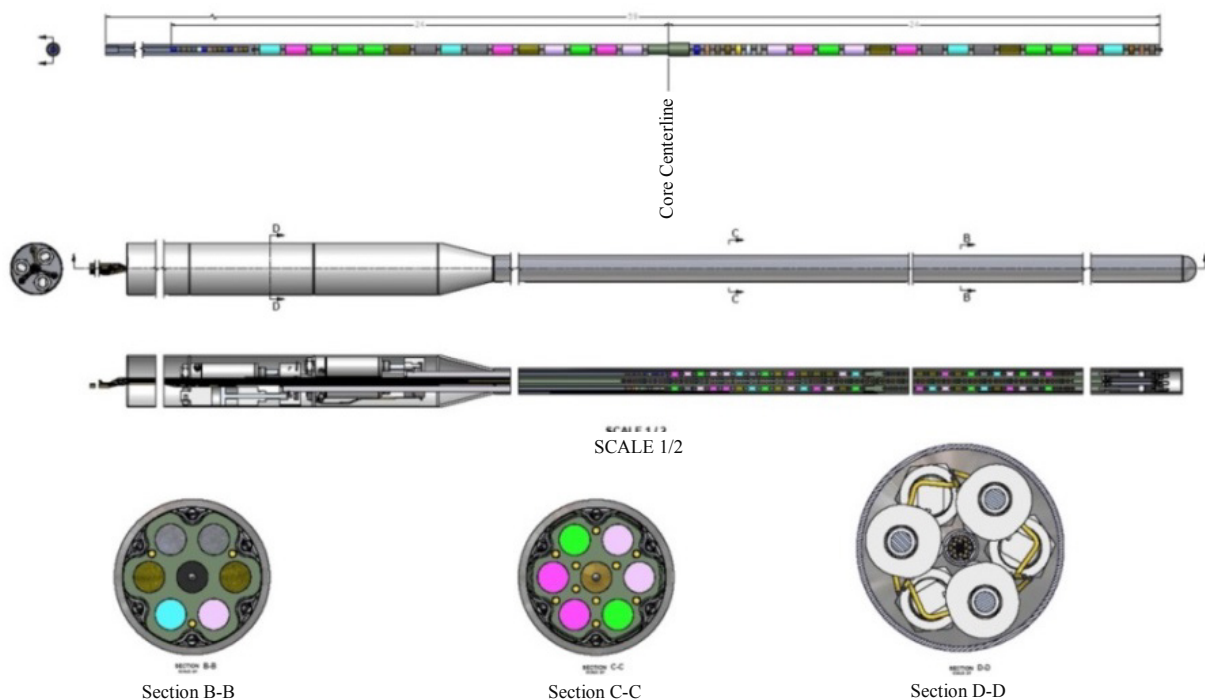


Figure 2. The AGC-2 creep capsule.

All AGC experiment capsules have six channels located in the outer perimeter of the graphite specimen holder body and a center channel. All channels are nominally 12.9 mm (0.51 in.) in diameter and are designed to hold all types of AGC experiment specimens. Specimens within the upper half of the capsule have a mechanical load applied to them via a pneumatic ram system. Specimens within the lower half remain unloaded and have no applied stress. The three applied stress levels—13.8 MPa, 17.2 MPa, and 20.7 MPa (2.0 ksi, 2.5 ksi, and 3.0 ksi) nominal—are imposed in all AGC capsules to provide a known stress on the graphite specimens during irradiation. These mechanical stress levels are high enough to produce irradiation-induced creep strain with the graphite specimens.

To achieve the desired dose range in the specimens the capsule designs use the symmetric flux profile generated within ATR to achieve similar dose conditions for specimens within the upper and lower sections of the capsule. Both specimens from a “matched pair” are positioned within the capsule at locations in the upper and lower sections where the flux level is the same. This allows the matched pair to receive similar dose while the specimens in the upper part of the capsule are exposed to the applied mechanical stress and the specimens in the lower half are unstressed.

Finally, the shape and design of the capsule internal components provide a constant irradiation temperature to all specimens. Thus, all specimens in an AGC experiment capsule are exposed to the same irradiation temperature over a range of neutron dose with half the specimens experiencing a mechanical stress and the other half remaining unstressed. These conditions provide the necessary parameters to determine the effects of neutron dose and irradiation strain on the graphite behavior. The effect of temperature is determined by differences in the graphite behavior between the various AGC capsules (i.e., specimens in AGC-1 and AGC-2 are irradiated at 600°C while specimens in AGC-3 and AGC-4 are irradiated to the same dose range and stress levels but at 800°C).

2.4 Establishing Specimen Dose and Temperature

A careful specimen loading order within the irradiation capsule is required to ensure similar dose for each “matched pair.”^{15,16} Other considerations include the size of each creep specimen, the need for periodically placed spacers containing flux wires, and space requirements in the top of the stacks for the pneumatic push rods. The core flux mid-plane, in relation to the capsule arrangement, was established so that the reactor neutron flux field could be correlated to the physical elevations and positions in the capsule to yield accurate “match pair” irradiation dose (Figure 3).¹⁷

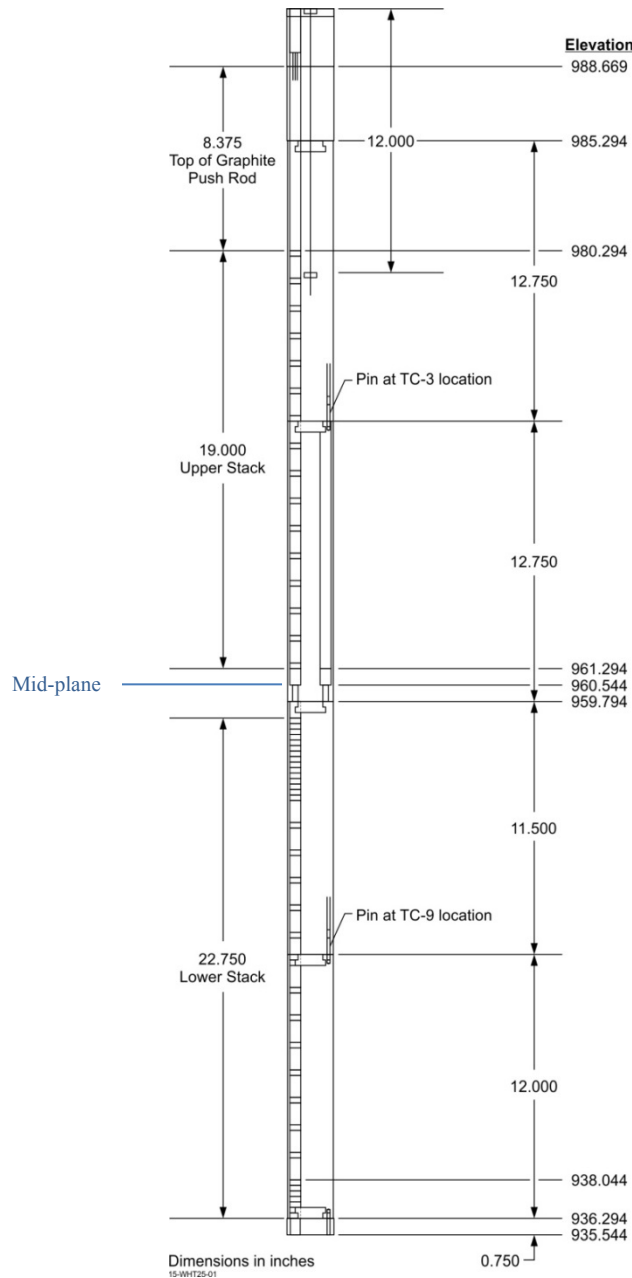


Figure 3. Elevation sketch of the AGC experiment capsule.

Irradiation dose values, as a function of distance from the reactor core centerline, are calculated from the total calculated fluence using standard conversion factors for carbon in a fast neutron irradiation field ($E > 0.1$ MeV).¹⁸ A neutron flux gradient across the capsule radius requires the capsule to be rotated 180 degrees at the irradiation midpoint. If the capsule is rotated, a uniform neutron-fluence profile is achieved for all stacks, regardless of their position within the capsule.

As described in previous reports,¹³ the ATR neutron flux profile is not completely symmetrical along the vertical axis. Thus, to produce matched-pair specimens that have similar dose profiles both above and below the core mid-plane, an offset position from the mid-plane is required. An offset distance of 31.75 mm (1.25 in.) from the core mid-plane for the bottom creep specimens produces the closest dose matches between specimens. While it was impossible to exactly match the dose for both the upper and lower specimens, the dose for each specimen pair were fairly close, ranging from 0 to 2%.^{18,19}

Temperature values within all AGC capsules are calculated based on thermocouple readings at select positions within the capsule. Specimen temperature is calculated with a finite element model that has been calibrated to predict the known thermocouple readings in the capsule. Dose range are calculated using Monte Carlo N-Particle Transport Code models and operating conditions in the ATR core and are corroborated from flux wire data.

2.5 Physical Positions of Creep Specimens in the Stacks

Once the specimen-position offset was established for the bottom half of the specimens, the number of total number of creep specimens for each grade of graphite was determined. It should be noted that the specimen stacking order for subsequent AGC irradiation capsules was changed from that initially established for the AGC-1 test train. In the initial AGC experiment capsule design, AGC-1 utilized 6.35 mm (0.25 in.) long NBG-25 graphite spacers between all creep specimens to separate them from each other. It was determined that this was not necessary, and most of the 6.35-mm (0.25-in.) long NBG-25 graphite spacers were eliminated. The decision to eliminate the spacers increased the total number of creep specimens in an AGC experiment capsule to 216 total specimens (or 36 matched pairs in each of the six outer perimeter channels). This allowed more specimens per graphite grade to be irradiated within the AGC-2 capsule.

As mentioned above, the six outer stacks in the capsule allow the specimens in two of the channel stacks to be loaded at the same stress level. Two channels are loaded to 13.8 MPa, two channels at 17.2, and two channels at 20.7 MPa. Because two stacks are at similar applied stress levels, the specimen loading order can be shifted between the two stacks, allowing the same grade of graphite to be mechanically loaded over a broader neutron dose range (see Figure 4). Assuming that both stacks have the same applied stress level, receive similar dose per position, and have a constant temperature allows this shifting of specimens and, consequently, a more uniform, smoother dose profile for each graphite grade.

A final consideration when establishing specimen loading positions is grain orientation of the specimens. All AGC capsules attempt to account for grain orientation relative to irradiation behavior. For extruded graphite grades, the against-grain (AG) and with-grain (WG) directions are obviously perpendicular and parallel to the extrusion direction, respectively. Iso-molded grades have little-to-no grain direction and there is no consideration for their orientation. However, in the case of vibration-molded graphite grades (i.e., NBG-17 and 18), there are actually two WG directions and one AG direction as a consequence of the fabrication process. The total number of WG and AG specimens is dependent on the particular capsule (i.e., AGC-1 and AGC-2 have the same number of specimens with similar orientation).

Once these considerations are accounted for, the dose-level profiles are determined for each graphite grade within each channel stack. It should be noted that due to elimination of the majority of the NBG-25

spacers from the AGC-1 design, the dose-level profiles for each graphite grade have been altered for the succeeding capsules.^{20,21,22} However, the changes are modest, allowing nearly direct comparison between AGC-1 and the subsequent AGC experiment capsules.

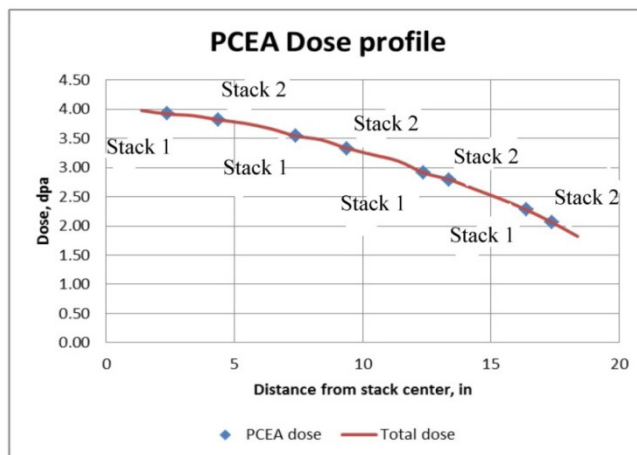


Figure 4. A typical dose profile for creep graphite specimens using similar applied stress levels in matched stacks.

3. AGC-2 TEST TRAIN CAPSULE

The AGC-2 capsule was irradiated in ATR beginning with Cycle 149A on April 12, 2011, and ending with ATR Cycle 151B on May 5, 2012.²³ In general, the average estimated irradiation temperature for all samples in the AGC-2 test train was 600°C, with a standard deviation of 64°C and a total range of 392 to 707°C. The average radiation dose of all specimens was 3.41 dpa, with a standard deviation of 1.03 dpa and a total range of about 1.2 to 4.7 dpa. This includes the piggyback specimens in the extreme top and bottom positions of the irradiation capsule. While the temperature range was much better than the prototype AGC-1 irradiation capsule, the AGC-2 irradiation temperature range exceeded the design (600 ± 50°C).²⁴ Irradiation temperature, applied stress, and total received dose for the AGC-2 creep and control specimens have narrower ranges than the total capsule range due to their centralized position within the irradiation capsule. Specific creep and control specimen irradiation ranges are reported later in this analysis report. All AGC-2 design documents and drawings pertinent to the AGC-2 graphite specimens have been referenced in the previous AGC-2 graphite pre-irradiation data package (INL/EXT-10-19588).²⁵

The AGC-2 irradiation capsule is the companion capsule for AGC-1. The original AGC-2 capsule design was intended to be identical to AGC-1, but would be irradiated within ATR for twice as long to achieve the higher dose. However, because of the large and unintended temperature variation across the AGC-1 capsule, it was decided that AGC-1 would be exposed to the higher neutron dose (i.e., nominal 3.5 to 7 dpa) to provide additional high-dose data. Consequently, the AGC-2 design was modified to provide lower dose data across a range of 1 to 5 dpa (i.e., the capsules were reversed with AGC-1 being the higher dose capsule and AGC-2 being the lower dose capsule).²⁴ ATR irradiation cycles were chosen to achieve this new dose range.

While some significant modifications were made to the AGC-2 irradiation specimens and layout (e.g., elimination of the majority of NBG-25 spacers to provide more space for creep specimens), overall design of AGC-2 was kept as similar to AGC-1 as possible. All minor and experimental graphite grades were retained, and only one alternate graphite grade was replaced with a new nuclear grade. This allowed results from both capsules to be compared and combined into a larger data population.

3.1 Design Parameters of AGC-2 Test Train

Since the silicon carbide temperature monitor results verified the thermocouple measured temperatures during AGC-1 capsule irradiation, it was decided that AGC-2 and subsequent capsules did not require the addition of silicon carbide temperature monitors to provide independent temperature verification.²⁶ Consequently, the central hole in each of the central piggyback specimens was not machined to accommodate the silicon carbide temperature monitors. By eliminating these monitors, the independent temperature monitoring capability for the AGC-2 capsule was excluded, but it was determined that being able to measure the changes to the thermal diffusivity at high temperatures was more important. Central holes in all AGC experiment piggyback specimens for the subsequent remaining irradiation capsules were also eliminated.¹²

As discussed previously, a majority of the 6.35-mm (0.25-in.) long NBG-25 graphite spacers between all AGC-1 creep specimens was eliminated. Four spacers were left in each channel (two in the upper section of the channel and two in the lower section) to allow flux wires to be placed within them. Eliminating most of the spacers allowed 12 additional creep specimens to be tested within the AGC-2 capsule. The total number of creep specimens in the AGC-2 capsule was increased to 216 total specimens (or 36 matched pairs in each outer perimeter channel).²⁵ This stacking configuration with minimal spacers will also be used with subsequent AGC irradiation capsules (e.g., AGC-3, AGC-4, etc.).

3.2 AGC-2 Graphite Grades

With only a few minor changes, the graphite grades irradiated in AGC-2 were the same as grades irradiated in AGC-1. One of the graphite grades in AGC-2 was changed at the request of the graphite vendor (Mersen, USA). Piggyback specimens of graphite grade 2114 were directly substituted for graphite grade 2020 and irradiated within the AGC-2 central stack (axial spine of capsule). All other graphite grades irradiated within AGC-2 remain the same as in AGC-1.

The sample numbers for two major grades, H-451 and IG-430, were reduced to allow for more creep test specimens in the remaining major grades. All AGC-2 major, minor, alternate, and experimental grades of graphite are as follows:

1. Major graphite grades: NBG-17, NBG-18, PCEA, IG-110, H-451, and IG-430
2. Minor graphite grades: NBG-25, NBG-10, HLM, and PGX
3. Alternate grades: PPEA, PCIB, and 2114 (replaced grade 2020)
4. Experimental grades: BAN and A3-3/A3-27 fuel compact matrix material
5. Single crystal graphite: HOPG.

A more complete description of all of the graphite samples included in capsule AGC-2 is given in Table 1. Code letters were given to each graphite grade to replace their name designations to shorten the specimen identification number for each specimen. This allowed the specimen to have a short ID number, which was necessary for laser engraving of each specimen. For grades NBG-17, NBG-18, and PCEA (codes A, B, and D), both WG and AG specimen orientations are included in the capsule.

Table 1. Major, minor, alternate, and experimental graphite grades within the AGC-2 capsule.

Graphite Grade	Forming Method	Intended Purpose	AGC Code Letter
NBG-17	Vibrational molded	AREVA Next Generation Nuclear Plant design	A
NBG-18	Vibrational molded	Pebble Bed modular reactor (not currently being pursued)	B
H-451	Extruded	Historical grade (reference grade)	C
PCEA	Extruded	AREVA Next Generation Nuclear Plant design	D
IG-110	Isostatically pressed	HTR– Pebble-Bed module (China)	E
IG-430	Isostatically pressed	Candidate graphite	F
HOPG	Vapor deposited	Fundamental studies	G
A3 matrix	Hot pressed	Fuel matrix material	H
HLM	Molded	Low dose core component	J
PGX	Extruded	Low dose core component	K
PPEA	Extruded	Alternate candidate	L
NBG-25	Isostatically pressed	Low dose core component	M
PCIB	Isostatically pressed	Alternate candidate	P
BAN	Isostatically pressed and extruded	Experimental graphite	R
NBG-10	Extruded	Low dose core component	S
2114	Isostatically pressed	Candidate graphite	T

3.3 AGC-2 Specimen Stack Positions

The final loading configuration for the outer channel/stacks was determined for each graphite grade to optimize the number of specimens for each grade, create a smooth irradiation profile for creep and piggyback specimens, and ensure proper position of creep specimens to create matched pairs.

The further decision was also made to increase the creep specimen number population for the newer graphite grades, because little-to-no irradiation data are available on these grades. Specifically, more specimens of graphite grades NBG-18 and PCEA were chosen to be irradiated instead of the IG-110, IG-430, and NBG-17 graphite grades (see Table 2).²⁵ NBG-18 and PCEA were chosen to have 16 specimens per applied stress level for a total of 48 specimens within AGC-2. Graphite grades IG-110 and IG-430 were represented by 12 specimens per applied stress level (for a total of 36 specimens) and NBG-17 and H-451 had the fewest with only 8 specimens per applied load (total of 24 specimens) within AGC-2.

Table 2. Total number of irradiated-creep specimens in the AGC-2 test series capsule.

Graphite Grade	Number of Creep Specimens
PCEA	48
NBG-18	48
IG-110	36
IG-430	36
NBG-17	24
H-451	24
Total Creep	216

In AGC-2, approximately 75% of extruded specimens (H-451 and PCEA) were oriented in the WG direction and 25% of the specimens were AG. As discussed previously, iso-molded grades (IG-110 and IG-430) have little to no grain direction, and there is no consideration of specimen orientation for these grades. However, in the case of vibration-molded graphite grades (i.e., NBG-17 and -18), which possess two WG directions and one AG direction,⁶ it was logical to split the WG and AG specimens evenly (i.e., 50/50 ratio) rather than following the 75/25 ratio established for the extruded specimens.

Orientation of the specimen is designated by the second digit in the sample identification number. Specimen identification numbers possessing a “W” in the second digit are specimens in the WG orientation (e.g., CW101). Specimen identification numbers possessing an “A” in the second digit are specimens machined from an AG orientation (e.g., DA402). As discussed previously, vibrationally molded grades are designated with an “L” or “P” for the two WG orientations (e.g., BP402 for an NBG-18 grade specimen).

The final loading configuration documented in INL-EXT-16-39682, *AGC-2 Irradiation Creep Strain Data Analysis*⁸ for AGC-2, including creep specimen matched-pair positions (above and below the capsule mid-plane), piggyback order, lower stack offset, and flux wire spacers, was mapped for each graphite specimen as it was loaded into the AGC-2 irradiation capsule during assembly. Following irradiation in ATR at INL, the AGC-2 capsule was disassembled.^{27,28} All specimens recovered from disassembly were visually inspected and physically measured within the INL Carbon Characterization Laboratory (CCL) before being stored in the irradiated graphite storage vault. It should be noted that NBG-25 Specimen S101 was lost (i.e., missing) during AGC-2 disassembly activities.²⁷ After accounting for all recovered specimens from the AGC-2 capsule, PIE and testing were performed for each specimen at the CCL.

4. AGC-2 AS-RUN IRRADIATION CONDITIONS

AGC-2 was designed to provide irradiation conditions similar to AGC-1 (i.e., the same graphite grades, a nominal irradiation temperature of 600°C, and the same applied mechanical loading) but it was irradiated for a shorter period of time to provide material property values for the graphite samples at lower dose range than those achieved in AGC-1. An additional objective was to incorporate capsule design improvements learned from AGC-1 to reduce the large specimen temperature range experienced in AGC-1.

AGC-2 was irradiated in the south flux trap of ATR between April 12, 2011, and May 5, 2012.^{23,27} AGC-2 was irradiated over five reactor cycles, Cycles 149A, 149B, 150B, 151A, and 151B (there was no Cycle 150A) for a total of 5,539 MW days or approximately 230 effective full-power days. The final specimen dose ranged from 1.3 to 4.7 dpa, with the specimens at the mid-plane elevation receiving the highest accumulated dose.²⁹ It should be noted that the majority of piggyback specimens were located within the unloaded central stack of the AGC-2 capsule. However, a small fraction of the piggybacks were used in the outer stacks, primarily near the bottom of the capsule to ensure the creep specimens were centrally located within the reactor core mid-plane. Because these select piggyback specimens were near the bottom end of the capsule, they received much lower dose than the creep specimens.

Irradiation creep is defined as the difference in dimensional change between stressed (i.e., creep) and unstressed (i.e., control) samples irradiated at similar dose and temperature levels. ECAR-2925 gives details on how the specimen stresses were calculated for each stack of specimens. This report also describes the uncertainty in the load data.³⁰

Modifications to the AGC-2 capsule design were made to reduce the range of specimen irradiation temperatures. The desire was for all specimens be irradiated as close to 600°C as possible. The AGC-2 creep and control specimen temperatures ranged from 541 to 681°C,^{31,32} which was markedly better than the AGC-1 specimens (with a range of 468 to 716°C),^{22,33,34} but it is still considered less than optimal as defined for AGC-2 capsule irradiation specifications (i.e., average capsule temperature maintained at 600°C ±50°C).¹⁰ Maximum and minimum temperatures between stacks were significantly improved (i.e., maximum temperature range of 666 to 681°C and minimum temperature range of 541 to 553°C) as were temperatures between AGC-2 matched-pair specimens. A detailed uncertainty analysis of the temperature model used to derive the specimen temperatures was given in ECAR-3017.^{35,36} A summary of the AGC-2 capsule experimental conditions was explained in more detail in INL/EXT-16-38431.²

5. MATERIAL PROPERTY DATA

Pre-irradiation material property data for all major graphite grades were reported in INL's *AGC-2 Graphite Pre-irradiation Data Package* (INL/EXT-13-28612, Revision 1).²⁵ The data package report also details dimensional sizes of the specimens in the capsule, creep, control, and piggyback specimens. Post irradiation material property data are provided in *AGC-2 Specimen Post-Irradiation Data Package Report* (INL/EXT-15-36244).⁹ An uncertainty analysis on material property measurements can be found in *AGC Inter-laboratory Comparison of Graphite Testing Procedures* (TEV-2530).³⁷ Table 3 shows the breakdown of specimens in the AGC-2 capsule by graphite grade, grain orientation, and specimen type.

Table 3. Number of with-grain, against-grain, creep, and piggyback specimens for the major graphite grades in the AGC-2 capsule.

	Creep/Control Specimens		Piggyback Specimens	
	With-Grain	Against-Grain	With-Grain	Against-Grain
H-451	24	0	4	2
NBG-17	18	6	12	3
IG-110	36	0	21	0
IG-430	36	0	13	0
NBG-18	36	12	8	5
PCEA	36	12	10	5

Dimensional measurements were made on all specimens (i.e., creep, control, and piggyback). However, the larger creep and control specimens were subjected to density, resistivity, elastic modulus (both by sonic resonance method and sonic velocity method), shear modulus, and thermal expansion measurements, while only density and thermal diffusivity measurements were made on the smaller piggyback specimens.

Dimensional change was calculated and recorded for the AGC-2 creep analysis and reported in the AGC-2 creep analysis report.⁸ All measurements were made according to the applicable American Society of Testing and Materials (ASTM) standard.

Table 4 lists the ASTM standards that were used when making the graphite material properties measurements. Further details of how these measurement standards are applied to the graphite specimens can be found in PLN-4657.28 This plan describes the measurement techniques, equipment, and standards used to gather data analyzed in this report.

Table 4. ASTM standards used for AGC-2 property measurements.

Measurement	ASTM Standard	Material Property
Physical Dimensions and Mass	ASTM C559-90 (Reapproved 2010)	Bulk density
Fundamental Frequency	ASTM C747-93 (Reapproved 2010), ASTM C1259-08	Elastic modulus (flexural mode)
Sonic Velocity	ASTM C769-98 (Reapproved 2005)	Young's modulus, Shear modulus
Four-Point Electrical Resistivity	ASTM C611-98 (Reapproved 2010)	Electrical resistivity
Laser Flash Diffusivity	ASTM E1461-07	Thermal diffusivity
Push Rod Dilatometry	ASTM E228-06	Coefficient of thermal expansion

When interpreting the material property measurements and property changes, measured data were analyzed against the five variables within the experiment. These variables are specimen dose, specimen temperature, specimen stress, specimen grain orientation, and graphite grade/type. It should be noted that there is a strong correlation between specimen temperature and specimen dose due to the larger-than-designed irradiation temperature range over the full length of the AGC-2 capsule. This relationship makes it more difficult to draw definitive conclusions on dose versus temperature variations (Figure 5), which illustrates the AGC-2 specimen temperatures versus received dose. In an attempt to determine any effects from irradiation temperature, any potential change resulting from specimen irradiation temperature are analyzed for all material properties.

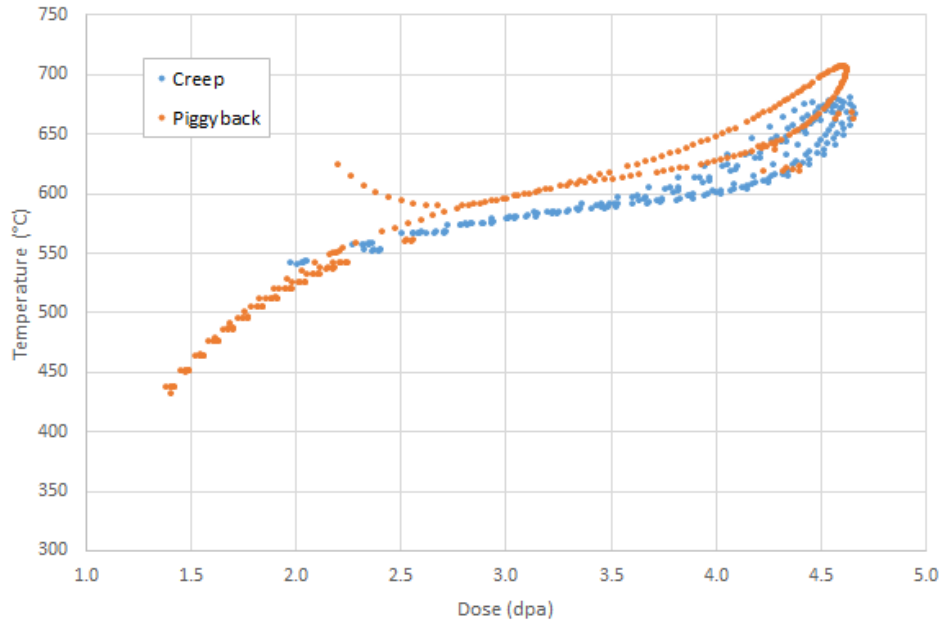


Figure 5. AGC-2 specimen irradiation temperature versus dose plot.

Finally, the irradiated material property data are presented as a percentage change from the unirradiated material property values. This approach allows quantitative irradiation-induced changes to be easily illustrated. In addition, the AGC experiment was originally designed to provide irradiation-induced change in each material property rather than the absolute irradiation value. The mean irradiation-induced changes for each material property measured in this analysis will then be added to the more statistically accurate virgin (i.e., Baseline) material property mean values to arrive at the absolute irradiation value for each property. This methodology was used because this sample population for irradiated specimens is limited (i.e., only a few hundred irradiated specimens for each capsule), while the Baseline sample population was designed to be significantly larger and more statistically accurate. Therefore, all data presented in this analysis will be the calculated relative difference between the pre-irradiation and post-irradiation material property values for each specimen.

Relative changes between the un-irradiated and irradiated material were evaluated using the following percent difference formula:

$$\%Difference = \left(\frac{X_{post} - X_{pre}}{X_{pre}} \right) \times 100 \quad (1)$$

where, X represents a specific material property.

5.1 Density

Studies from the Advanced Reactor Technologies Graphite Baseline program have demonstrated that density has a large effect on graphite material property values, illustrating that even small variations in a graphite grade can lead to significant changes in property values. Any irradiation-induced density changes to the graphite grades will be important to analysis of graphite behavior. Dimensional and mass measurements are performed to ASTM Standard C559-90 (Reapproved 2010). This standard describes, in detail, the procedure for making dimensional and mass measurements for calculating bulk density of manufactured carbon and graphite articles. The bulk density of the specimen is calculated as follows:

$$D = M/V$$

(2)

where:

D = bulk density, mg/mm^3

M = mass, mg

V = volume, mm^3

Density measurements were made on all AGC-2 graphite specimens before and after irradiation. Density changes in the AGC-2 specimens ranged from 0.3 to 5.2%, as a function of dose (Figure 6). It should be noted that the density change appears to be linear with respect to the received dose of the specimens. From past research, irradiation induced changes should appear nonlinear since density is proportional to inverse volume change ($1/V$) and volume change will be represented by a curve. However, AGC-2 density changes appear to be linear because the dose is low and the temperature range is narrow. The density change is also related to the dimensional change experienced within irradiated graphite, and the observed changes compare well with the behavior seen for dimensional and irradiation creep response in AGC-2 specimens.⁸ Linear regression of data between the dose range of about 1.25 and 4.7 dpa shows a change of 0.603% per dpa with a square of residuals of 0.48%.

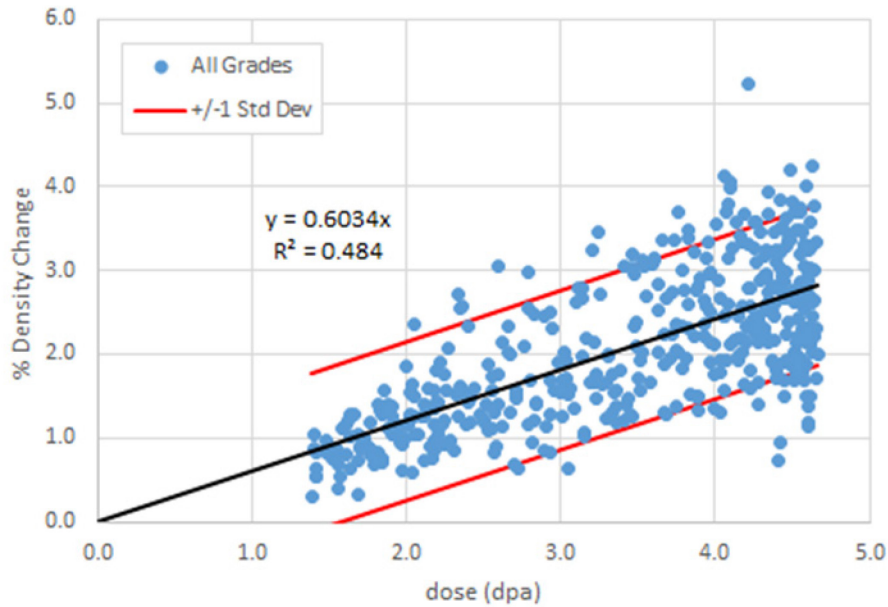


Figure 6. Percentage change of density for all AGC-2 graphite specimens.

Figure 7 and Figure 8 demonstrate the induced density changes resulting from irradiation only (no mechanically loaded specimens are considered). Figure 7 illustrates the density change for all unstressed AGC-2 graphite grades, with increasing received dose (i.e., control and piggyback specimens). As expected, due to irradiation-induced dimensional change, the density of all graphite grades increases simply as a result of exposure to neutron dose. The extent of change is less than observed in Figure 6 because the additional dimensional changes resulting from mechanical loading are not considered.

Figure 8 isolates these density changes to only major graphite grades in order to clarify the data trends. It is observed that with the exception of the IG-430 grade, the regression slopes for all grades are very similar, demonstrating a similar density change response. However, there are some differences in the initial offset. The regressions shown in Figure 8 may serve as refinement by limiting data to control

(i.e., unstressed) specimens only, but various grain orientations and irradiation temperatures are still factors in the overall data trend.

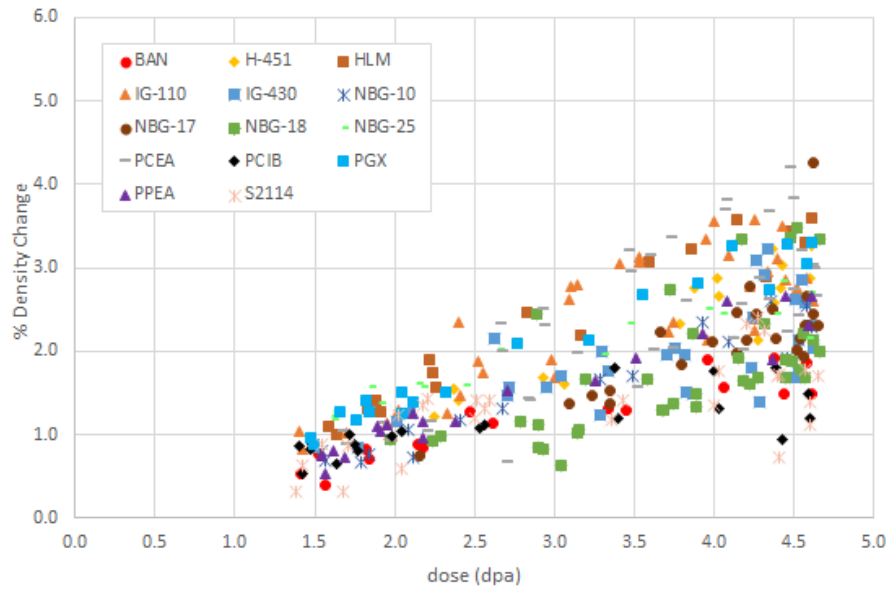


Figure 7. Percent density change versus dose by graphite grade for all unstressed specimens only (no applied mechanical loads).

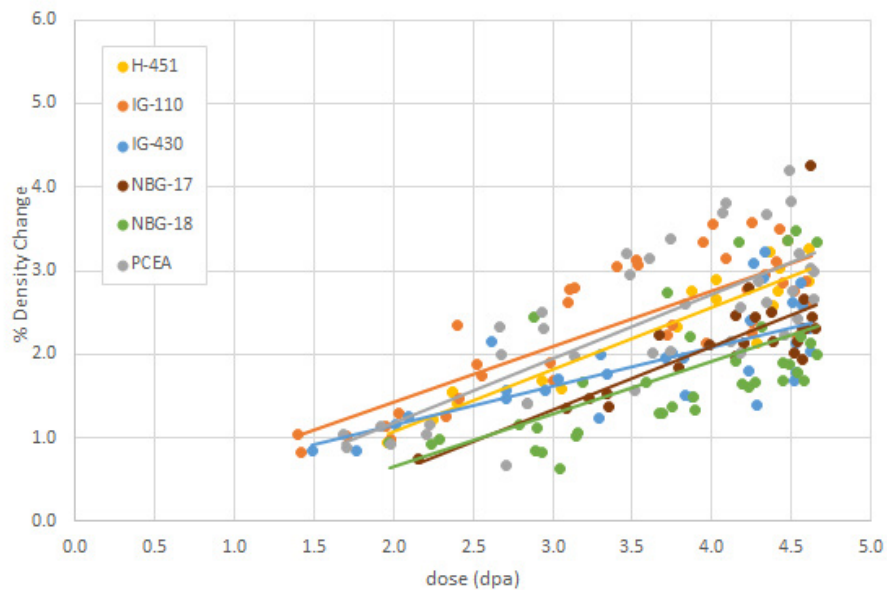


Figure 8. Percent density change versus dose of control (unstressed) major graphite grades only.

The effect of applied mechanical stress on average percent change in specimen density for the six major grades of graphite is shown in Figure 9. Control specimens are not stressed in the experiment; therefore, they are represented by the “0 MPa” grouping on the left hand side of the plot. Three levels of applied stress are shown as 13.8 MPa, 17.2 MPa, and 20.7 MPa. The number of specimens tested for each grade of graphite at the various stress conditions are shown inside each bar. Plus and minus one standard deviation is represented by the error bars. These standard deviations are relatively large due to

incorporation of all grain orientations, specimen irradiation temperatures, and all received doses being included in the average percent change in specimen density. However, it can be observed that the density change generally increases as the applied stress (and resulting irradiation-induced strain) increases. This results from the greater dimensional change seen for stressed specimens as observed in the AGC-2 creep analysis report.

It can be seen that grade IG-110 had the highest average percent change in density (for specimens with stress levels of 20.7 MPa) at 3.25 and NBG-18 had the least at 1.75. This corresponds well to the average longitudinal creep coefficients determined previously with IG-110 $K_{\text{long}} = 0.122$ as the second highest value and NBG-18 $K_{\text{long}} = 0.095$ as the lowest value ($K = 10^{-30} \text{ cm}^2/\text{n}\cdot\text{Pa}$).

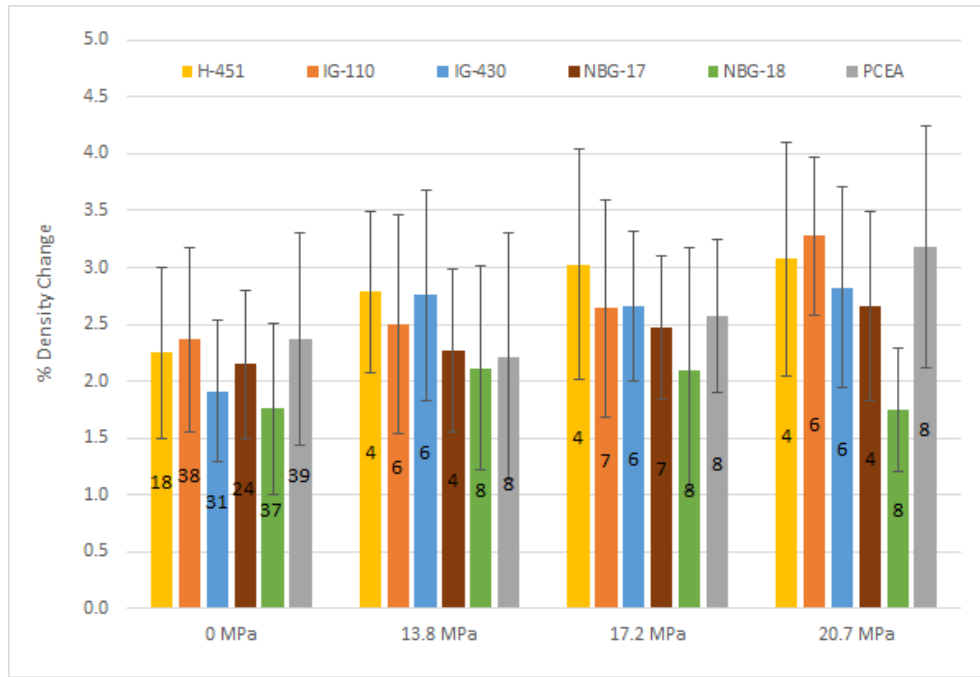


Figure 9. Average percent density change by graphite grade and applied load. The error bars represent ± 1 standard deviation from the mean and the numbers in the bars represent the sample size.

Figure 10 shows the percent density change as a function of observed strain in the loaded direction. All stressed (creep) specimens are depicted by large symbols and unstressed (control and piggyback) specimens are shown by smaller symbols. As expected, the loaded specimens with the highest strain yield slightly larger density changes, and unstressed specimens have a different density change behavior than stressed specimens. However, an interesting result is that rather large strain ranges can result in similar density changes. At 2.0% density change, the strain in specimens of NBG-18 can range from -0.5 to -2.5 (% strain). This behavior is not well understood and will require additional analysis.

Figure 11 demonstrates the effects of combining irradiation dose and applied load with the density changes on stressed (● creep) and unstressed (• control) specimens. An attempt is made to discriminate between density change for applied mechanical stresses and received dose by plotting data with large (stressed) and small (unstressed) data points as a function of received dose. Figure 9 appears to show the expected slight increase in density for creep specimens over unstressed control specimens. This effect from irradiation strain is illustrated more clearly in Figure 12, where the graphite grades have been grouped into their respective fabrication processes of vibration, isostatic, and extrusion. This result is expected from the creep analysis results, where stressed specimens demonstrate greater dimensional change than unstressed specimens receiving the same dose.

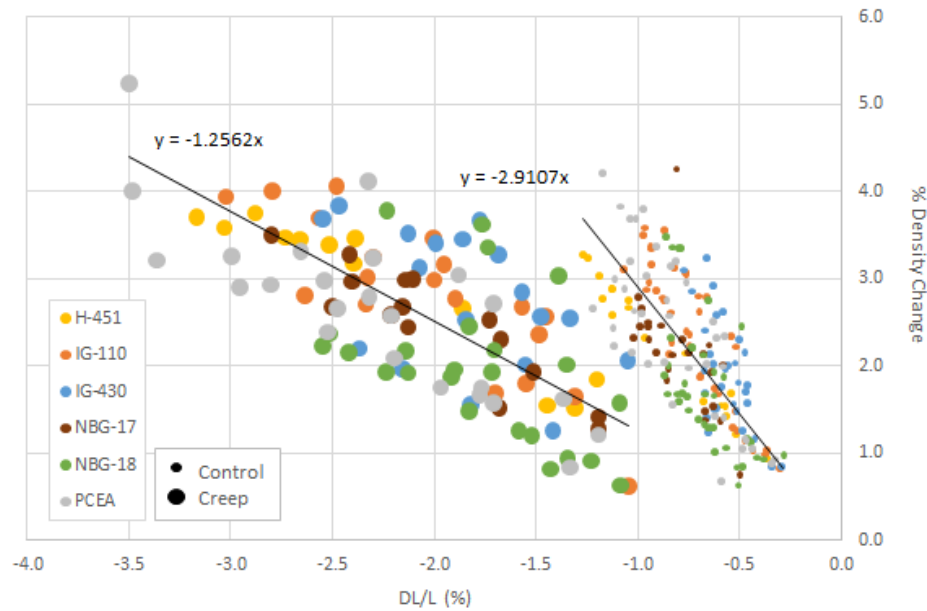


Figure 10. Percent density change versus specimen strain by graphite grade for creep, control, and unstressed piggyback specimens. Note negative strain increases from right to left (from 0.0 to -4.0%)

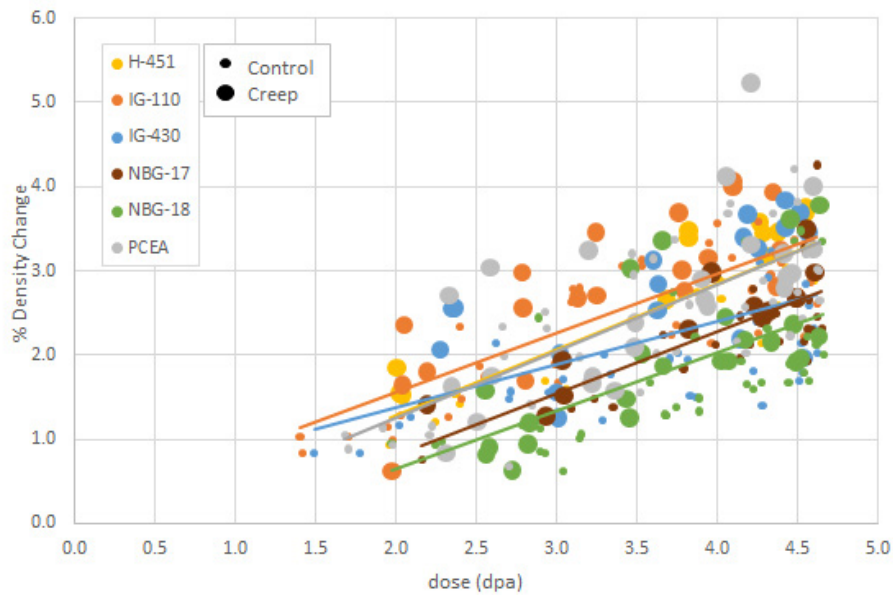


Figure 11. Percent density change versus dose by graphite grade for control and creep specimens.

It is interesting to note the slope of density change is approximately equal for all three forming processes. The linear regressions are very similar for the extruded and iso-molded forming processes with the vibra-molded being offset by about 1%. As shown in Figure 9, the percent change in density is less for the unstressed control specimens. This difference is greatest for the iso-molded process and least for the vibra-molded. Also note the difference between creep and control specimens in the percent change of density depicted by the linear regressions was constant for all three forming processes.

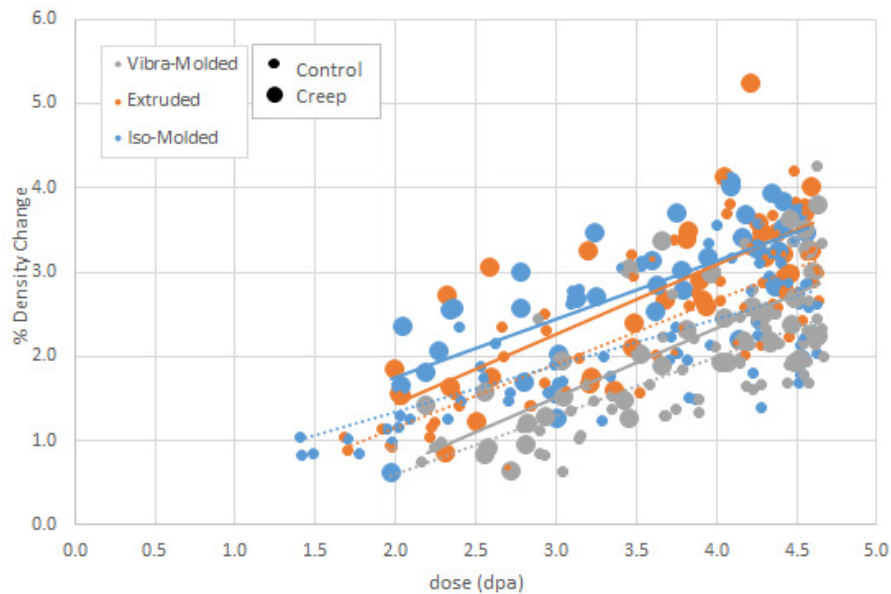


Figure 12. Percent density change versus dose by fabrication process for creep and control specimens.

While dose, applied stress, and graphite grade are considered major factors in density changes, grain orientation of the specimen can affect the response as well. There are four graphite grades included in the specimen population that possess distinct grain orientation directions. Figure 13 and Figure 14 show the effects of grain orientation on density changes for grades PCEA, NBG-17, NBG-18, and H-451 in both a stressed and unstressed conditions. Neither figure shows a clear correlation observed with-grain direction. Note the error bars (\pm one standard deviation) are relatively large due to inclusion of multiple variables and a lower number of specimens. Also note the H-451 data are incomplete due to no AG creep samples being included in the AGC-2 capsule.

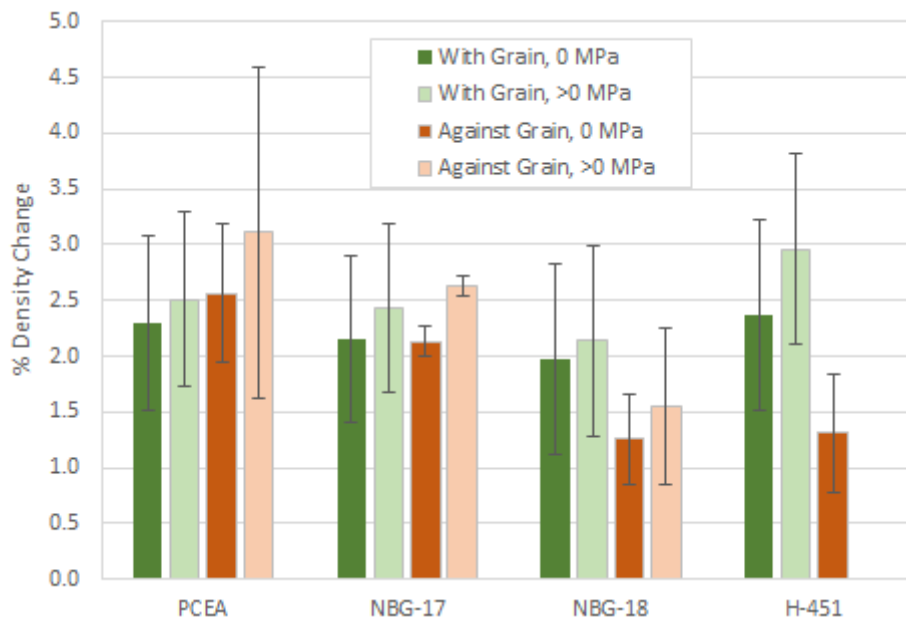


Figure 13. Average percent density change by grain orientation and graphite grade for control and creep specimens.

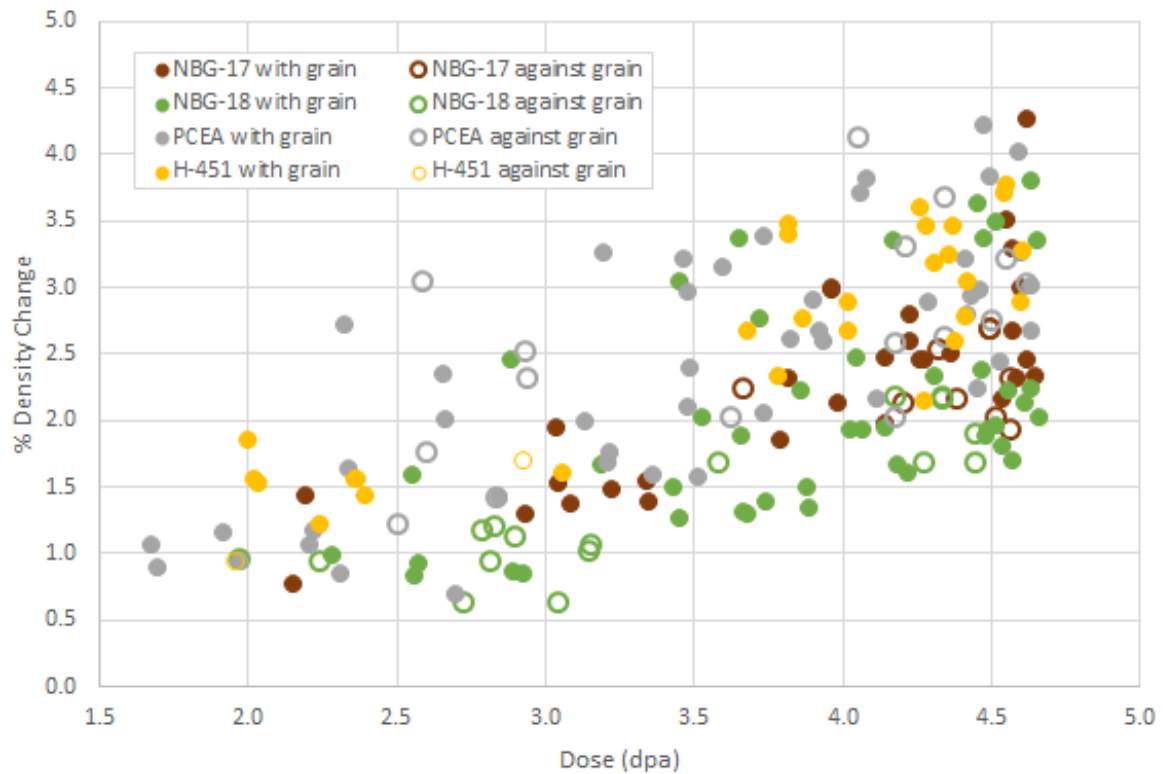


Figure 14. Percent density change versus dose by grade and specimen grain orientation.

Finally, as described previously, AGC-2 was designed for a nominal irradiation temperature of 600°C, but contained specimens with irradiation temperatures between 432 and 708°C. In an attempt to discern whether the larger-than-designed specimen irradiation temperature range might affect the measured density change, data for the three forming process grades are plotted in a very narrow dose range (i.e., between 3.5 and 4.5 dpa) as a function of the irradiation temperature range (Figure 15). The temperature range in Figure 15 is about 110°C (between 590°C and 700°C) and stressed and unstressed specimens are depicted by the size of the plotted symbol.

For these specific ranges of temperature and dose, no distinct trend in percent density change as a function of irradiation temperature is seen for any grade of graphite. However, this is a relatively narrow temperature range and only indicates there is limited temperature effect on the density change for the AGC-2 capsule. A more accurate determination of temperature effects will be derived as data from other AGC capsules are gathered with nominal temperatures of 800°C and 1,100°C. With data taken over a much broader temperature range, it will be possible to calculate the actual role of irradiation temperature versus irradiation dose for nuclear graphite.

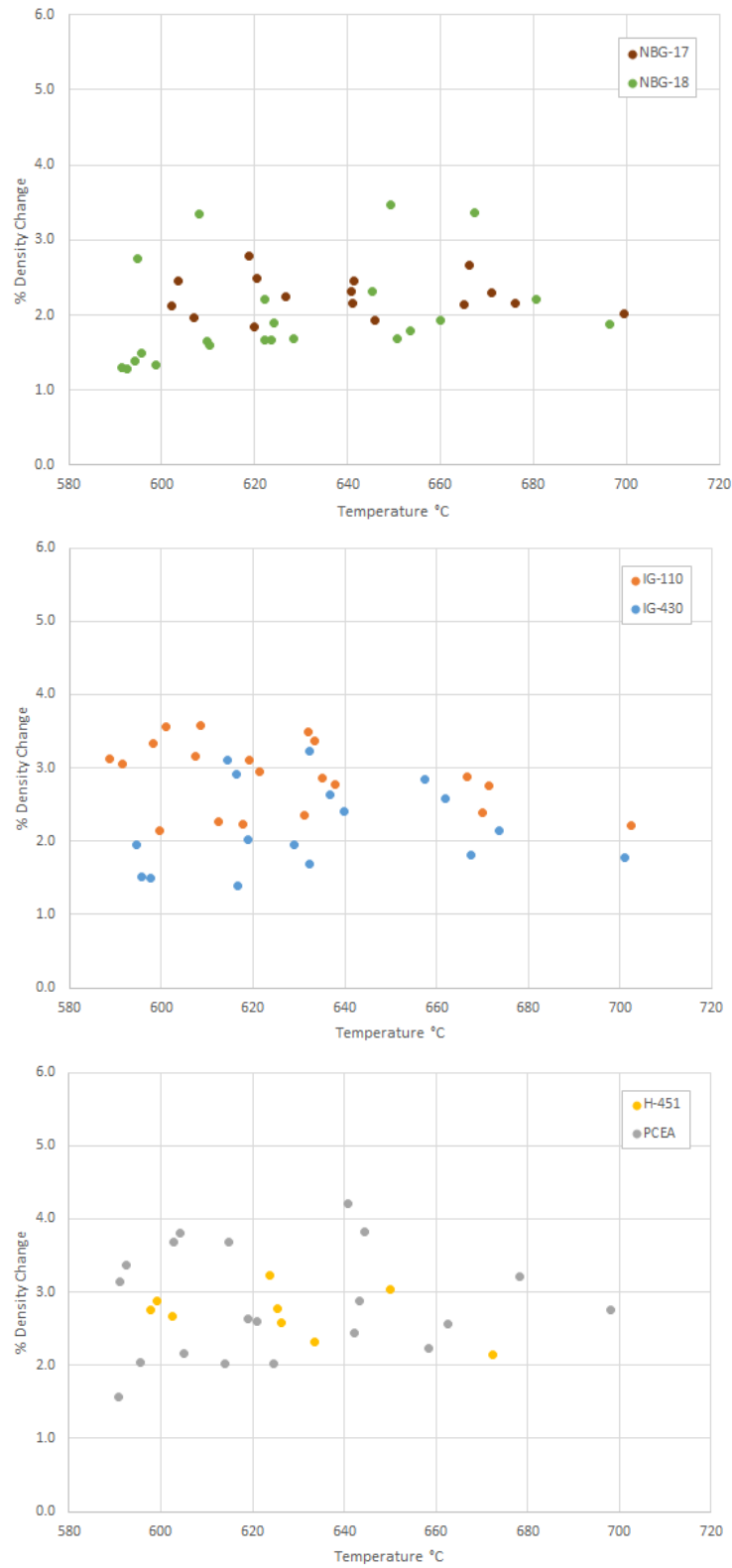


Figure 15. Percent density change in unstressed specimens versus specimen irradiation temperature for a narrow dose range of 4.0 ± 0.5 dpa for different graphite grades.

5.2 Resistivity

Electrical resistivity is used as a rapid, simple means for determining the isotropy or grain orientation of manufactured graphite. Changes in electrical resistivity can be used to ascertain irradiation-induced microstructure and crystallinity changes. When used in conjunction with optical microscopy, it can be used to determine the microstructural texture of graphite components with little sample preparation. Resistivity is measured following ASTM C 611-98 (Reapproved 2010). The measurement technique is commonly referred to as four-point probe. It consists of passing a known current through the sample and measuring voltage across the sample at known locations. Based on Ohms law, the resistance is determined and the resistivity, ρ , is calculated from

$$\rho = R \cdot A / L \quad (3)$$

where:

R = measured resistance

A = cross-sectional area

L = length over which the voltage is measured.

Resistivity measurements were made on the creep and control specimens both before and after irradiation. The overall increase in resistivity was significant for all grades and ranged from 106 to 232% (Figure 16). The average change for all graphite specimens is about 162% (shown as a green line with ± 1 standard deviation shown as red lines). The scatter in data reflects the different variables within the experiment, including irradiation temperature, dose, applied stress, graphite grade, and grain orientation. However, 67% of the data still lie within ± 1 standard deviation.

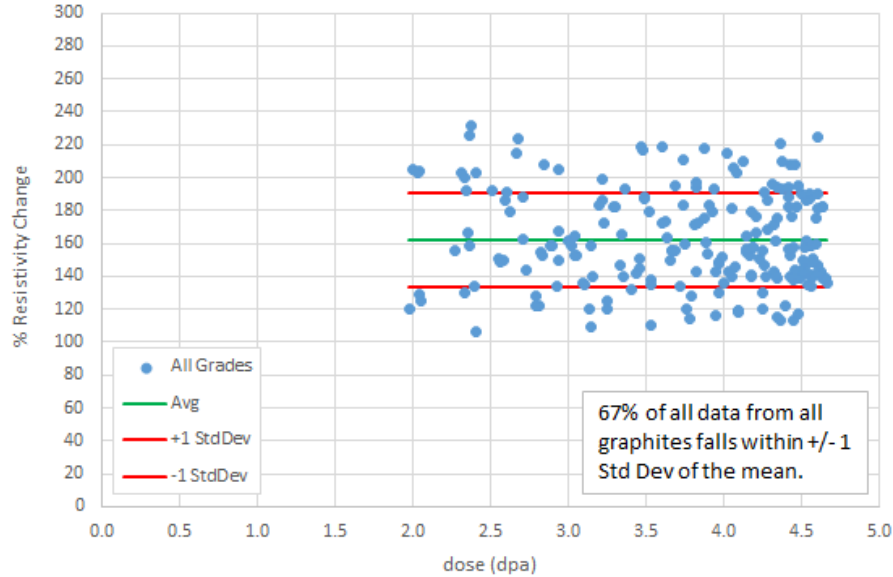


Figure 16. Percent change in resistivity as a function of fast neutron dose for AGC-2 resistivity measurement specimens.

Figure 16 is remarkable in that all specimens, including different grades, different grain sizes, stressed, unstressed, and with different grain orientations, respond so similarly. While the resistivity for all irradiated specimens rises significantly, the increase is accomplished at relatively low dose (less than 2.0 dpa) and the change is generally constant over the entire received dose range of AGC-2 (1.9 to 4.7 dpa). This indicates that electrical resistivity is increased rapidly during initial irradiation

(i.e., less than 2.0 dpa), but once the maximum change has been reached, the resistivity does not continue to change as the dose is increased over the dose range of the AGC-2 capsule (1.9 to 4.7 dpa).

Microstructural factors (such as grain size, pore size, fabrication process) and changes to the pore microstructure appear to have minimal effect on the electrical resistivity response once this maximum change has been achieved at these relatively low dose (less than 2.0 dpa). Past research indicates that the initial change may result from in-crystal reduction due to electron scattering at irradiation induced defects. The later changes expected from structure effects are not observed because of the relatively low dose range.

While there are significant similarities between all tested specimens, there are some differences between the different graphite grades. Figure 17 illustrates the resistivity effects from irradiation only (i.e., no mechanical loaded specimens are considered). Again, all grades exhibit a significant increase in electrical resistivity from irradiation (i.e., percent change in resistivity) by a dose less than 2.0 dpa. However, the extruded grades of H-451 and PCEA show an approximate 200% increase in resistivity, while the iso-molded grade of IG-110 had a lower approximate 125% increase. As noted in Figure 16, it is interesting that all graphite grades have such a significant rise in resistivity for received dose of less than 2.0 dpa, followed by a near constant change in resistivity from a dose of 2.3 to 4.7 dpa. As seen in Figure 17, only a slight general decrease in the resistivity change is shown as a function of increasing irradiation dose for the six major grades of graphite. This general trend is very weak and scatter in the data would indicate that the resistivity change for all grades generally stays constant over the AGC-2 dose range.

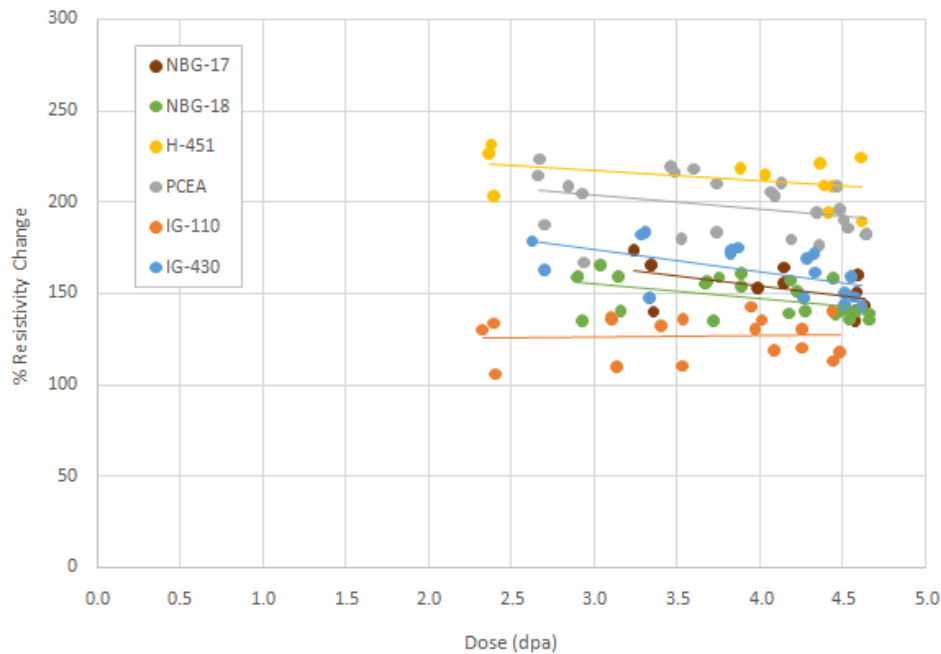


Figure 17. Percent resistivity change versus dose by graphite grade for control specimens.

Figure 18 and Figure 19 investigate the effect of stress on the percent change in resistivity. Figure 18 illustrates the resistivity change for four stress levels experienced by the different graphite grades. The average percent change in resistivity is indicated by the bar length, and error bars represent ± 1 standard deviation. On average, resistivity changes for all graphite grades remained relatively constant across the increasing applied stresses. It appears resistivity changes for unstressed specimens may be slightly higher than stressed specimens for all graphite grades, but the difference is very small. As noted in Figure 17,

extruded creep specimens demonstrate the largest change in resistivity, while the IG-110 specimens exhibits the least change.

Figure 19, like Figure 17, is a plot of percent change in resistivity versus irradiation dose; however, now the control (unstressed) and creep (stressed) specimens are shown separately. Linear regression lines are established through data for each individual grade. As seen, there appears to be minimal difference between creep or control specimens for all graphite grades. Any decrease in resistivity resulting from increasing dose or stress is extremely small and is well within data scatter.

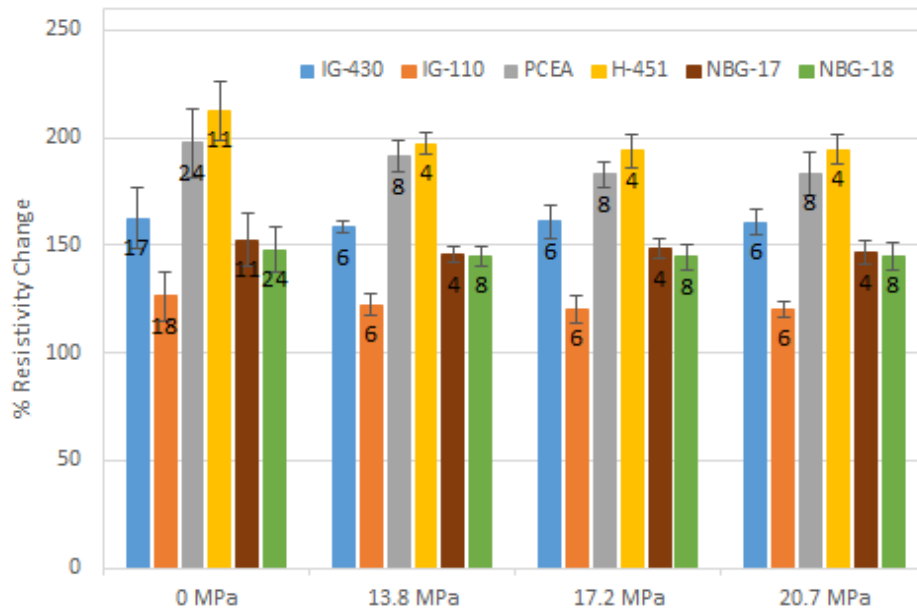


Figure 18. Average percent resistivity change by graphite grade and applied stress. The error bars represent ± 1 standard deviation from the mean and numbers in the bars represent the sample size.

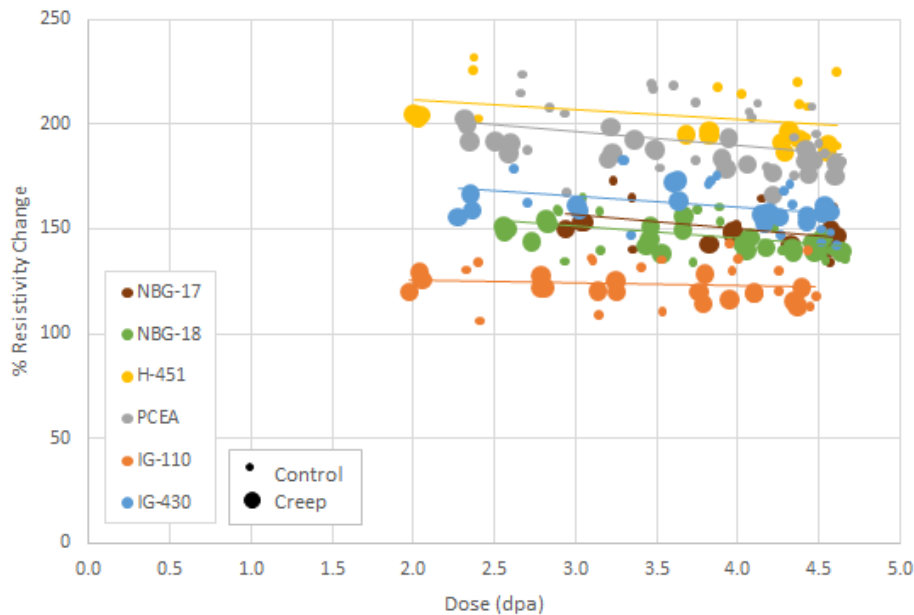


Figure 19. Percent resistivity change versus dose by graphite grade for both control and creep specimens.

Figure 20 adds together the effects of irradiation and applied stress for the three separate forming processes. As noted earlier, the extruded grades have the greatest percent increase in resistivity, while the iso-molded grades have the least. No clear trend in resistivity change exists as the dose increases with the extruded and vibrationally molded grades showing a slight decrease in change, but the iso-molded exhibiting a slight increase in resistivity change. These slight trends are very weak and scatter in the data would indicate the resistivity change for all grades stays generally constant over the AGC-2 dose range. As noted previously in Figure 19, differences between stressed conditions (solid lines) and unstressed conditions (dotted lines) are small; however, the percent change in resistivity of the control (unstressed) specimens is consistently higher for all forming processes.

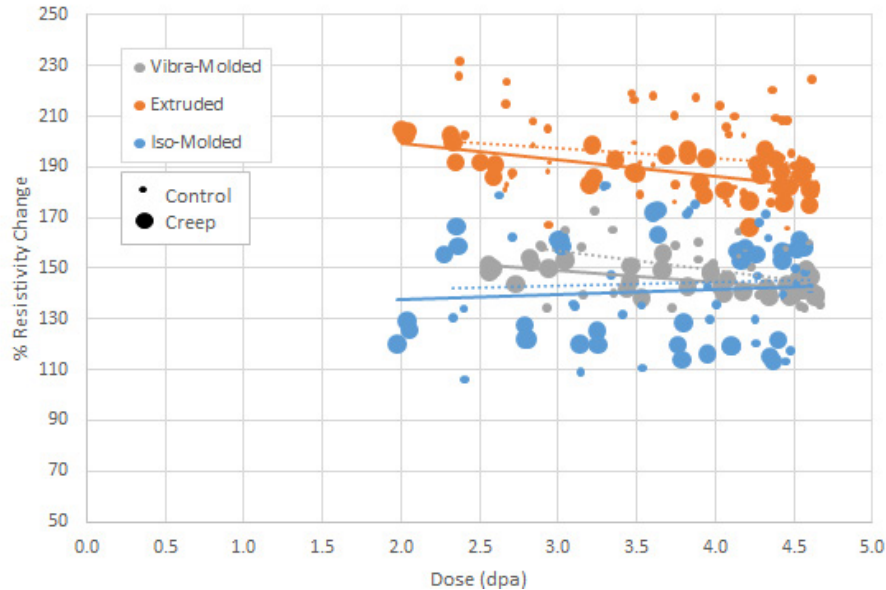


Figure 20. Percent resistivity change versus dose for similar graphite fabrication processes for creep (—) and control (---) specimens. Solid lines represent linear fits of the creep specimens, while the dotted lines represent linear fits of the control specimens.

Figure 21 and Figure 22 investigate the dependence of grain orientation on the resistivity change for the three major graphite grades that have forming processes resulting in distinct grain orientations. Figure 21 examines the effect of grain orientation on electrical resistivity for stressed and unstressed specimens. Minimal differences exist for either orientation or stress on the change in resistivity for the AGC-2 specimens, indicating that irradiation and stress affect electrical resistivity similarly for any specimen orientation. Figure 22 shows percent change in resistivity over the irradiation dose range for the two grain orientations (hollow and solid symbols are representative of against and with-grain, respectively). Similar to the applied stress analysis, grain orientation appears to have no difference in the percent change in resistivity with respect to irradiation dose.

Figure 23 illustrates the effects of specimen density (before irradiation) on the change in electrical resistivity after irradiation. Changes in the density of graphite can significantly affect the material property values in all nuclear graphite grades, with lower density resulting in a reduction in mechanical strength, lower thermal diffusivity, and lower modulus values. As seen in Figure 23, the change in electrical resistivity is shown to be lower for grades with higher pre-irradiation density, with the exception of the IG-110 iso-molded grade. This behavior cannot be directly attributed to only pre-irradiation density because other factors (such as fabrication process, grain size, and coke source) may also contribute.

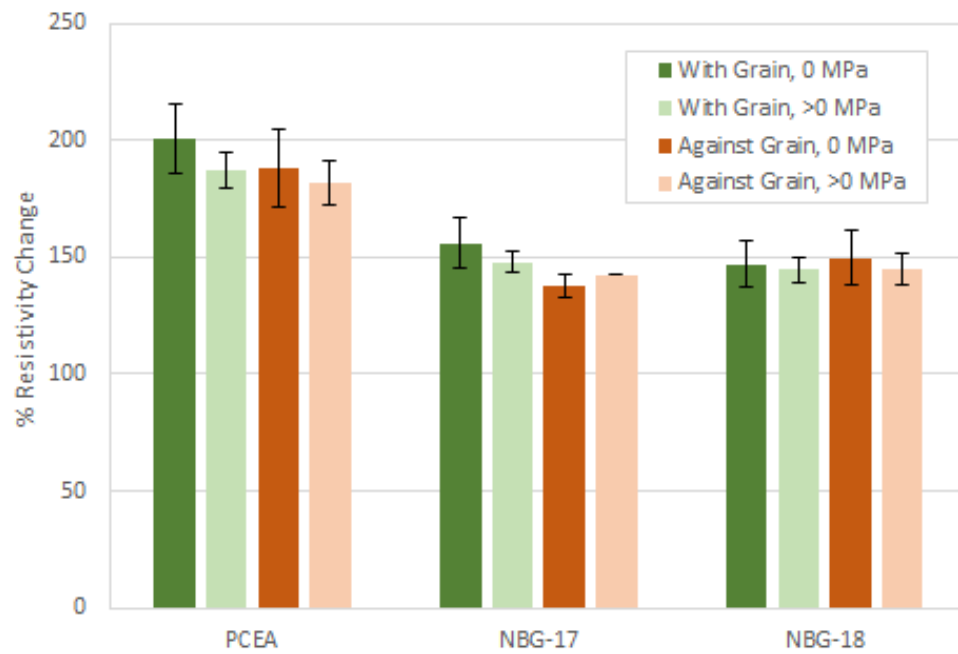


Figure 21. Average percent resistivity change by grain orientation and graphite grade.

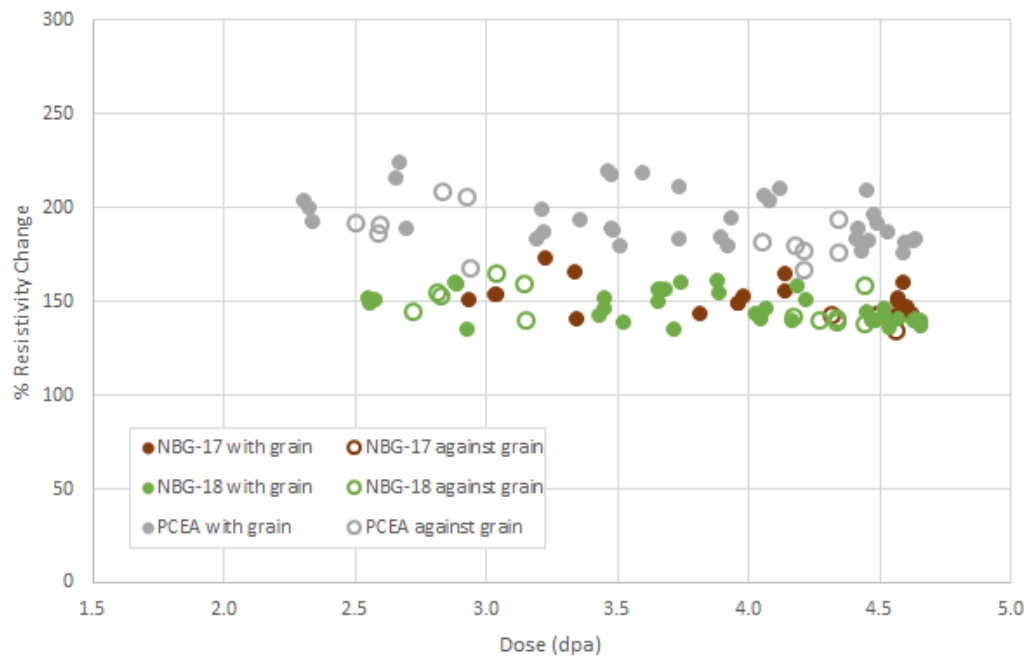


Figure 22. Percent resistivity change versus dose by grade and specimen grain orientation.

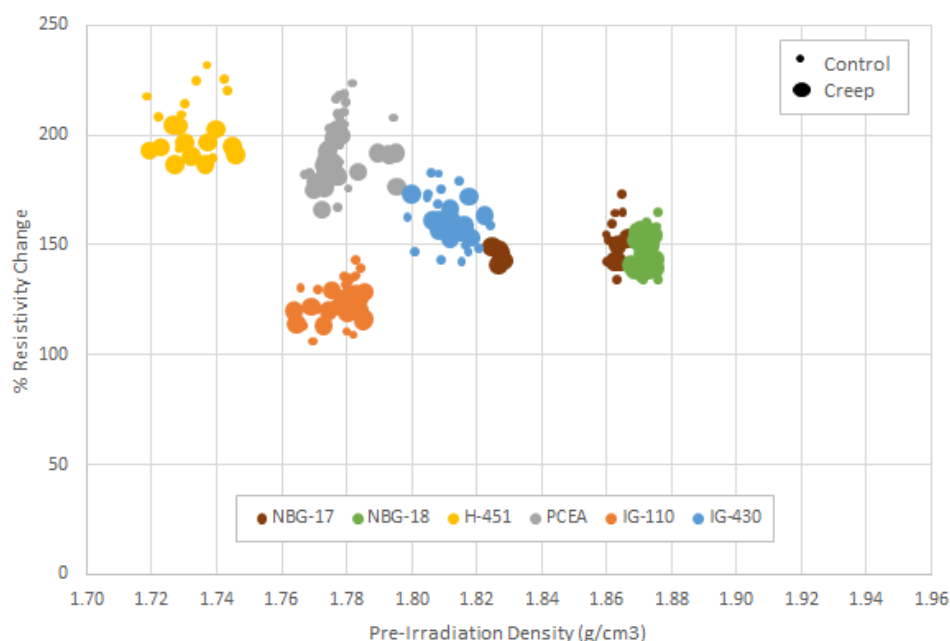


Figure 23. Percent resistivity change post irradiation versus specimen pre-irradiation density for control and creep specimens.

One further observation for density effects is the comparison of lower and higher density specimens of NBG-17 grade. NBG-17 specimens with a lower density than normal were chosen to be irradiated within the AGC-2 capsule under the same conditions as the higher density specimens. This small NBG-17 sampling was intended to observe any possible effects of lower density on material performance under irradiation. As seen in Figure 23, while density for the two sets of NBG-17 specimens varies from 1.82 to 1.87 g/cm³, the observed changes to electrical resistivity are minimal. There appears to be no significant affect for density variations of approximately $\pm 2\%$.

The effect on electrical resistivity from irradiation-induced strain is shown in Figure 24. Data for all grades show a small but consistent trend toward lower percent change in resistivity as the specimens experience negative strain (i.e., shrinkage) in the specimen axial direction. This slight trend was noted in Figure 17 (resistivity change from increasing irradiation dose), but it is somewhat more pronounced in Figure 24, where dimensional change/strain has been applied. As noted previously, the change to resistivity is greatest in the extruded grades and least in the iso-molded grade IG-110.

Finally, in an attempt to discern whether the larger-than-designed specimen temperature range in AGC-2 might affect the electrical resistivity change, data for the three forming processes are plotted in a very narrow dose range (between 3.5 and 4.5 dpa) as a function of the irradiation temperature range (Figure 25). This temperature range is approximately 100°C from 590 to 690°C. Creep and control specimens are depicted by the size of the plotted symbol. It can be seen that for these specific ranges of temperature and dose, the resistivity change is minimal. Because this depicts a relatively narrow temperature range, the fact that there is no trend with temperature is only an indication that the constant percent change in resistivity versus dose (initially shown in Figure 17 for all radiation temperatures) is not a result of the competing effects of dose and temperature. This was expected based upon the previous AGC-1 analysis but is shown here to assure that any temperature affects from the larger-than-designed AGC-2 specimen temperature range do have minimal effect on the electrical resistivity results. It should be noted that there will be an expected change in all material properties for the substantially higher irradiation temperatures anticipated in the later AGC capsules (nominal temperatures of 800 and 1100°C).

As data from the later AGC capsules are gathered, it will be possible to ascertain the role of irradiation temperature on the observed material property changes.

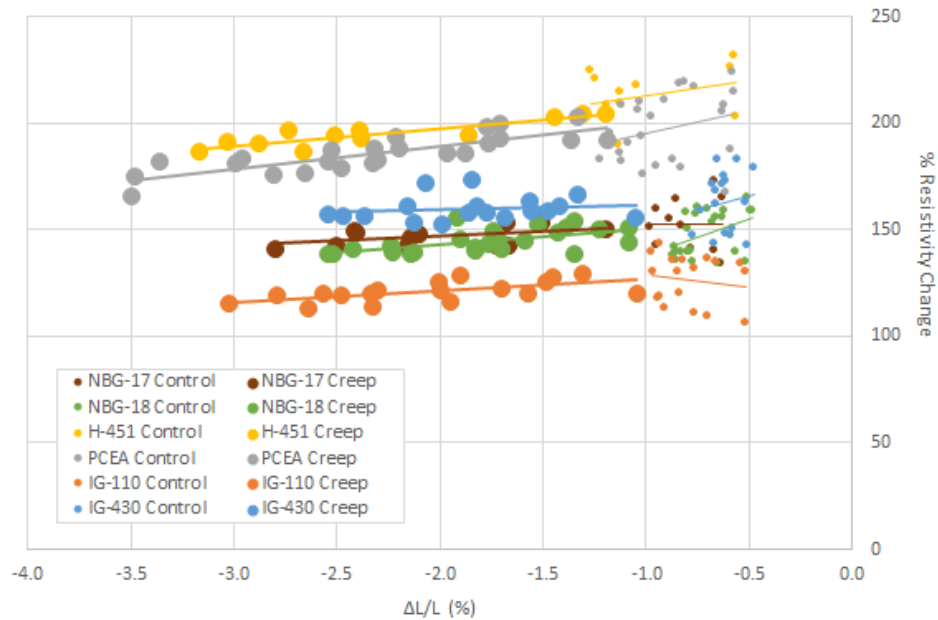


Figure 24. Percent resistivity change versus specimen strain by graphite grade for both control and creep specimens. Note negative strain increases from right to left (from 0.0 to -4.0%)

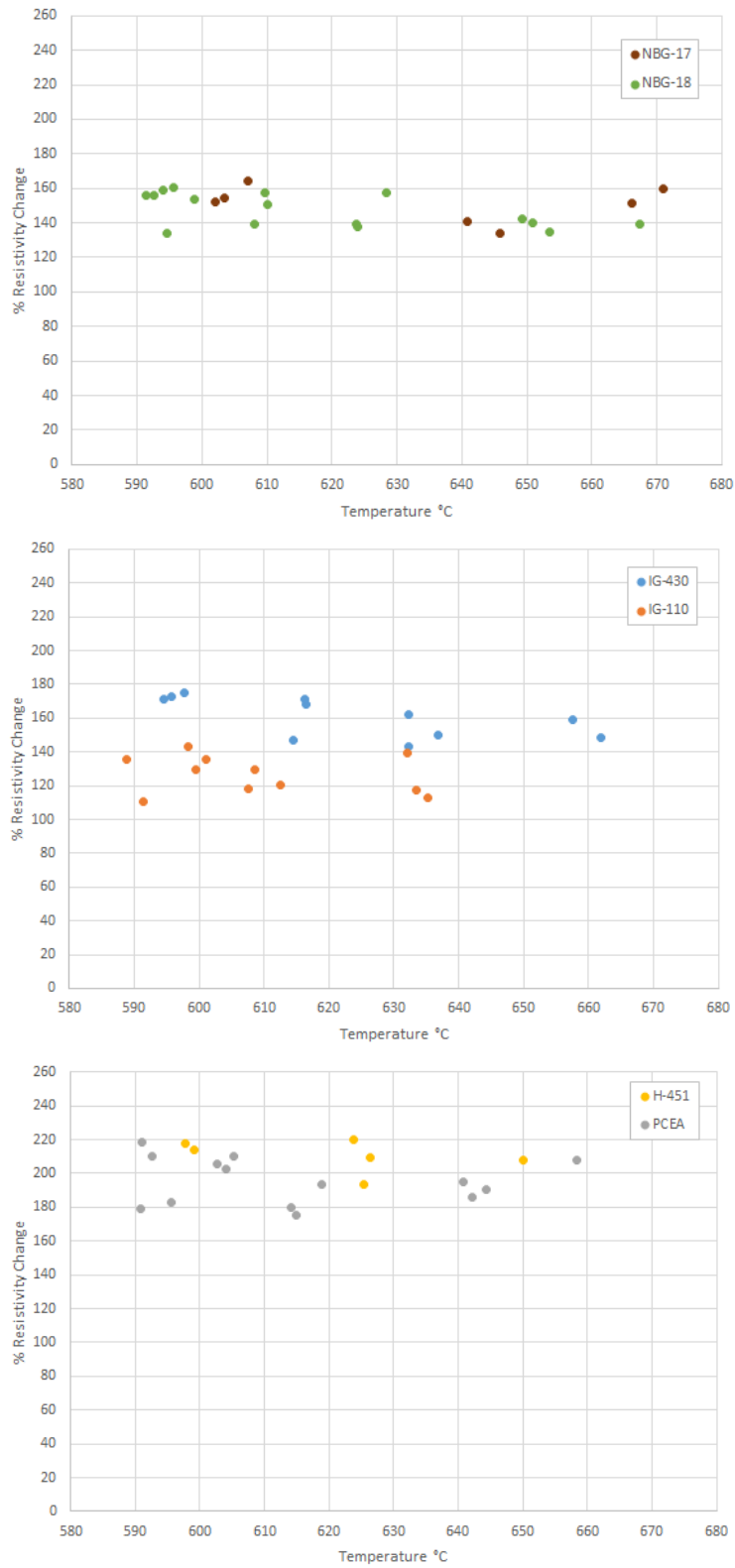


Figure 25. Percent resistivity change versus specimen irradiation temperature for a narrow dose range of 4.0 ± 0.5 dpa for different graphite grades.

5.3 Elastic Modulus by Sonic Velocity Method

A material's elastic moduli are a measure of how compliant (or stiff) the material behaves and is useful for ascertaining a graphite grade's mechanical properties, irradiation creep response, and the structural strength and integrity of graphite components. The measurement of elastic constants by the sonic velocity method is carried out in accordance with ASTM C 769-09. In this measurement, a transmitting piezoelectric transducer sends a sound wave through the sample. At the opposite end of the sample, the acoustic wave is received by another piezoelectric transducer. The sonic velocity of the sound wave through the specimen is the ratio of specimen length to the signal time lapse between transducers. Approximate values for Young's modulus are obtained from the square of the velocity multiplied by the density of the graphite.

$$E = \rho V^2 \quad (4)$$

where:

E = Young's modulus

ρ = specimen density

V = sonic velocity.

Elastic modulus measurements were made on the creep and control specimens both before and after irradiation. The overall increase in Young's modulus for all measured AGC-2 specimens was significant for all grades and ranged from about 38 to 120% (Figure 26). The average change for all graphite specimens is about 72% (shown as a green line with ± 1 standard deviation shown as red lines). Scatter in the data reflects the different variables within the experiment, including irradiation temperature, dose, applied stress, graphite grade, and grain orientation. However, 58% of the data still lie within ± 1 standard deviation.

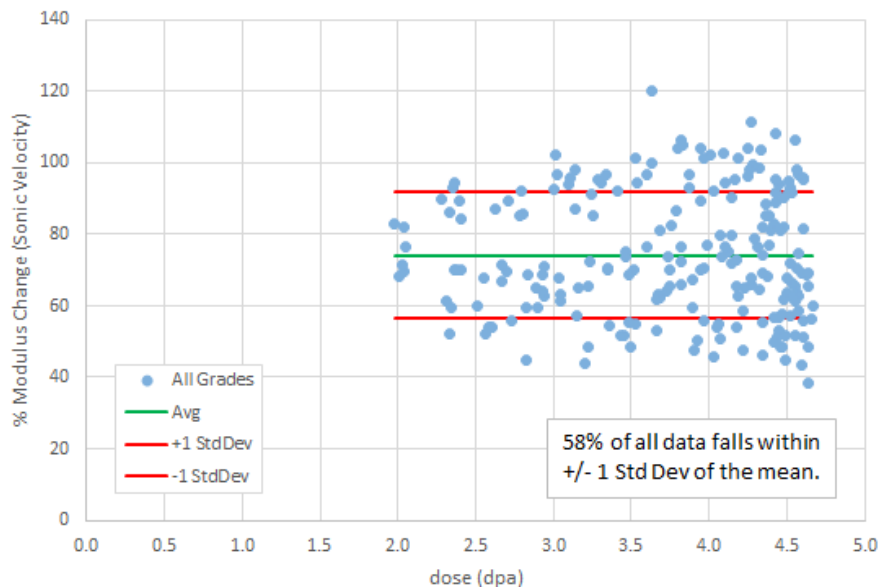


Figure 26. Scatter plot of the percentage of modulus change from all AGC-2 graphite grades, stress conditions, and irradiation temperatures.

Similar to the results for electrical resistivity, Figure 26 demonstrates remarkable similarity in irradiation modulus values for all AGC-2 specimens regardless of nuclear grade, grain size,

stressed/unstressed condition, or grain orientation. Additionally, the initial increase in modulus is significant for all specimens and reaches a maximum at relatively low dose (i.e., less than 2.0 dpa). The change appears to remain generally constant over the entire received dose range of AGC-2 (1.9 to 4.7 dpa), but the scatter is much greater than for electrical resistivity, indicating the modulus may not be as universally constant. Finally, modulus changes from irradiation do not appear to be as sensitive to microstructural factors (such as grain size, pore size, fabrication process, and changes to the pore microstructure) over this relatively small irradiation dose range. Past studies in this area indicate that these changes result primarily from in-crystal defects which in turn impede the flow of dislocations increasing the stiffness modulus. Obviously the dislocation movement is saturated (i.e., constant stiffness) and any changes due to structural evolution have minimal effect over this narrow dose range.

Figure 27 illustrates the irradiation-induced modulus changes between the six major graphite grades from irradiation only (i.e., no mechanical-loaded specimens are considered). A small increase to modulus occurs with increasing dose for the iso-molded grades and the extruded H-451 (note the number of H-451 control specimens is rather small for the dose range of 2.5 to 3.75 dpa). However, the modulus change for extruded PCEA and vibration-molded grades is seen to be generally constant over the entire AGC-2 dose range. It should be noted that the primary difference between these graphite grades besides fabrication processes (if H-451 is ignored for the moment) is grain size and the resulting defect pore structures. The difference between grain and pore size between the different grades is significant (about 15 to 1,600 μm) and could provide some explanation for the differences in behavior. Traditionally, from past studies of irradiated graphite, the irradiated modulus values will initially rise sharply with increasing dose and then level off as turnaround is approached. Once the turnaround dose has been reached, the modulus decreases rapidly with increasing dose. However, none of the AGC-2 specimens reached turnaround dose as demonstrated in the AGC-2 creep analysis report.⁸

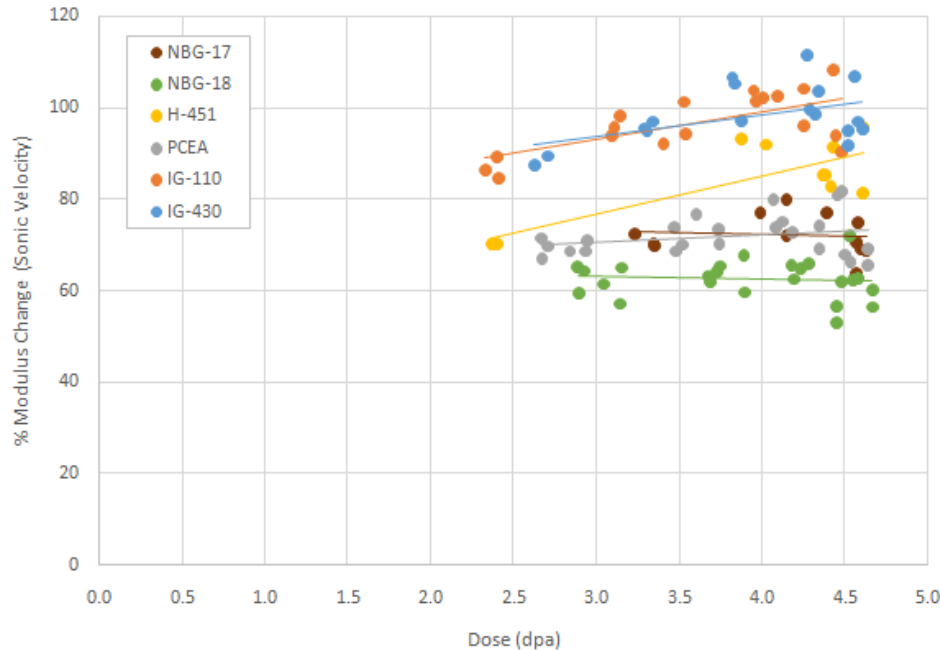


Figure 27. Percent modulus change versus dose by graphite grade for control specimens only.

Figures 28 and 29 investigate the effect of stress on the percent change in resistivity. Changes to the measured modulus resulting from the three applied stress levels are clearly shown in Figure 28. The percent modulus change for all graphite grades gradually decreases as the applied stress (and the resulting

sustained creep strain) is increased. The stressed specimens exhibiting larger plastic strain are shown to experience less change in modulus than the unstressed control specimens exhibiting smaller plastic strain. This implies that the modulus changes can be affected by a change in microstructure (i.e., pore, grain, and connected cracks). The iso-molded grades appear to experience the smallest decrease, while the extruded grades exhibit the largest. The average percent change in stiffness modulus is indicated by the bar length and the error bars represent ± 1 standard deviation.

Figure 27 and Figure 29 are plots of percent change in modulus versus irradiation dose; however, Figure 27 shows the control (unstressed) and creep (stressed) specimens separately. Linear regression lines are established through the data for each individual grade. Similar to Figure 27, the modulus percentage change for both iso-molded grades are seen to increase with increasing dose while the extruded PCEA and vibration-molded grades show a generally constant change in modulus. With the larger H-451 sample population of both creep and control specimens measured, the H-451 trend is still rising but much less rapidly. The change in stiffness remains significantly greater for the iso-molded grades than the vibration-molded grades and extruded PCEA for all stress levels.

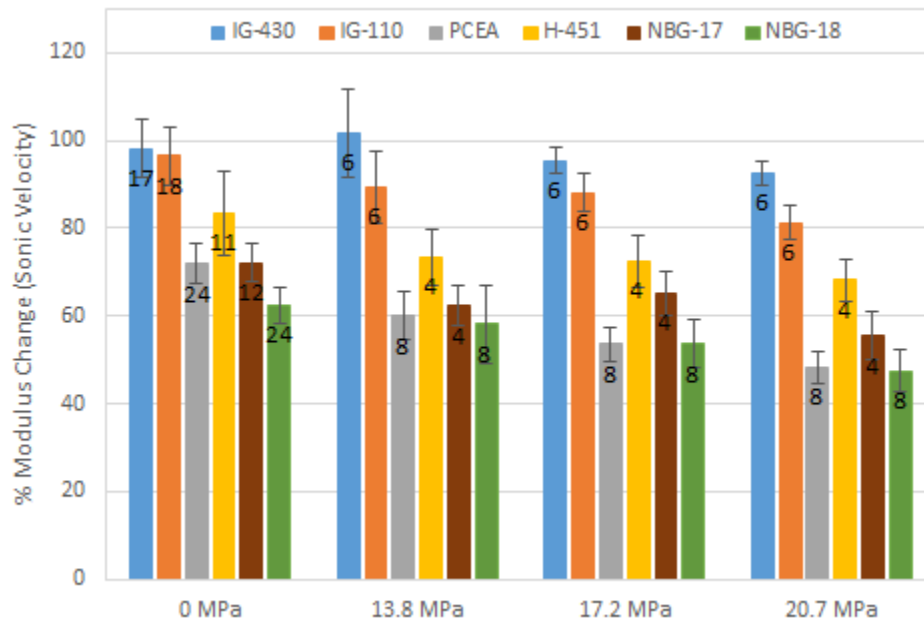


Figure 28. Average percent modulus change by graphite grade and applied stress. The error bars represent ± 1 standard deviation from the mean and the numbers in the bars represent the sample size.

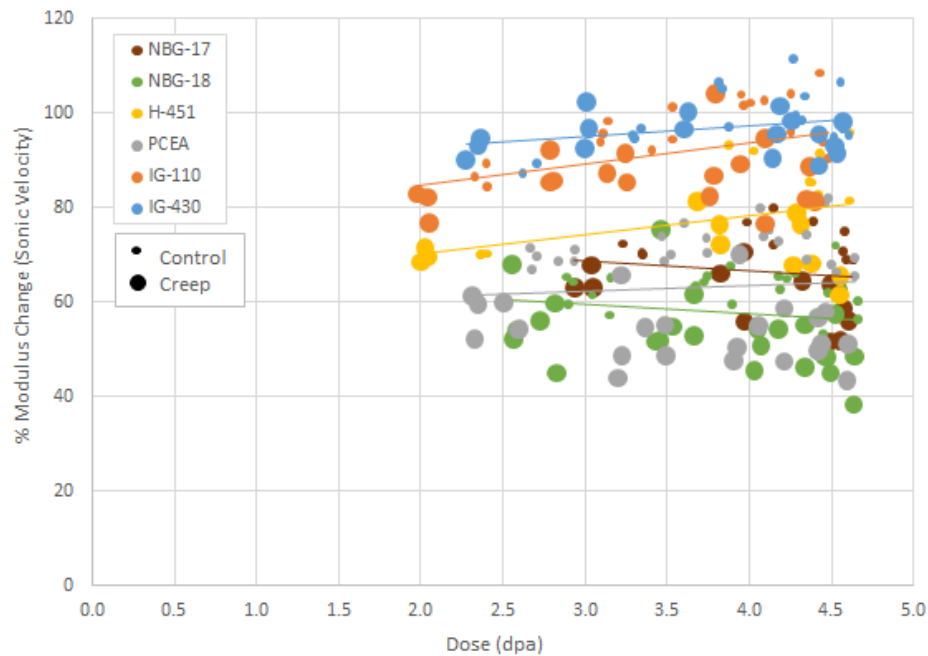


Figure 29. Percent modulus change versus dose by graphite grade for control and creep specimens.

Figure 30 represents the combination of irradiation and applied stress effects for three separate forming processes. As noted earlier, iso-molded graphite exhibits the greatest percent change in modulus and the vibra-molded graphite shows the least change. The control specimens (dashed line) exhibit greater increases in modulus change, while the creep specimens (solid line) are generally lower (as noted previously). However, it is interesting to note that modulus changes increase much less for the creep (stressed) specimens than what is observed in the control (unstressed) specimens. Increases for the iso-molded grade creep specimens show a lower increase, while the vibra-molded grades demonstrate an actual reduction in percent change in modulus as the dose increases.

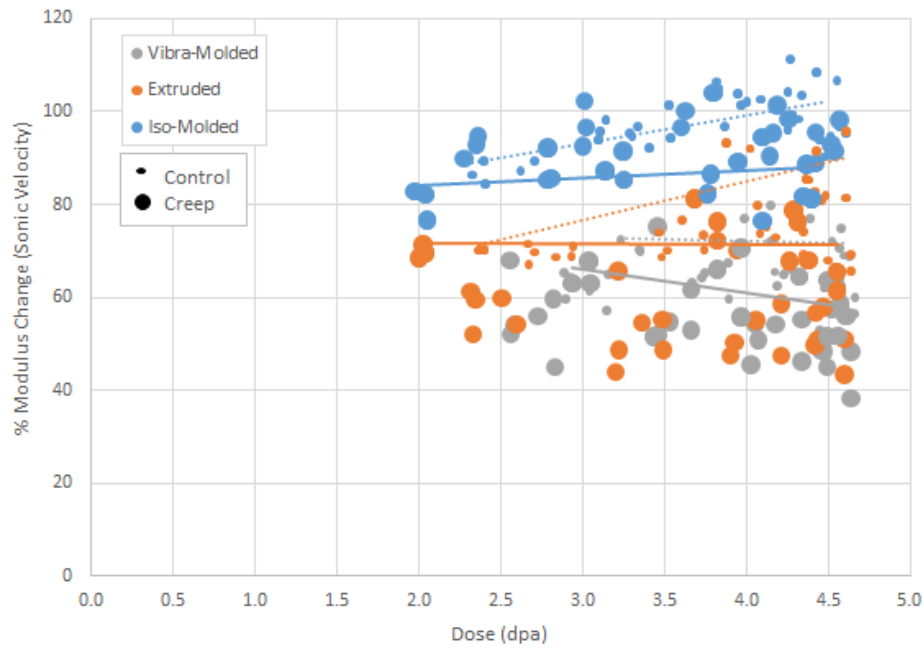


Figure 30. Percent modulus change versus dose by fabrication process for creep (—) and control (---) specimens.

Figure 31 and Figure 32 investigate the dependence of grain orientation on the change in modulus for the three major graphite grades that have forming processes which result in distinct grain orientations. Figure 31 examines the effect of grain orientation on the change in modulus for stressed and unstressed specimens (error bars represent ± 1 standard deviation in the data). While no significant change in modulus was observed between the two grain orientations for all grades in the unstressed specimens, there was a definitive reduction when stress is applied, as noted previously.

Figure 32 shows the percent change in modulus over the irradiation dose range for the two grain orientations (hollow and solid symbols are representative of against and with-grain, respectively). Similar to the applied stress analysis, grain orientation appears to have no difference in the percent change in modulus with respect to irradiation dose. No differences in percent modulus change are observed for grain orientation as a function of irradiation dose.

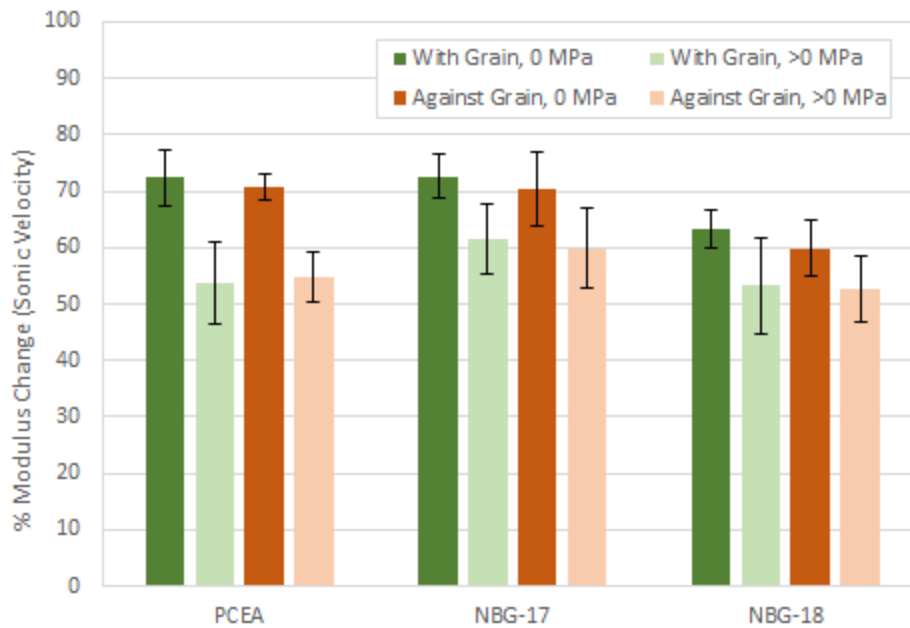


Figure 31. Average percent modulus change by grain orientation and graphite grade.

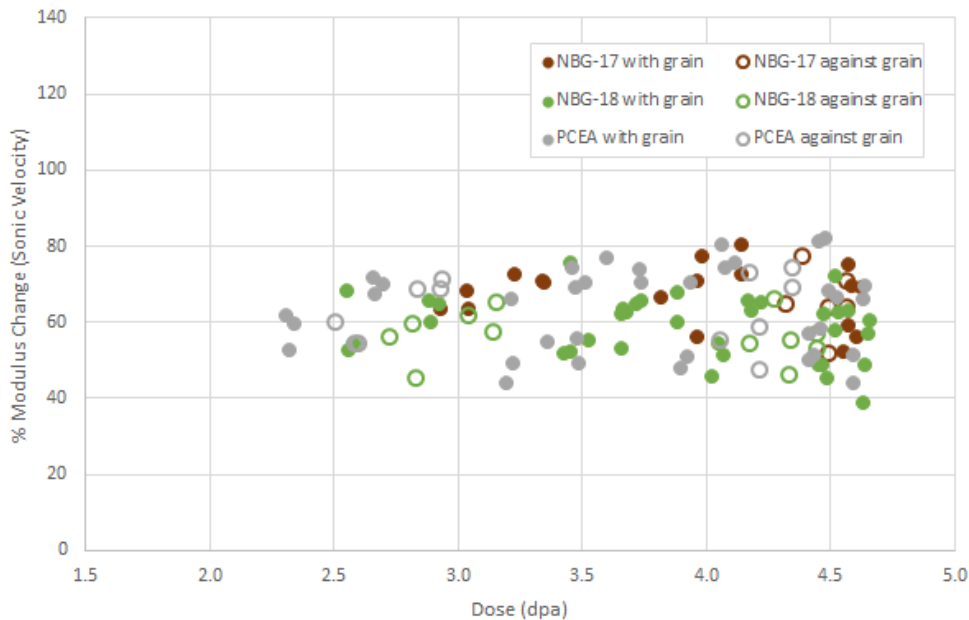


Figure 32. Percent modulus change versus dose by graphite grade and specimen grain orientation.

Figure 33 illustrates the effects of specimen density (before irradiation) on the change in Young's modulus. As noted previously, density has a large effect on material property values; density-related differences may be exacerbated under irradiation. However, the data in Figure 33 show no obvious changes to the irradiation modulus percentage change as a function of density changes, even for the NBG-17 specimens for which data was gathered for two density ranges having a 2% density variation between specimens. The effects of loading (increased strain) does show a reduction in the modulus change as easily seen.

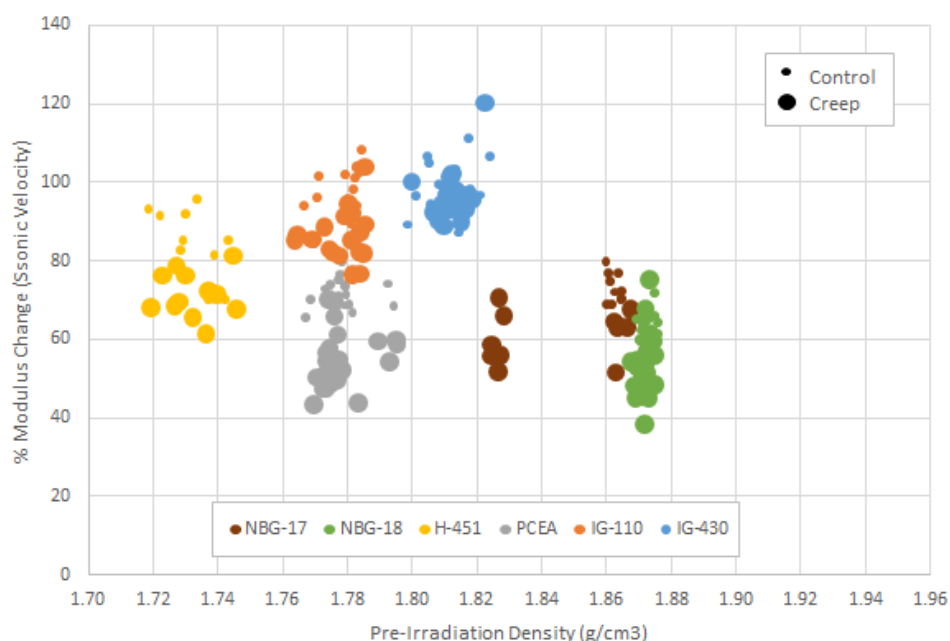


Figure 33. Percent modulus change versus specimen pre-irradiation density by graphite grade for control and creep specimens.

The affect from irradiation-induced strain on elastic modulus change is shown in Figure 34. Data are presented as the change in Young's modulus due to increasing strain experienced in the specimen axial direction as analyzed in the AGC-2 creep analysis report.⁸ Data are separated into control and creep specimens of the major grades of graphite, including all irradiation temperatures and received dose. As demonstrated previously, while all specimens (i.e., creep and control) experienced similar neutron irradiation doses and temperatures the stressed creep specimens showed much larger strains due to the added mechanical stresses. With this understanding, Figure 34 illustrates two trends of interest: (1) the unstressed control specimens for all grades show increasing modulus change and (2) the stressed creep specimens for all grades demonstrate a slight decrease in modulus change with increasing dose.

The fact that these two trends are in opposite directions is an indication of competing processes. As discussed previously, the rapid (and large) initial increase in modulus change is most likely due to neutron damage in the graphite crystal structure, leading to dislocation pinning that will result in a less compliant and stiffer graphite. For the unstressed control specimens, this change to the modulus continues for all graphite grades. However, for the stressed creep specimens, the change is reversed and the modulus begins to demonstrate increased compliance as the strain (and applied stress) is increased. This difference in behavior is most easily seen for those creep and control specimens that experienced similar strain levels. Consistently, unstressed control specimens for all grades demonstrate larger modulus change than the stressed creep specimens for similar strain levels. This implies that a microstructural change resulting from the increased strain on the material (i.e., irradiation creep strain) is competing with irradiation damage, which tends to increase the stiffness of graphite. These microstructural changes in the creep specimens may include increased microcracking from the large applied mechanical stresses, pore/grain structure realignment, or pore closure. Further fundamental studies will be necessary to assist in interpretation of these data trends.

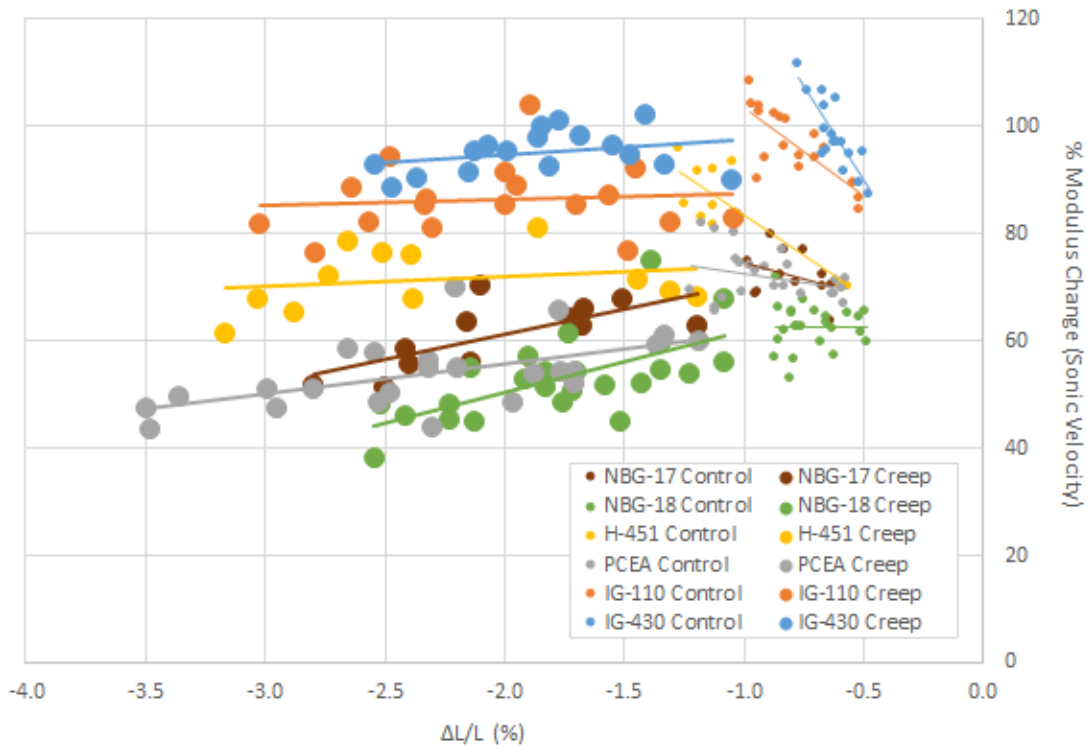


Figure 34. Percent modulus change versus specimen strain by graphite grade for control and creep specimens. Note negative strain increases from right to left (from 0.0 to -4.0%)

Finally, Figure 35 is intended to determine the influence that irradiation temperature may have on the change in Young's modulus for these AGC-2 specimens. Percent change in Young's modulus data that falls in a narrow dose range of 3.5 to 4.5 dpa is plotted as a function of irradiation temperature. Similar to a previous analysis, this temperature range is about 100°C, from 590 to 690°C. Graphite grades are separated into the three forming processes to aid in clarity, while creep and control specimens are depicted by the size of the plotted symbol.

As seen in Figure 35, data in this narrow range show no obvious trend in the modulus change as the irradiation temperature is increased. This indicates that there is no obvious effect from the larger-than-designed irradiation temperature range within the AGC-2 capsule for elastic modulus. As data from future high-irradiation AGC capsules are gathered (800 and 1,100°C), it will be possible to calculate the true role of irradiation temperature versus irradiation dose over much broader ranges.

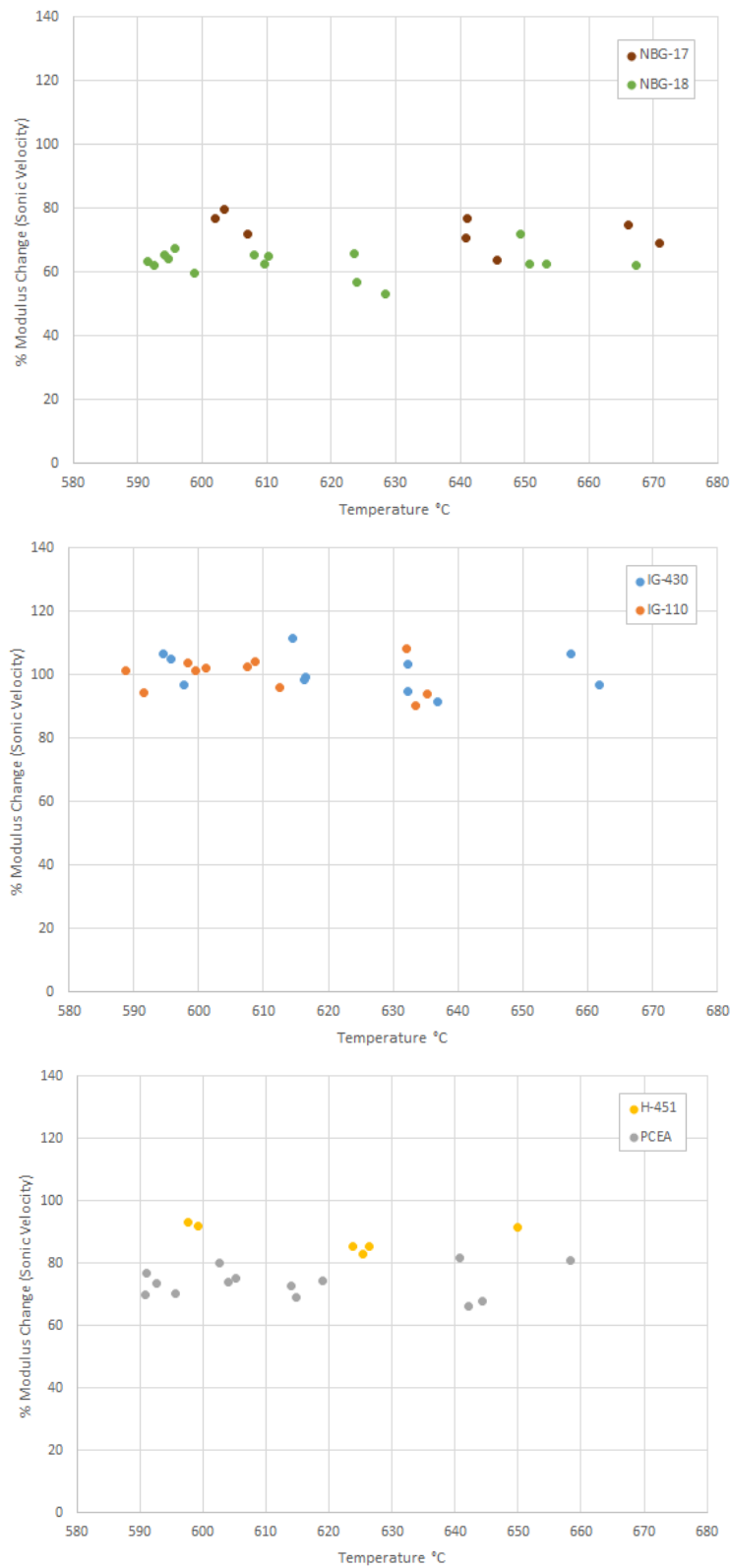


Figure 35. Percent change in Young's modulus versus specimen irradiation temperature for a narrow dose range of 4.0 ± 0.5 dpa for different graphite grades.

5.4 Elastic Modulus by Sonic Resonance Method

Measurements of Young's elastic modulus were also made from a different testing methodology (i.e., the sonic resonance method). This test method measures the fundamental resonant frequency of test specimens of suitable geometry by exciting them mechanically with a singular elastic strike. Specimen supports, impulse locations, and signal pick-up points are selected to induce and measure specific modes of the transient specimen vibration. The transient signals are analyzed and the fundamental resonant frequency is isolated by a signal analyzer. Measured fundamental resonant frequency, specimen dimensions, and mass are used to calculate Young's modulus in accordance with ASTM C747-93 (Reapproved 2010). For the fundamental flexural frequency of a rod of circular cross section

$$E = 1.6067 \left(\frac{L^3}{D^4} \right) (mf_f^2) T'_1 \quad (5)$$

where:

E = Young's modulus, Pa

m = mass of the bar, g

L = length of the bar, mm

μ = Poisson's Ratio,

f_f = fundamental resonant frequency of bar in flexure, Hz

D = diameter of rod, mm

T'_1 = correction factor for fundamental flexural mode to account for finite thickness of bar, Poisson's ratio, etc.

Similar to elastic modulus measurements made from the sonic velocity technique, measurements were made on creep and control specimens both before and after irradiation. The percent change of the calculated elastic modulus and analysis were, unsurprisingly, very similar to the results of the modulus measurements made with the sonic velocity technique. Irradiated Young's modulus data by resonance method show nearly identical results to those determined from sonic velocity testing: (1) a significant increase for all specimens at relatively low dose (less than 2.0 dpa), (2) an average percent change increase of 79% (green line) with a range of about 40 to 105% increase, and (3) and no apparent increase or decrease over the dose range of the AGC-2 capsule (Figure 36). Approximately, 77% of the data lie within ± 1 standard deviation (shown as red lines) of the data scatter; again this results from differences in irradiation temperature, dose, applied stress, graphite grade, and grain orientation. The two outliers in the plot are AG PCEA specimens. During testing, it was noted that the PCEA AG specimens were particularly difficult to obtain consistent fundamental frequency values.

As expected, the elastic modulus results from sonic resonance and sonic velocity are extremely similar. Because of these similarities, the analysis and conclusions are the same, and no further analysis for the sonic resonance results will be presented in the main report. Specific data results of the sonic resonance data may be found in Appendix A for further analysis.

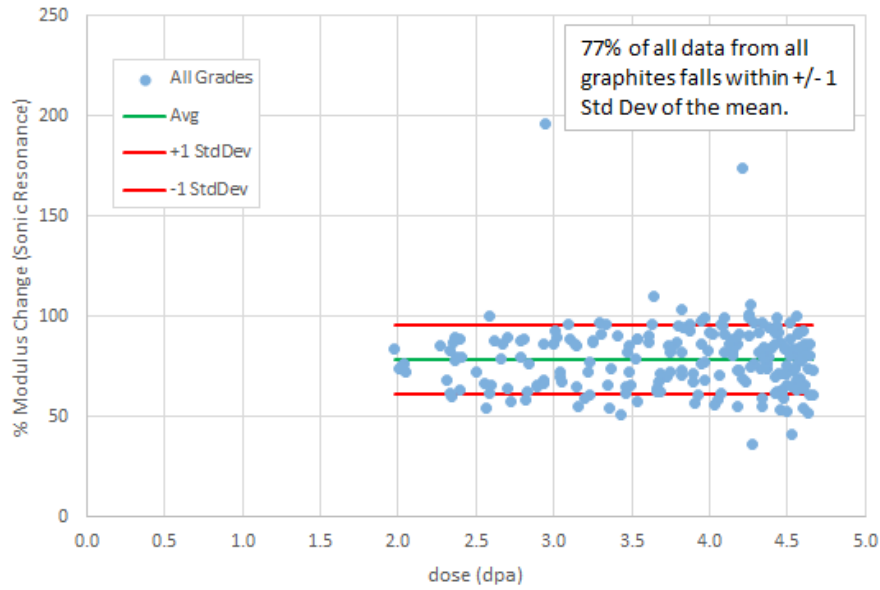


Figure 36. Scatter plot of the percentage of modulus change from all graphite grades, irradiation temperatures, and stresses.

5.5 Shear Modulus

A material's shear modulus (i.e., modulus of rigidity) is a measure of how compliant (or stiff) the material behaves when shearing or torsion forces are applied. Shear modulus is part of a material's elastic response and has similar uses to the Young's elastic modulus. The determination of shear modulus using the sonic velocity method was also carried out in accordance with ASTM C 769-09. Much like determining Young's modulus, a transmitting piezoelectric transducer sends a transverse shear wave through the sample. At the opposite end of the sample, the wave is received by a second piezoelectric transducer. The sonic velocity of the shear wave through the specimen is the ratio of specimen length to the signal time lapse between transducers. Approximate values of the shear modulus are obtained from the square of the velocity multiplied by the density of the graphite.

$$G = \rho V^2 \quad (6)$$

where:

G = shear modulus

ρ = specimen density

V = sonic velocity.

Elastic shear modulus measurements were made on the creep and control specimens both before and after irradiation. Shear modulus percent changes were extensive, averaging a 73% increase for all grades (green line) and ranging from 28 to 108% with the ± 1 standard deviation shown as red lines (Figure 37). The scatter in data is not as broad as Young's modulus measurements using the same ASTM method (see Section 5.3). These shear data cover all irradiation temperatures between 425 and 710°C for all grades, all stress levels, and all grain orientations.

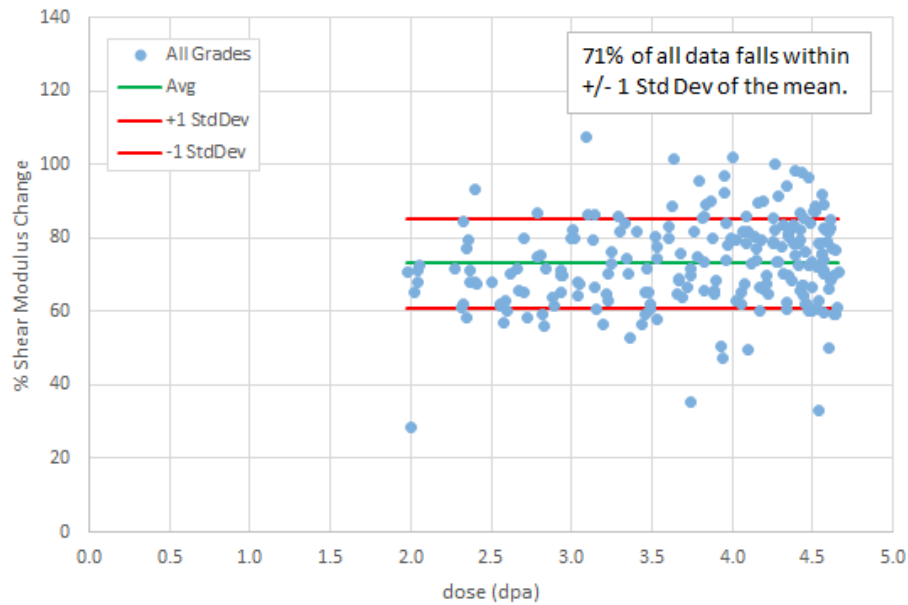


Figure 37. Scatter plot of the percentage of shear modulus change from all graphite grades.

Similar to the results for Young's modulus shown previously, Figure 37 demonstrates remarkable similarity in irradiation modulus values for all AGC-2 specimens, regardless of nuclear grade, grain size, stressed/unstressed condition, or grain orientation. As before, the initial increase in modulus is significant for all specimens and reaches a maximum at relatively low dose (i.e., less than 2.0 dpa). The change appears to remain generally constant over the entire received dose range of AGC-2 (1.9 to 4.7 dpa); however, the scatter is much less than found for Young's modulus values for either sonic velocity or fundamental frequency testing methods. Thus, shear modulus changes from irradiation do not appear to be as sensitive to microstructural factors (such as grain size, pore size, fabrication process, or changes to the pore microstructure) over this relatively short irradiation dose range.

Figure 38 illustrates the irradiation-induced shear modulus changes between the six major graphite grades from irradiation only (no mechanical-loaded specimens are considered). In general, no significant change was observed to the shear modulus percentage change with increasing dose for all graphite grades. There may be a slight increase as the dose increases, but any difference is well within the data scatter for each grade. As seen, IG-110 exhibits the largest shear modulus change (i.e., approximately 80 to 90% increase), while the NBG-18 grade exhibits the smallest change (i.e., approximately 60 to 70%), over the relatively small dose range experienced by the AGC-2 capsule.

The next two figures investigate the effect of stress on the percent change in modulus. Changes to measured shear modulus that result from the three applied stress levels are clearly shown in Figure 39. Error bars represent ± 1 standard deviation from the mean, and numbers in the bars represent sample size. The size of the standard deviation and small differences in averages combine to make it difficult to identify any clear trend in the percent change in shear modulus with the level of stress. However, it does appear that the shear modulus change for creep specimens is slightly less than the control specimens, implying a very weak effect from applied stress.

Figure 40 (similar to Figure 38) is a plot of percent change in modulus versus irradiation dose; however, the control (unstressed) and creep (stressed) specimens are now shown separately. Linear regression lines are established through the data for each individual grade. Similar to Figure 38, there is no strong correlation of shear modulus change to received dose for either creep or control specimens.

While the slight increase in shear modulus change as dose increases appears stronger when stressed specimens are included, any change is still well within the scatter of the complete data set for each graphite grade. Any difference would be expected to be small. It should be noted that this stress effect is much smaller for the shear modulus than what was found for the Young's modulus. Any change in shear modulus appears to be similar for all graphite grades.

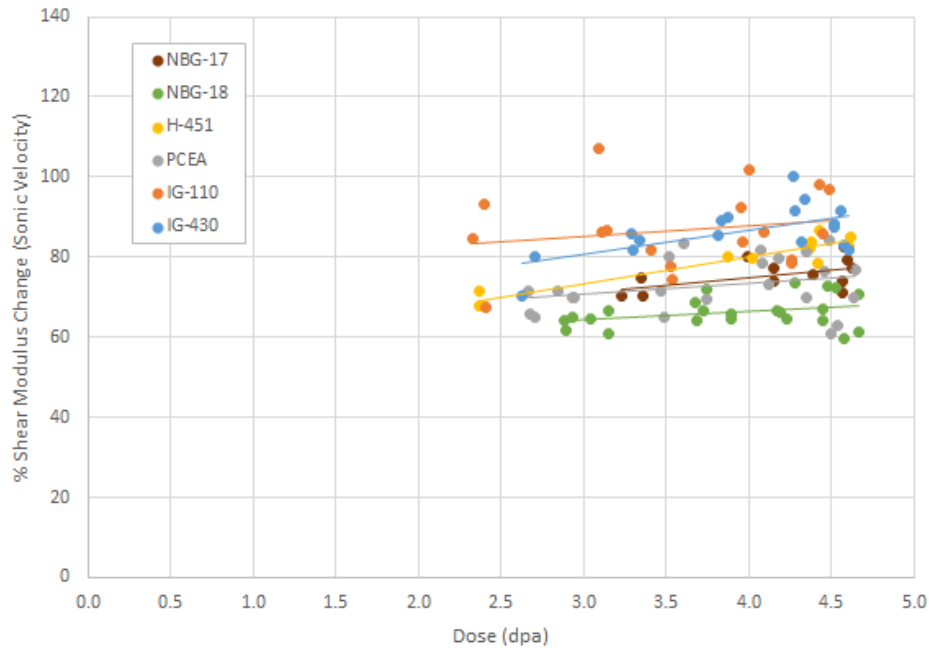


Figure 38. Percent shear modulus change versus dose by graphite grade for control specimens only.

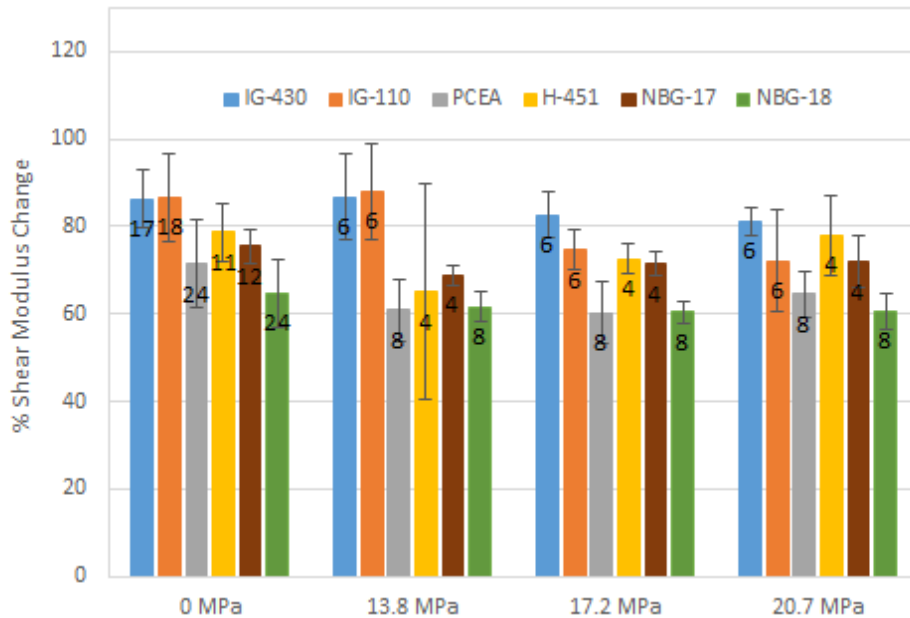


Figure 39. Average percent shear modulus change by graphite grade and applied load. The error bars represent ± 1 standard deviation from the mean and numbers in the bars represent sample size.

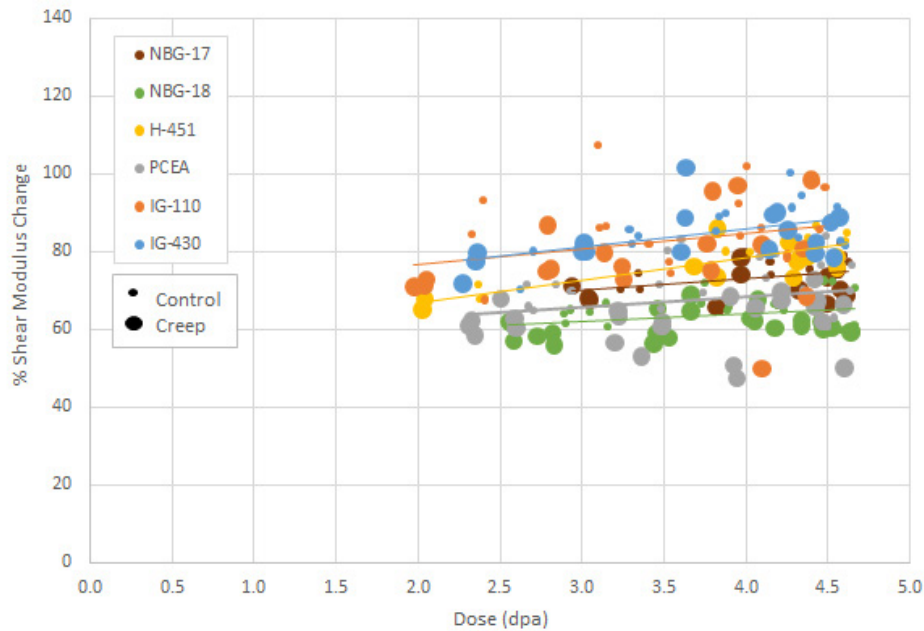


Figure 40. Percent shear modulus change versus dose by graphite grade for control and creep specimens.

Figure 41 combines the effects of irradiation and applied stress together for the three separate forming processes. The percent change in shear modulus shows the percentage modulus change for both stressed creep (—) and unstressed control and piggyback (···) specimens over the entire AGC-2 irradiation dose range. Figure 41 appears to show a slightly stronger trend for increased shear modulus change with increasing dose when both creep and control specimens are considered. However, the trends are still well within the scatter for all data sets, implying a weak relationship that most likely results from the weak applied stress effects noted in Figure 40. Similar to what has been observed previously, the iso-molded graphite experiences the largest percent change in shear modulus, and the vibra-molded and extruded graphite grades experience less change.

Figure 42 and Figure 43 investigate the dependence of grain orientation on the change in shear modulus for three major graphite grades that have forming processes that result in distinct grain orientations. Figure 42 examines the effect of grain orientation on the percentage change in shear modulus for stressed and unstressed specimens (error bars represent ± 1 standard deviation in the data). The percent change in shear modulus is nearly equal for the two grain orientations for all grades and average stress conditions. Figure 43 also demonstrates no significant difference in percent shear modulus change from grain orientation as a function of irradiation dose.

Figure 44 illustrates the effects of specimen density (before irradiation) on the change in shear modulus. As noted previously, density has a large effect on material property values, and density-related differences may be exacerbated under irradiation. However, data in Figure 44 show no obvious changes to the irradiation shear modulus percentage change as a function of density changes even for the NRG-17 specimens for which data were gathered for two density ranges (a 2% density variation between specimens).

The effect of irradiation-induced strain on elastic shear modulus is shown in Figure 45. This figure shows the changes in shear modulus as a function of strain in the specimen axial direction. The data are presented as the change in shear modulus as a function of increasing strain experienced in the specimen axial direction as analyzed in the AGC-2 creep analysis report.⁸ Data are separated into control and creep

specimens of the major grades of graphite, including all irradiation temperatures and received dose. While the trends are not quite as strong as demonstrated for the Young's modulus data, the percent change in shear modulus follows the same pattern of competing effects as seen for Young's modulus changes: (1) the unstressed control specimens for all grades show increasing shear modulus change, and (2) the stressed creep specimens for all grades demonstrate little to no change to irradiated shear modulus values with increasing dose.

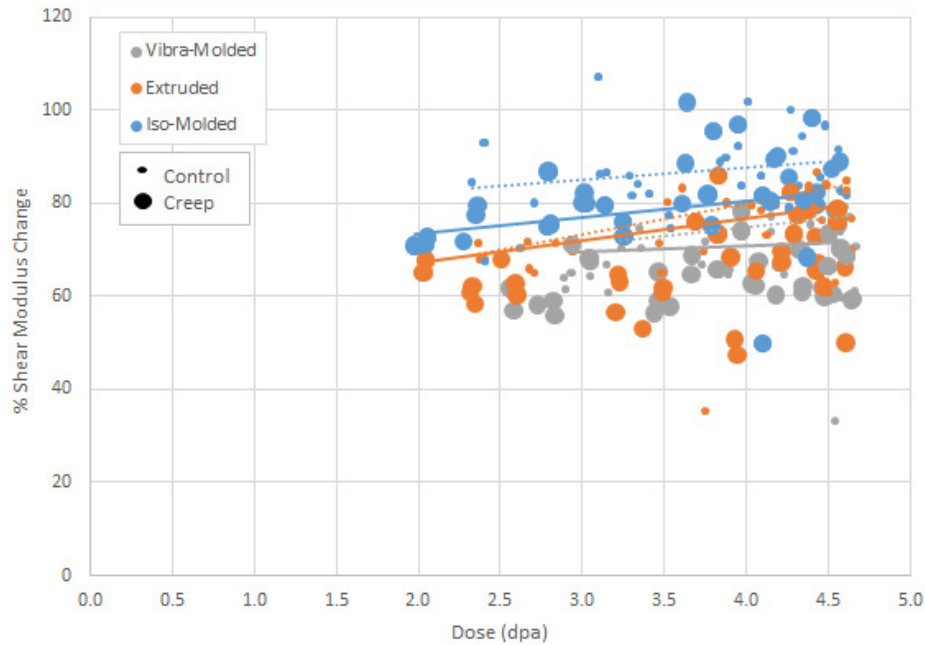


Figure 41. Percent shear modulus change versus dose by graphite fabrication process for control and creep specimens.

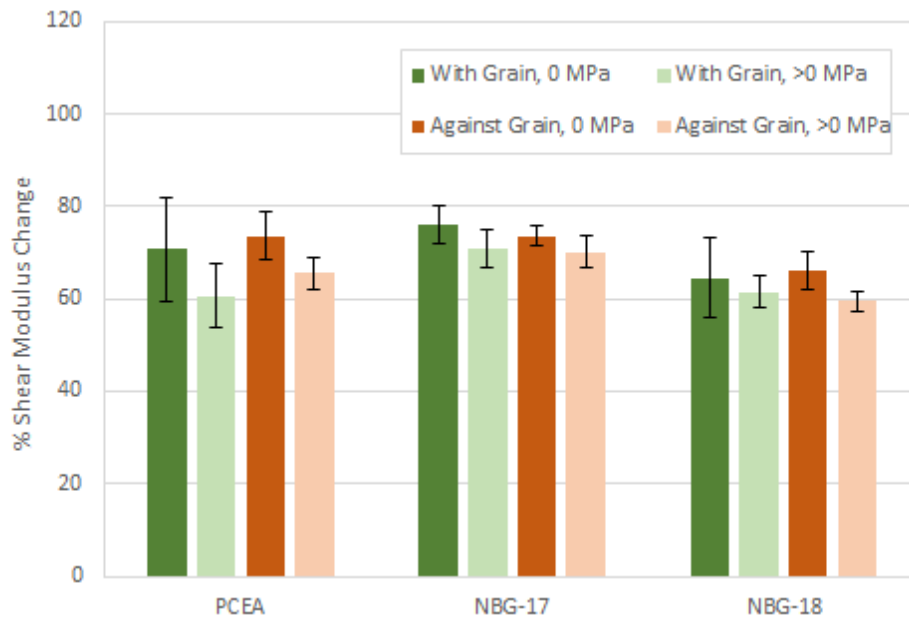


Figure 42. Average percent shear modulus change by grain orientation and graphite grade.

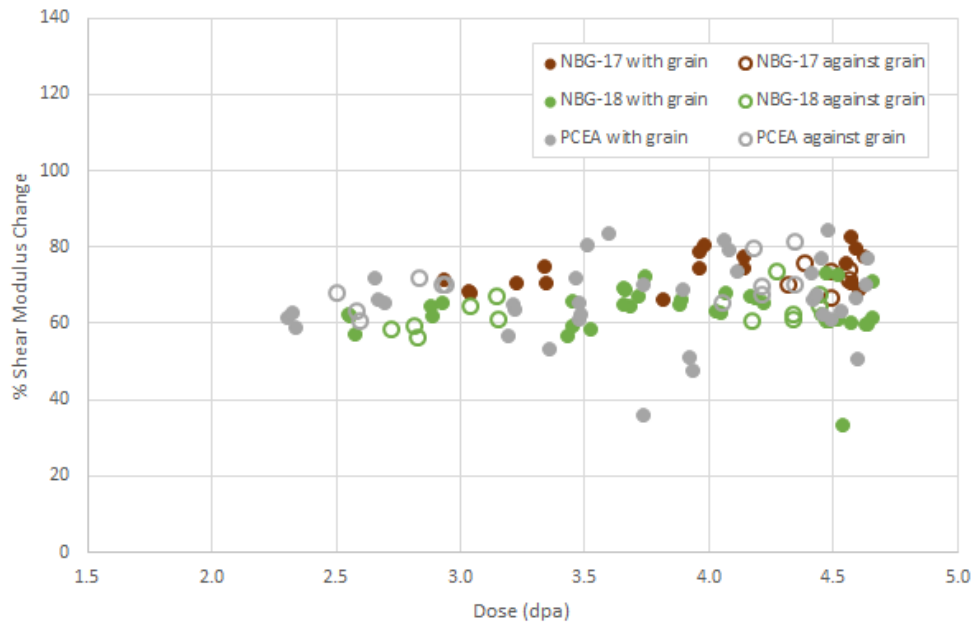


Figure 43. Percent shear modulus change versus dose by graphite grade and specimen orientation.

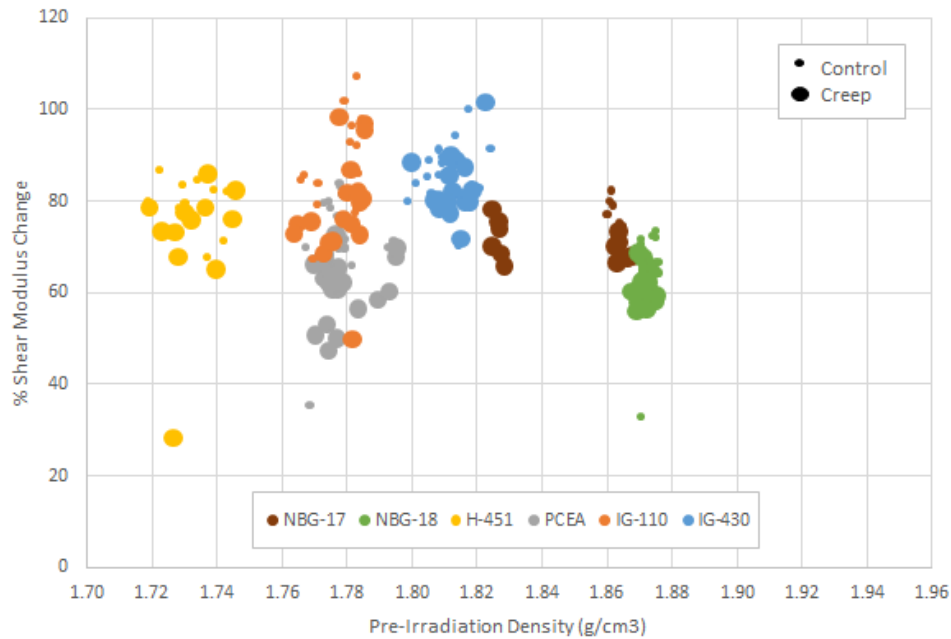


Figure 44. Percent shear modulus change versus specimen pre-irradiation density by graphite grade for control and creep specimens.

While the stressed creep specimens do not clearly demonstrate a distinct decrease in the shear modulus percent change as is shown in the Young's modulus measurements, the fact that creep and control specimen data trends are different still indicates the presence of competing mechanisms as discussed in Section 5.3. As a consequence, similar conclusions can be made for irradiated shear modulus behavior as were made for Young's modulus.

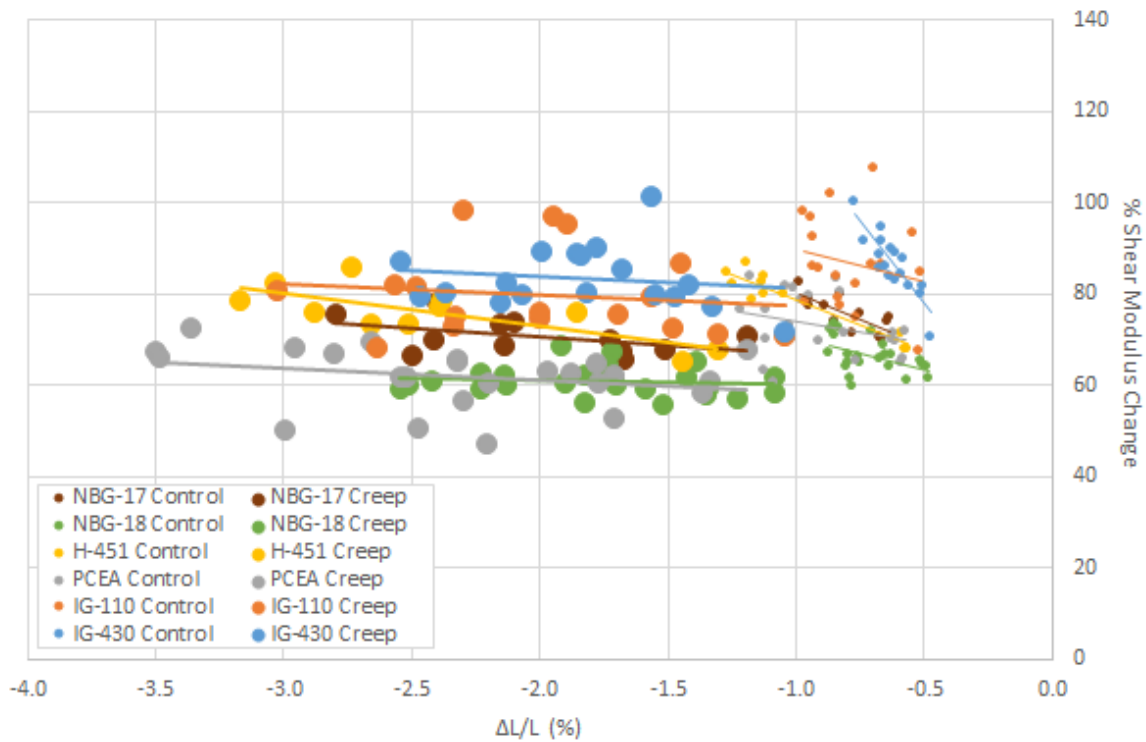


Figure 45. Percent shear modulus change versus specimen strain by graphite grade for control and creep specimens. Note negative strain increases from right to left (from 0.0 to -4.0%)

Finally, as described in previous sections, Figure 46 is intended to depict the influence that irradiation temperature may have on the change in shear modulus. Percent change in shear modulus data that falls in a narrow dose range of 3.5 to 4.5 dpa are plotted as a function of irradiation temperature. This temperature range is about 100°C from 590 to 690°C. Graphite grades are separated into three forming processes to aid in clarity, and stressed and unstressed specimens are depicted by the size of the plotted symbol. As seen for these specific ranges of temperature and dose, the shear modulus percentage change stays constant for the specimen irradiation temperatures shown. Because this is a relatively narrow temperature range, the fact that there is no trend with temperature is only an indication that the constant percent change in shear modulus versus dose is not a result of competing effects of dose and temperature. As data from the other AGC capsules are gathered with nominal irradiation temperatures of 800 and 1100°C, it will be possible to understand the role of irradiation temperature versus dose over much broader ranges.

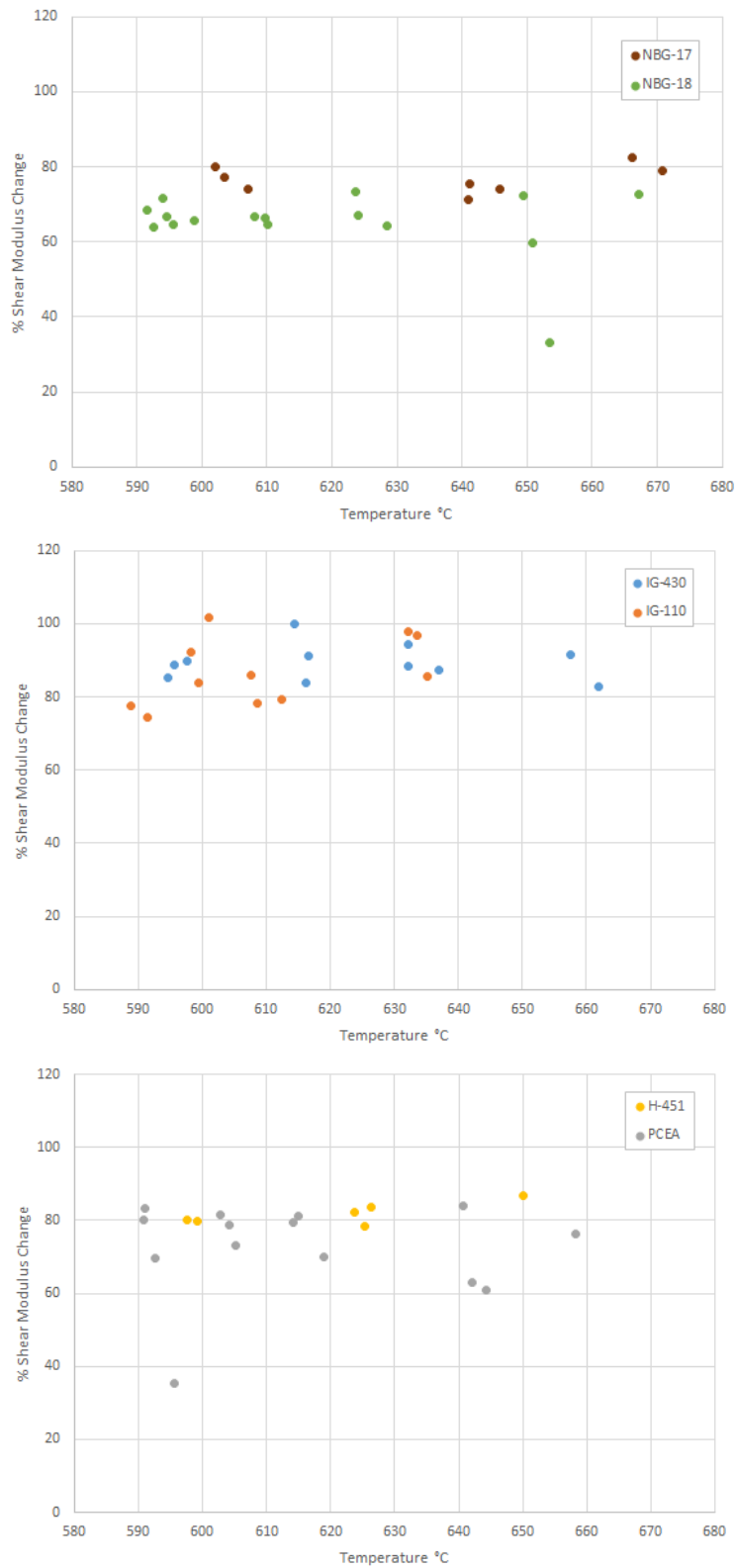


Figure 46. Percent change in shear modulus versus specimen irradiation temperature for a narrow dose range of 4.0 ± 0.5 dpa for the AGC-2 major graphite grades.

5.6 Coefficient of Thermal Expansion

The coefficient of thermal expansion (CTE) defines how the physical size of an object changes with a change in temperature. Specifically, it measures the fractional change in size per degree change in temperature at a constant pressure. CTE is a key parameter for determining thermally induced stress states within graphite components, volumetric changes, and irradiation creep rates. These stresses occur from thermally induced dimensional changes, any mechanical (internal or external) stresses induced from differential dimensional changes, and external stresses resulting from interlocked graphite core components as the individual pieces suffer differential thermal expansion.

CTE is measured in accordance with ASTM E228-06. This test method uses a push-rod dilatometer to determine the change in length of a graphite specimen relative to that of the holder as a function of increasing/decreasing temperature. The temperature is varied over the desired range at a slow constant heating or cooling rate. Using calibration to subtract the growth of instrument fixtures, the change in specimen length is recorded as a function of temperature. The mean CTE is calculated from the slope of a line drawn from the reference temperature, typically 20°C, and a specified temperature using Equation 7. This is performed for specific temperatures covered by the growth curve to produce mean CTE values like those shown as an example in Figure 47:

$$\alpha = \frac{\Delta L}{L_0} \cdot \frac{1}{\Delta T} \quad (7)$$

where:

α = CTE

ΔL = change in length

ΔT = change in temperature

L_0 = initial length at 20°C.

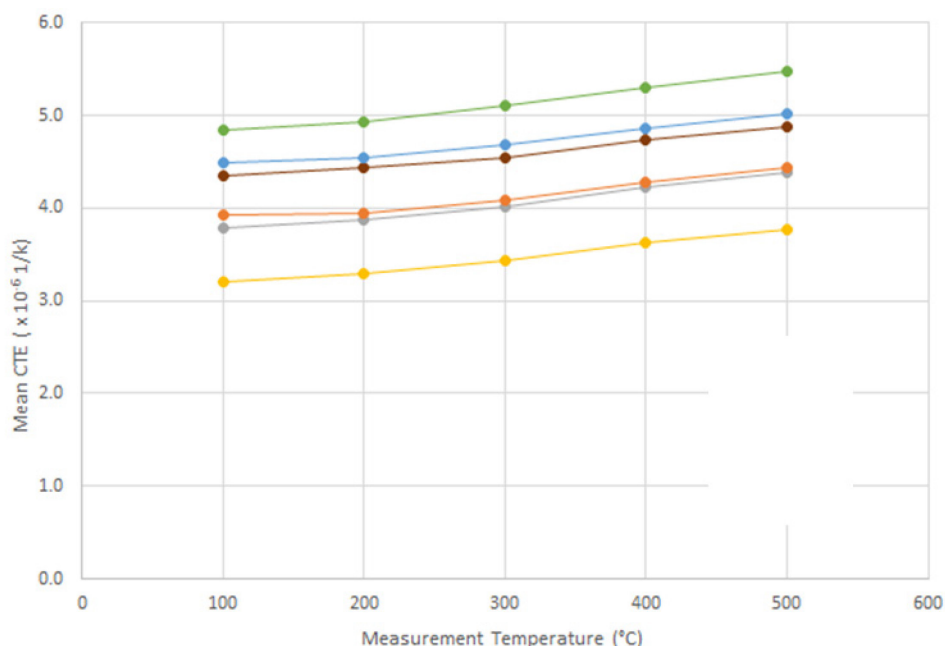


Figure 47. Typical mean CTE measurement plot of nuclear grades over a range of temperatures (note: the graphite CTE data at each temperature are for illustration purposes only). It is observed that the CTE increases as temperature increases and the rate of increase also increases with increasing temperature.

Mean CTE measurements were made on the creep and control specimens both before and after irradiation up to temperatures of 500°C (just below the irradiation temperature to forestall any irradiation damage annealing). While changes to CTE after irradiation showed the least percent change for any material property tested, the changes were still significant with an average increase of about 24% (green line) and a ± 1 standard deviation of about 15% (Figure 48). It should be noted that Figure 48 incorporates CTE results at five different test temperatures for each specimen. This is different from the density, elastic modulus, and resistivity measurements that are tested only at room temperature. This adds an additional variable to the data scatter in addition to irradiation temperature, dose, applied stress, graphite grade, and grain orientation. However, even with this increased variable contributing to data scatter, approximately 63% of the data lie within ± 1 standard deviation.

Finally, it should be noted that a linear representation of all CTE data scatter is not accurate since, as was stated previously, CTE normally increases with increasing temperature. However, for the purposes of consistency a linear regression was performed to illustrate the level of scatter in the data and the average change in CTE over the entire AGC-2 irradiation dose range.

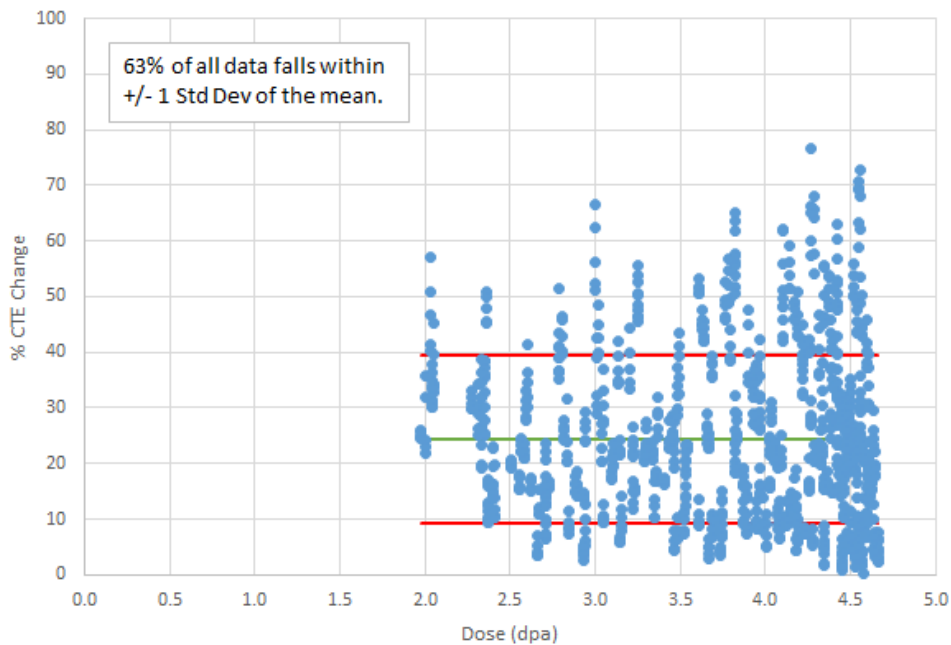


Figure 48. Percent change of CTE for all graphite specimens at all test temperatures (100, 200, 300, 400, and 500°C).

To allow CTE data to be analyzed comparably to the previous material properties, the CTE results for a single test temperature are analyzed against the test variables (Figure 49). As seen, for these single test temperature results, CTE is still observed to rise significantly with an average increase of about 24% (green line) with a ± 1 standard deviation of about 15% (shown as red lines) for 65% of the data, which is quite good. As discussed previously, the scatter in the data reflects the different variables within the experiment, including irradiation temperature, dose, load, graphite grade, and grain orientation.

While Figure 49 demonstrates a similar CTE response for all AGC-2 specimens (regardless of nuclear grade, grain size, stressed/unstressed condition, or grain orientation) the scatter in the data is considerable. The percent change in CTE has a large range from less than 5% to larger than 50% for all data, which is most likely a result of differences in grade and applied stress (i.e., irradiation-induced strain) (Figure 50 and Figure 51). Upon further analysis of the data, isolating the irradiation dose, applied stress, grade, and grain orientation are needed to determine these effects on CTE.

Figure 50 illustrates the irradiation-induced CTE changes between the six major graphite grades from irradiation only (no mechanical loaded specimens are considered). It can be easily seen that there is minimal common irradiation behavior between the different grades, something that has not been observed previously. The two small-grained, iso-molded grades demonstrate the largest CTE increase with a steady increase as dose is increased; NBG-18 has the lowest increase with the change in CTE nearly returning to unirradiated values for the higher dose specimens. While the linear regression analysis for each grade appears to show significant variation between the grades, it should be noted that there is considerable scatter within each specific graphite grade; this indicates that data trends for the individual grades are very weak. This weak relationship between irradiation dose and CTE change indicates that there are different mechanisms occurring in addition to irradiation damage mechanisms.

The effect of stress on the percent change in CTE was investigated next. Because CTE is measured over a range of temperatures, Figure 51 presents the average percent CTE change by graphite grade at measurement temperatures of 100°C through 500°C for both creep and control specimens. Error bars

represent ± 1 standard deviation from the mean. The large CTE difference between stressed and unstressed specimens is immediately observed with some stressed specimens demonstrating differences of more than a factor of 4 (i.e., PCEA at 500°C). The change in CTE within all grades is observed to be similar over all CTE test measurement temperatures, indicating no significant decrease for all specimens (creep and control) with increasing temperature.

Graphite grade H-451 demonstrates the largest increase in CTE (for both creep and control), while NBG-18 has the lowest irradiation-induced CTE change. The response of the extruded grade PCEA compared to H-451 is of interest. GrafTech, Inc. designed PCEA to be as similar to H-451 as possible, yet its irradiated CTE response is 40% lower than the H-451 CTE values. Because the dimensional change and creep coefficient are very similar,⁸ it is surprising that material property changes do not behave similarly. The other pairs of graphite within the same forming processes compared much closer (i.e., IG-110 and IG-430, NBG-17 and NBG-18). Finally, the fine grain grades, IG-110 and IG-430, appear to have significantly larger irradiation-induced change to the CTE than the larger medium grain grades (if H-451 is temporarily ignored).

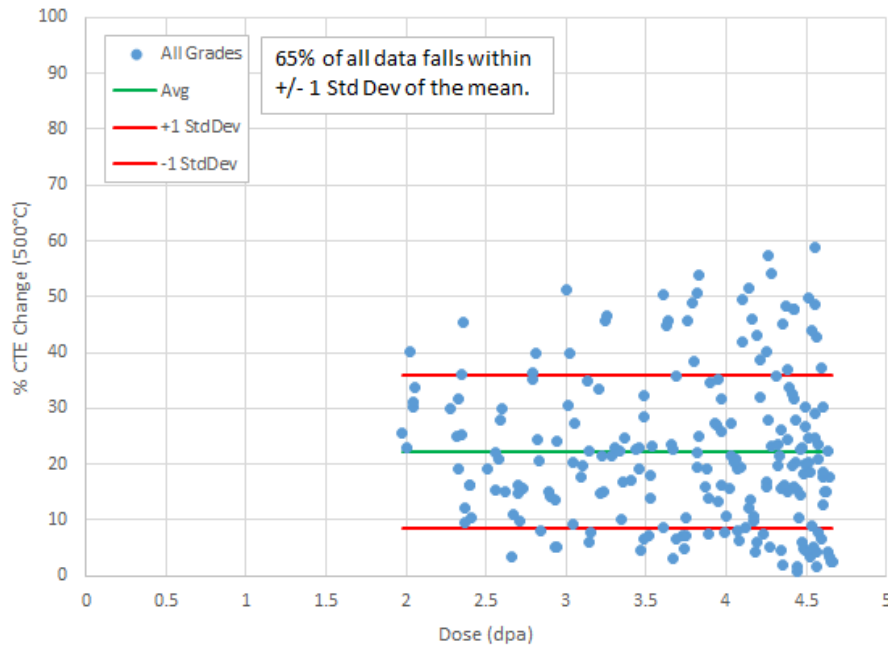


Figure 49. Percentage change of CTE at a single test temperature of 500°C for all tested specimens.

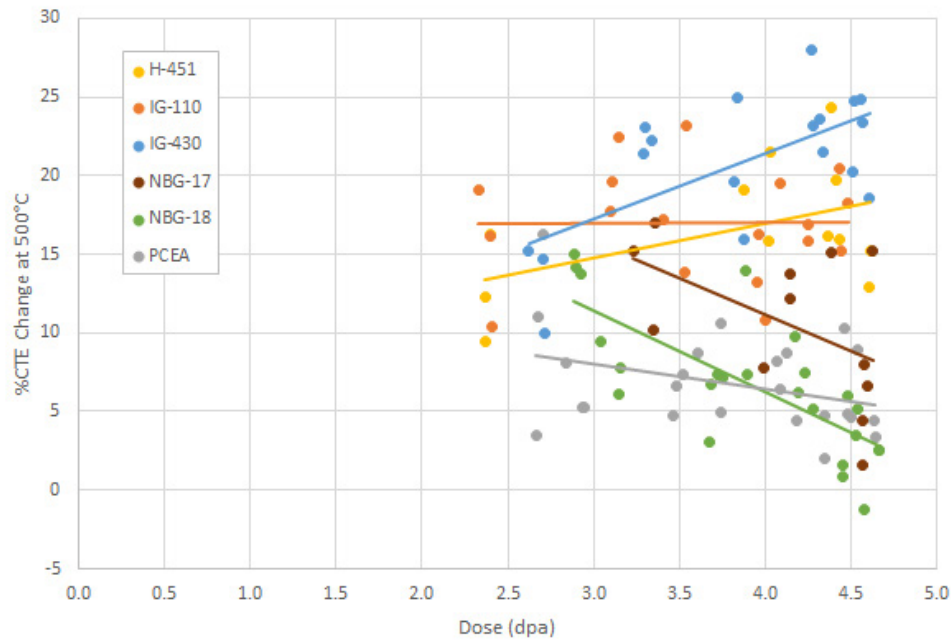


Figure 50. Percent change in mean CTE at 500°C versus dose by graphite grade for control specimens only.

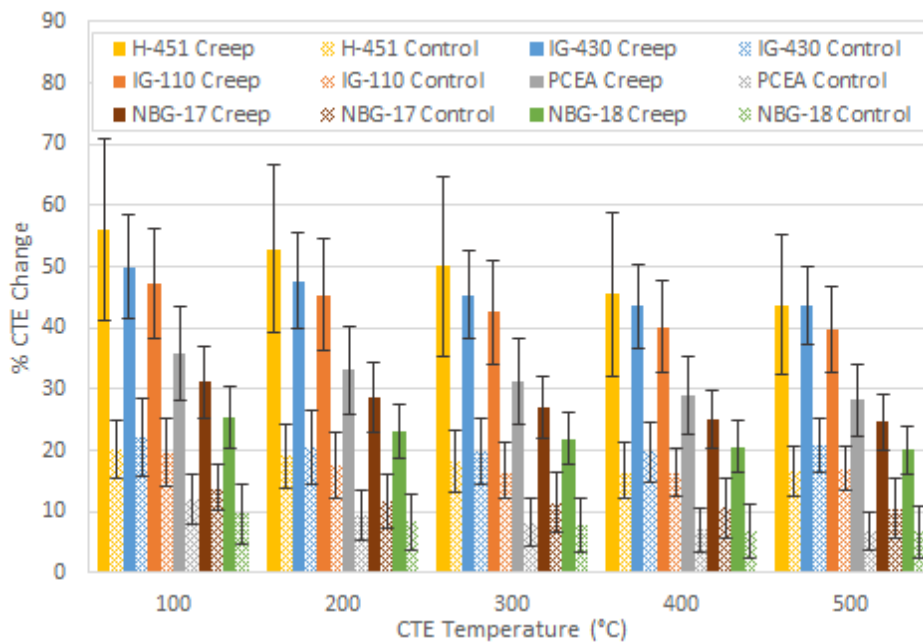


Figure 51. Average percent CTE change by graphite grade and applied load for measurement temperatures 100 to 500°C.

To assess the effects from different applied stress levels in the creep specimens, the changes to the measured CTE at 500°C at a single test temperature (500°C) for the three applied stress levels is shown in Figure 52. Error bars represent ± 1 standard deviation from the mean. The error bars are determined to be much larger than observed in the previous sections, indicating the much larger scatter in CTE data.

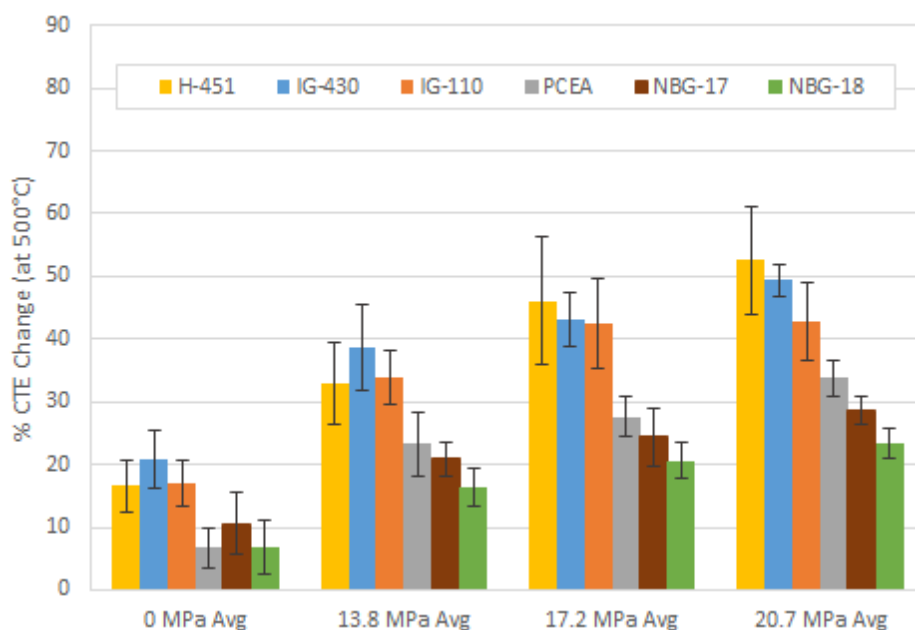


Figure 52. Percent CTE change by graphite grade and applied stress. The error bars represent ± 1 standard deviation from the mean and numbers in the bars represent sample size.

As in Figure 50, Figure 53 is a plot of percent change in CTE at 500°C versus irradiation dose; however, now the control (unstressed) and creep (stressed) specimens are shown separately. Linear regression lines are established for some individual grades to aid in clarity. To more accurately determine the effects from applied stress (and subsequent induced strain) the four stress levels are represented for each grade in Figure 53. The significant difference between stressed and unstressed specimens is apparent but it becomes clear that CTE generally increases with increasing applied stress, indicating that CTE is sensitive to changes in the microstructure occurring from the induced strain. This is true for all graphite grades, although the relationship is much weaker for the larger-grain PCEA and vibrational-molded grades.

This appears to be counterintuitive to the behavior observed in Figure 50, which shows increasing CTE change with increasing dose for the fine-grain grades and decreasing CTE change for the larger-grain grades. If the assumption that a change in large grain microstructure due to irradiation is responsible for a decrease in CTE is true, Figure 53 would show an acceleration in CTE decrease, not the opposite effect. Obviously, there is not enough data to come to a firm conclusion on the mechanisms that affect changes to CTE. Further fundamental studies will be required to assist in interpretation of these data trends.

Figure 54 adds together the effects of irradiation and applied stress on CTE at 500°C for the three separate forming processes. Only data from the 500°C testing temperature is used and linear regression lines are established for both creep (—) and control (---) specimens. From these data, the large difference in CTE behavior between the creep and control specimens is demonstrated along with the overall trend for each forming process. The small grain, iso-molded grades keep their trend of gradual CTE increase for both creep and control specimens, while the larger grain vibrational molded grades have the lowest CTE change and have started to decrease from their maximum peak. The extruded grades demonstrate a constant CTE response over the irradiation dose range. It should be noted that large scatter in the extruded data is due to the large difference in behavior between the H-451 and PCEA grades.

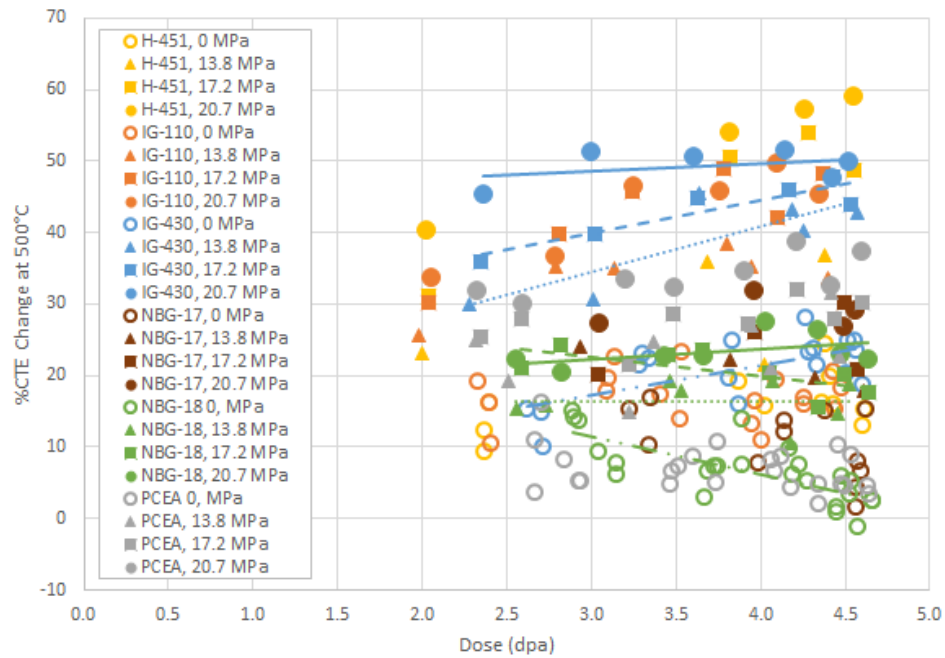


Figure 53. Percent CTE change at 500°C by graphite grade for stress levels of 0, 13.8, 17.2, and 20.7 MPa.

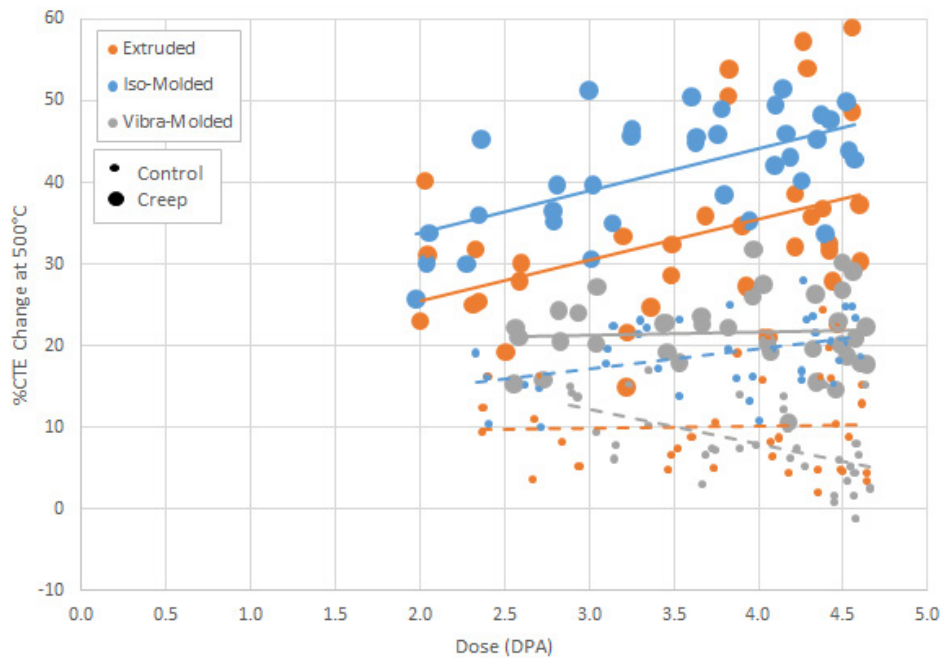


Figure 54. Percent change of post irradiation CTE measurements at 500°C versus dose by fabrication process for creep (—) and control (- -) specimens.

Figure 55 and Figure 56 investigate the dependence of grain orientation on the change of CTE at 500°C for the three major graphite grades with forming processes that result in distinct grain orientations. Figure 55 examines the effect of grain orientation on the change in CTE at 500°C for stressed and

unstressed specimens (error bars represent ± 1 standard deviation in the data). The percent change in CTE is nearly equal between the two grain orientations for all grades and average stress conditions. As observed previously, stressed specimens experience significantly more change in CTE than unstressed specimens regardless of grain orientation.

Figure 56 examines the percent change in CTE at 500°C over the irradiation dose range for the two grain orientations (hollow and solid symbols are representative of AG and WG, respectively). Similar to the applied stress analysis, no differences in percent CTE change are observed for grain orientation as a function of irradiation dose.

Figure 57 illustrates the effects of specimen density (before irradiation) on the change in CTE at 500°C. As noted previously, density has a large effect on material property values, and density-related differences may be exacerbated under irradiation. However, the data in Figure 57 show no obvious changes to the irradiation CTE percentage change as a function of density changes even for the NBG-17 specimens for which data were gathered for two density ranges that have a 2% density variation between specimens. The effects from applied stress (increased strain) do show the expected large increase in CTE change for all grades.

The affect from irradiation-induced strain on CTE at 500°C change is shown in Figure 58. Data are presented as the change in CTE at 500°C as a function of increasing strain experienced in the specimen axial direction as analyzed in the AGC-2 creep analysis report.⁸ Data are separated into control and creep specimens, including all irradiation temperatures and received dose, with linear regression lines established for each individual grade.

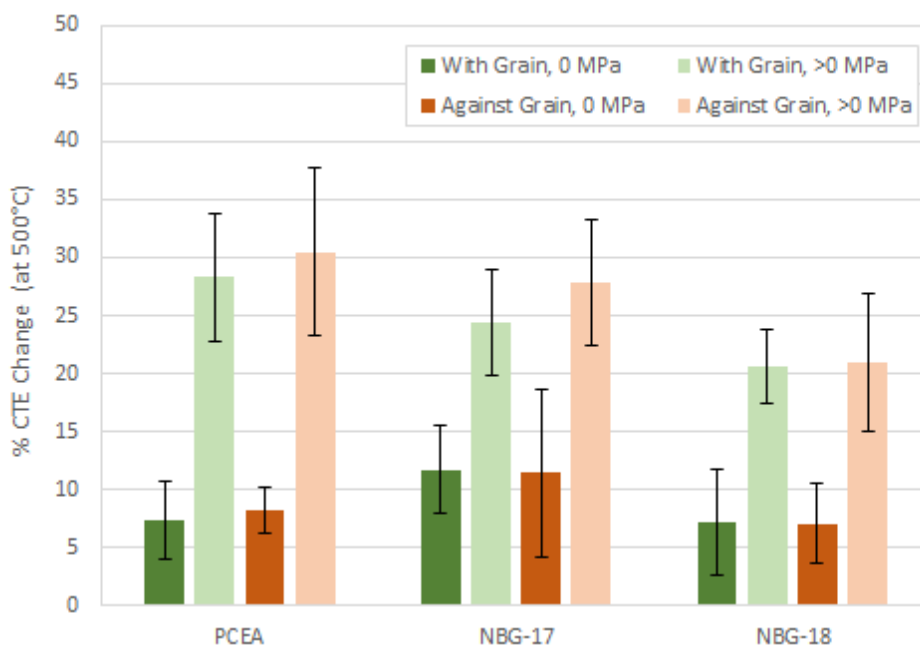


Figure 55. Average percent change CTE at 500°C by graphite grade, applied stress, and grain orientation for measurement temperatures at 500°C.

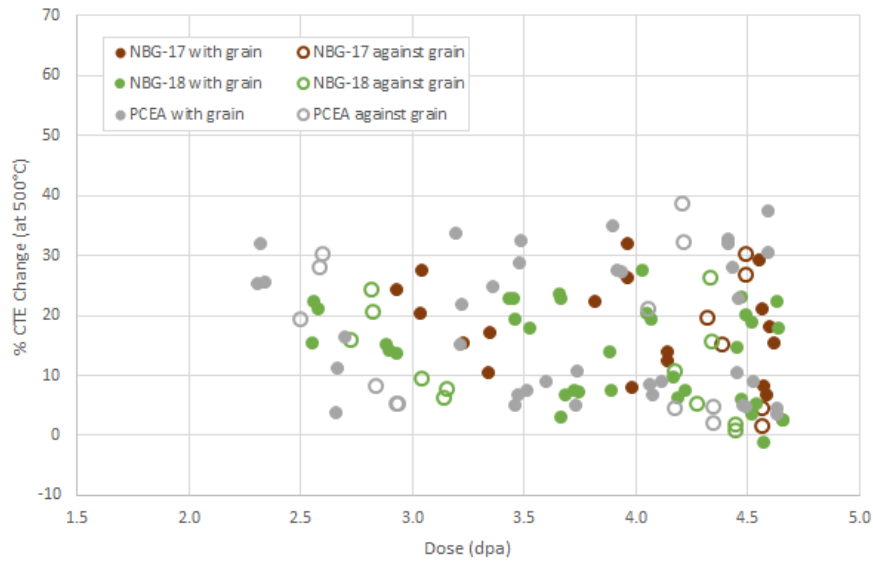


Figure 56. Percent change CTE at 500°C versus dose by graphite grade and specimen orientation.

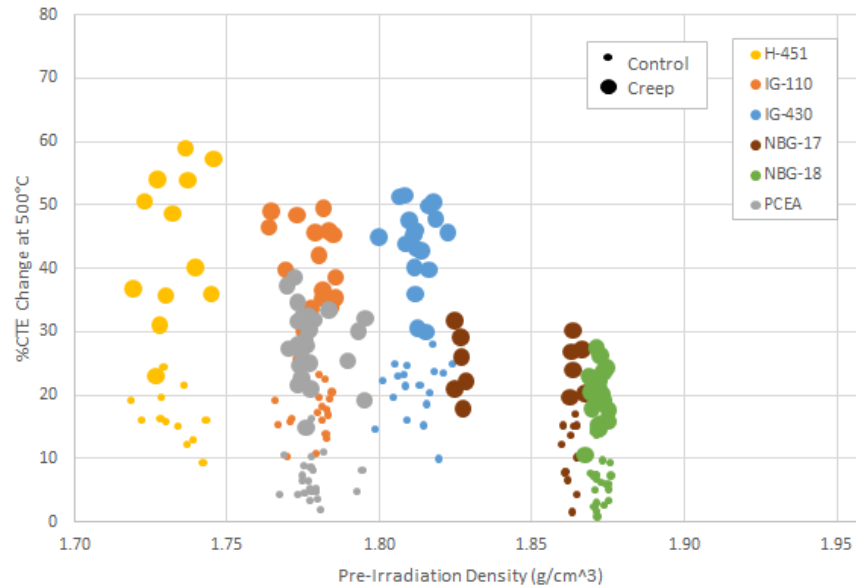


Figure 57. Percent CTE at 500°C change versus specimen pre-irradiation density by graphite grade for control and creep specimens.

As demonstrated previously, while all specimens (creep and control) experienced similar neutron irradiation doses and temperatures, the stressed creep specimens showed much larger strains due to the added mechanical stresses. With this understanding, Figure 58 illustrates three trends of interest: (1) CTE increases with increasing strain for creep specimens; (2) CTE change generally stays constant or decreases with increasing strain for control specimens; and (3) there is a small (i.e., about 5%) but consistent difference in CTE between creep and control specimens that have undergone similar strains.

Generally, it can be seen that CTE increases uniformly with increasing strain for the stressed creep specimens in all graphite grades. This indicates the CTE changes are strongly sensitive to strain imposed

upon the creep specimens by the applied stress as has been noted previously. However, the unstressed control specimens, which also undergo strain but at lower levels, do not have this uniform behavior across graphite grades. If the CTE is so strongly sensitive to strain, the response would be similar for both creep and control specimens. Further, for those creep and control specimens from the same grade that experience similar strain levels (where the creep and control data overlap), there is a significant difference in CTE response. It should be pointed out that in AGC-2, the highest strain control specimens received neutron dose approximately 2 to 2.5 times the exposure of the lowest strain creep specimens.

Strain-induced changes to CTE cannot completely explain the observations that neutron irradiation damage may continue to alter the CTE change at dose greater than 2 dpa. However, current data are not enough to form firm conclusions on how microstructure strain and irradiation damage directly affect changes to CTE. Further fundamental studies will be required to assist in interpretation of these data trends.

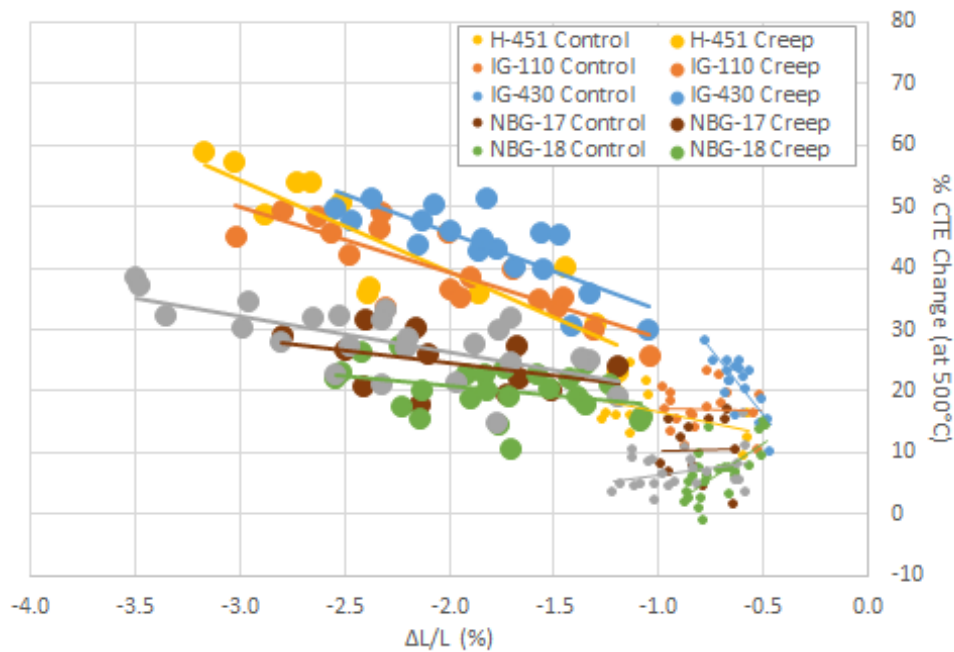


Figure 58. Percent CTE change at 500°C versus specimen strain by graphite grade for control and creep specimens. Note negative strain increases from right to left (from 0.0 to -4.0%)

Finally, Figure 59 is intended to provide an initial understanding of the influence irradiation temperature has on the level of change in CTE. Percent change in CTE data that fall in a narrow dose range of 3.5 to 4.5 dpa are plotted as a function of irradiation temperature. This temperature range is 590°C to 690°C. Graphite grades are separated into the three forming processes to aid in clarity and stressed and unstressed specimens are depicted by the size of the plotted symbol. For these specific ranges of temperature and dose, no trend in the level of CTE change as a function of irradiation temperature is visible. Because this is a relatively narrow temperature range, the fact that there is no trend with temperature is only an indication that the slight increase percent change of CTE versus dose, initially shown in Figure 50 for all irradiation temperatures, is not a result of competing effects between dose and temperature. As data from other AGC capsules are gathered with nominal temperatures of 800 and 1,100°C, it will be possible to understand the role of irradiation temperature verses irradiation dose over much broader ranges.

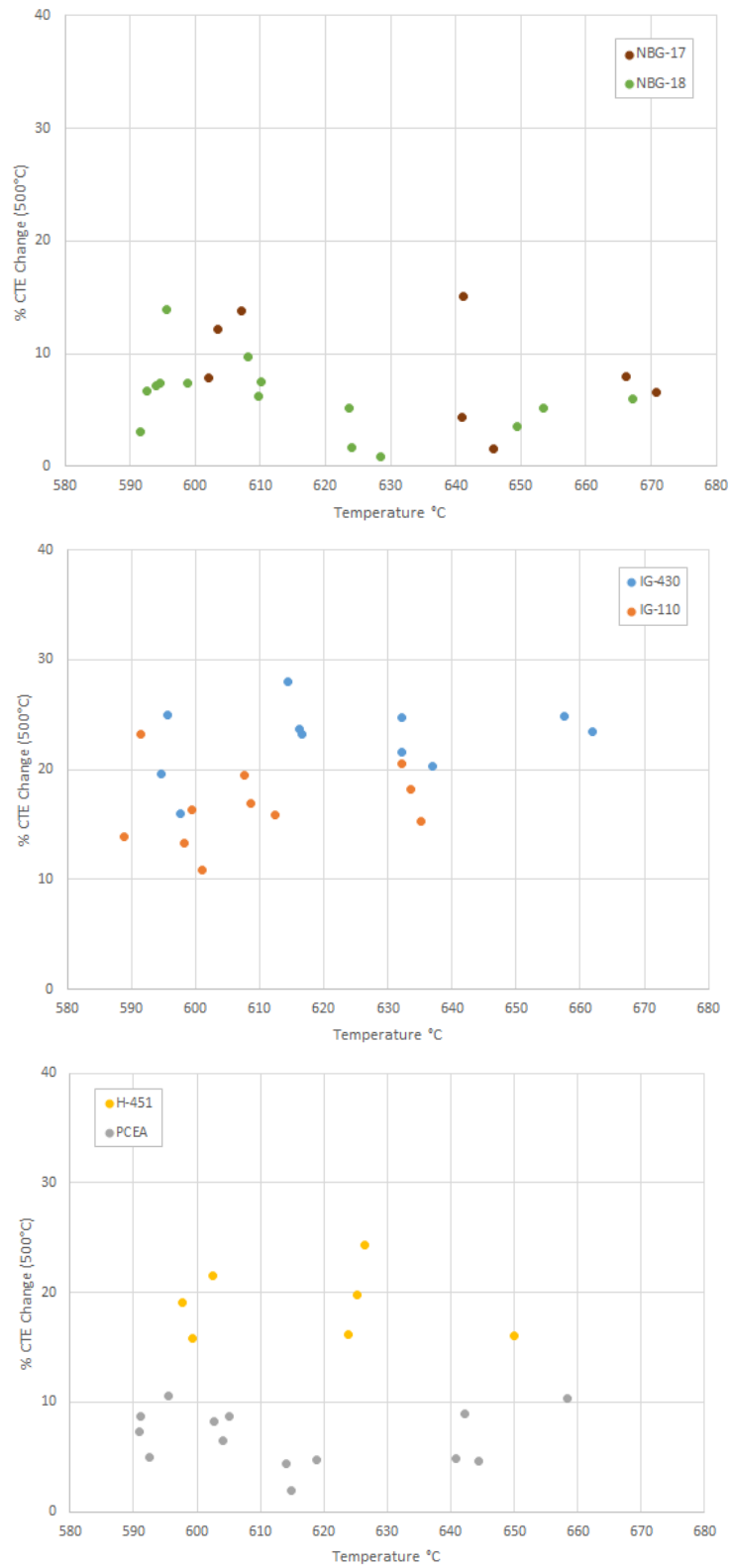


Figure 59. Percent change in CTE for unstressed specimens at 500°C versus specimen irradiation temperature for a narrow dose range of 4.0 ± 0.5 dpa for different graphite grades.

5.7 Thermal Diffusivity

Thermal conductivity and diffusivity are the most important thermophysical material parameters for describing the heat transport properties of a graphite component. Thermal diffusivity is a measure of the rate of heat transfer in a material (i.e., how fast heat is transferred from the hot side to the cold side of a material). It is useful for ascertaining heat conduction through the graphite core for passive decay heat removal, calculations of thermal stresses, and modeling core physics in a graphite moderated design.

The AGC-2 thermal diffusivity measurements were carried out in accordance with ASTM E1461-07. The measurement is performed on small, thin, disk-shaped specimens. A pulsed laser is used to subject one surface of the specimen to a high-intensity, short-duration energy pulse. The energy of this pulse is absorbed on the front surface of the specimen and the resulting rise in rear-face temperature is recorded. Thermal diffusivity is calculated from the specimen thickness and the time required for the rear face temperature to reach 50% of its maximum value.

$$\alpha = 0.13879 L^2/t_{1/2} \quad (8)$$

where:

L = specimen thickness

T_{1/2} = half rise time of the detector signal.

The more familiar thermal conductivity is derived from diffusivity values by multiplying thermal diffusivity by the material density and specific heat capacity:

$$K = \alpha \rho C_p \quad (9)$$

where:

K = thermal conductivity

α = thermal diffusivity

ρ = density

C_p = specific heat.

Thermal diffusivity is a strong function of unirradiated graphite temperature and is measured as a function of temperature. Because of the physical limitations necessary to conduct diffusivity measurements (i.e., a relatively thin specimen), the measurements were made on the piggyback specimens only. The piggyback specimens included all 14 different graphite grades (including the six major grades) analyzed in AGC-2. Resistivity was measured at successive 100°C increments over the temperature range of 100 to 500°C. Because of size and AGC-2 design limitations, none of the piggyback specimens were subjected to an applied mechanical stress during irradiation; accelerated creep was not attempted for these specimens. Because piggyback specimens did not receive applied stresses, there are no data comparing the effects of different stress levels (and induced accelerated strains).

Figure 60 shows the average pre- and post-irradiation diffusivity for all graphite grades and irradiation conditions as a function of measurement temperature. As with the other material property measurements, the percent change in thermal diffusivity was substantial, experiencing a maximum reduction of 79% at a measurement temperature of 100°C and a minimum reduction of 57% at 500°C (average diffusivity values are shown as a green line with ± 1 standard deviation shown as red lines). The scatter in data reflects the different variables within the experiment, including irradiation temperature, dose, applied stress, graphite grade, and grain orientation.

It should be noted that graphite thermal diffusivity is normally expected to gradually reduce as the testing temperatures increase due to grain boundary and phonon-phonon (Umklapp scattering) scattering effects.^{38,39} Grain boundary phonon scattering dominates thermal resistance at low temperatures but becomes insignificant above a few hundred degrees Celsius while the Umklapp scattering dominates at higher temperatures and defines the upper limit to the thermal conductivity for a “perfect” graphite. This gradual reduction due to temperature scattering effects is observed in both pre and post-irradiation data.

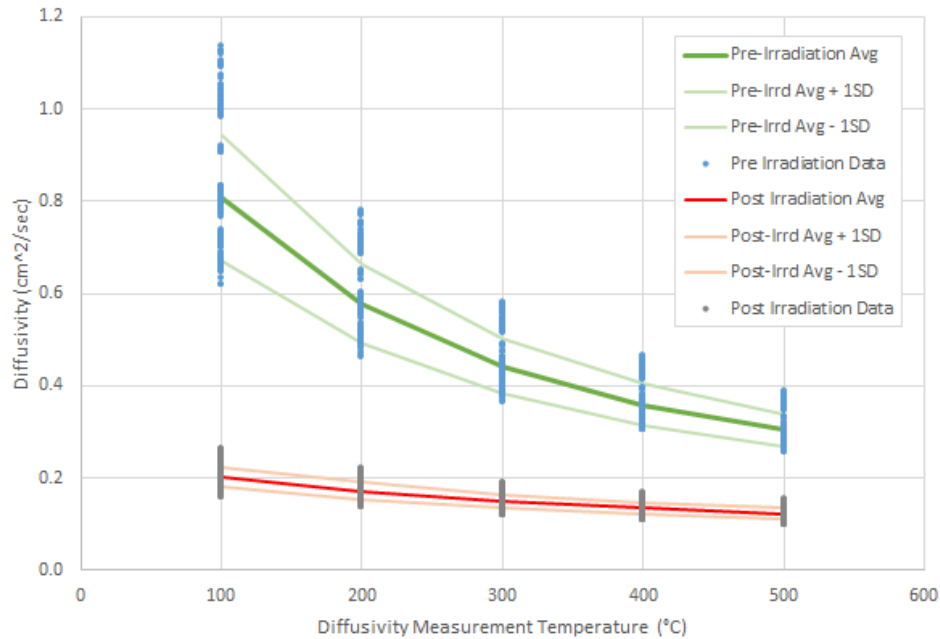


Figure 60. Specimen diffusivity versus measurement temperature for all AGC-2 piggyback specimens.

As seen in the previous analysis, thermal diffusivity data are remarkable in that all specimens, including different grades, different grain sizes, and with different grain orientations, respond so similarly over the relatively short irradiation dose range of AGC-2. In fact, the scatter in measurement data actually decreases after irradiation despite wide variations in the different graphite grades. This is illustrated in Figure 61, which shows the average percent change for all specimens tested at the five measurement temperatures. The similarity between the various grades (only an approximate 5% difference) is consistent over all measurement temperatures with all grades displaying a consistent behavior (i.e., grade HLM has the highest diffusivity measured values, while S2114 remains the lowest throughout all measurement temperatures).

Because of consistency among diffusivities for all grades and across all measurement temperatures, only the major grades of AGC-2 graphite will be considered in the remaining data figures to assist with clarity (Figure 62). Average diffusivity for the six major grades is indicated by the bar length and the error bars represent ± 1 standard deviation of the data for each grade. The standard deviations for all grades are extremely small and consistent between grades across the entire measurement temperature range, which is different from what has been observed for the other irradiated material properties that show large and variable data scatter for the different grades. As seen, the extruded graphite grades H-451 and PCEA had the greatest percent change, while iso-molded grade IG-110 had the least.

Because piggyback specimens did not receive applied stresses, there are no data comparing the effects of different stress levels (and induced accelerated strains). Only the effects from irradiation, fabrication processes, and irradiation-induced creep strain on the different tested grades are compared in this analysis.

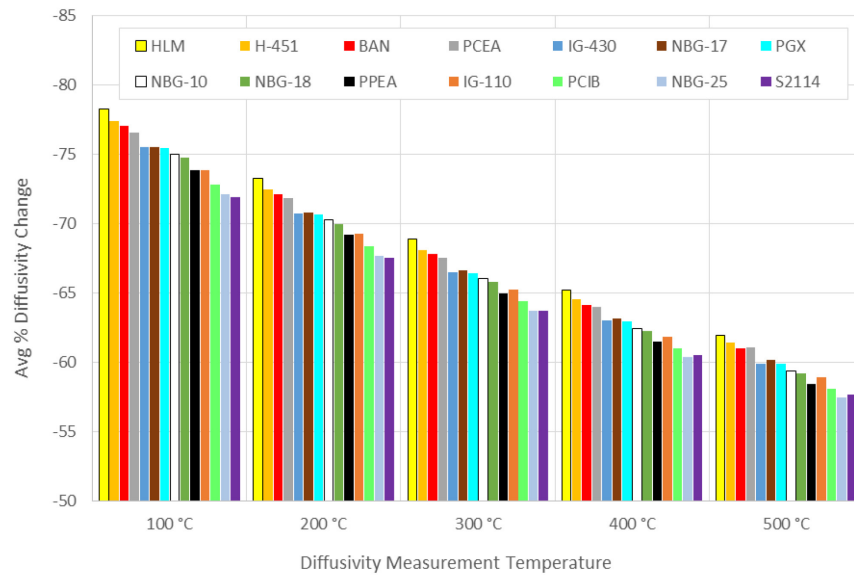


Figure 61. Average percent diffusivity change by graphite grade for measurement temperatures 100 to 500°C. Note the Y-axis is inverted.

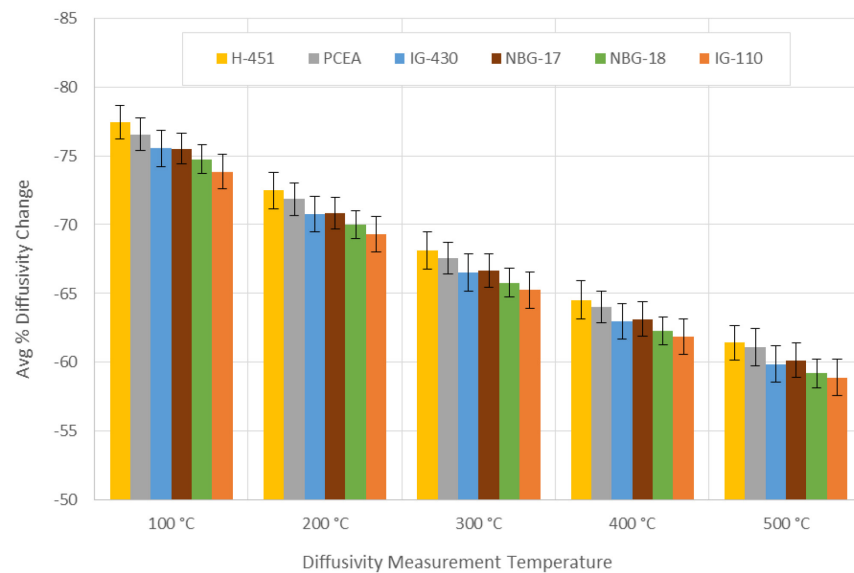


Figure 62. Average percent diffusivity change by graphite grade (major grades only) for measurement temperatures 100 to 500°C. Note the Y-axis is inverted. The error bars represent ± 1 standard deviation from the mean.

Figure 63 illustrates the thermal diffusivity behavior at 500°C from irradiation only (no mechanical-loaded specimens are considered). It should be noted that dose range for diffusivity specimens is larger (i.e., about 1.4 to 4.7 dpa) than the control and creep specimens, which were centered inside the capsule to ensure matching irradiation conditions for the matched control and creep pairs.²⁵ Unlike all previous material property measurements, thermal diffusivity is observed to show a large initial decrease (i.e., about 58%) for all graphite grades prior to the minimum AGC-2 dose of 1.4 dpa. It can also be seen that the change in diffusivity resulting from irradiation dose in Figure 63 continues to decrease

with increasing irradiation dose. This implies that irradiation damage or the effects resulting from irradiation damage (i.e., irradiation-induced dimensional change) continues to affect thermal diffusivity over the relatively short irradiation dose range in AGC-2. The extruded grades H-451 and PCEA exhibit the largest reduction in thermal diffusivity, while the isostatic-molded and vibration-molded grades exhibit similar changes to diffusivity as dose increases.

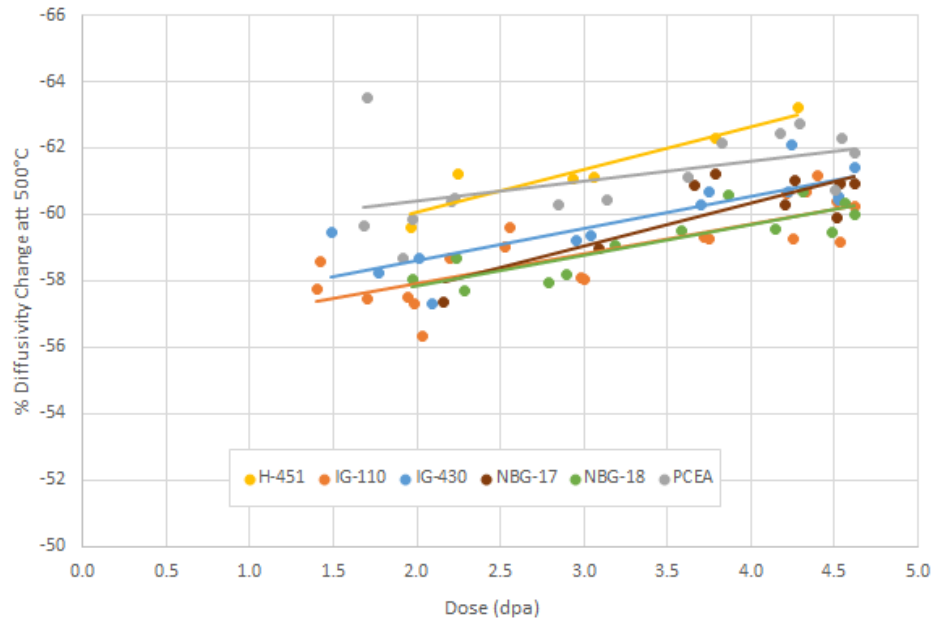


Figure 63. Percent change in diffusivity at 500°C as a function of irradiation dose. Note the Y-axis is inverted.

Figure 64 investigates the dependence of grain orientation on diffusivity change for the three major graphite grades that have forming processes which result in distinct grain orientations. The average percent change in thermal diffusivity for measurement temperatures of 100 and 500°C are shown with the error bars indicating ± 1 standard deviation. Minimal differences exist for either orientation at either measurement temperature, indicating irradiation affects thermal diffusivity similarly for any specimen orientation.

Figure 65 illustrates the effects of specimen density (before irradiation) on the change in thermal diffusivity. As noted previously, density has a large effect on material property values and density-related differences may be exacerbated under irradiation. However, data in Figure 65 show no obvious changes to the irradiation thermal diffusivity percentage change as a function of density change (i.e., less than an approximate 5% change as observed previously), even for the NBG-17 and H-451 specimens for which data were gathered for two density ranges that have a 2% density variation between specimens.

Figure 66 demonstrates the effect of irradiation-induced strain at 500°C on the thermal diffusivity response for the six major grades of graphite. As seen, there is a large initial reduction in diffusivity for all grades, but the diffusivity continues to decrease as the irradiation-induced strain increases, similar to what was observed for diffusivity changes from neutron dose in Figure 63. It should be noted that none of the specimens have experienced accelerated strain from an applied stress; therefore, any strain is due simply from irradiation-induced changes and the range is extremely short. Because there is no accelerated strain response data from applied stresses, any conclusions other than thermal diffusivity continues to decrease with increasing strain and dose cannot be made at this time.

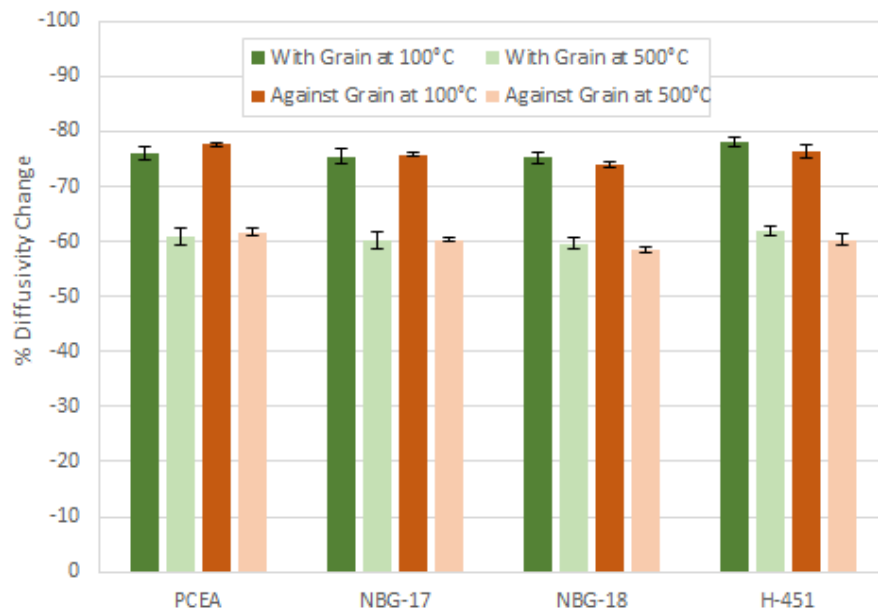


Figure 64. Average percent diffusivity change by graphite grade and grain orientation. Note the Y-axis is inverted.

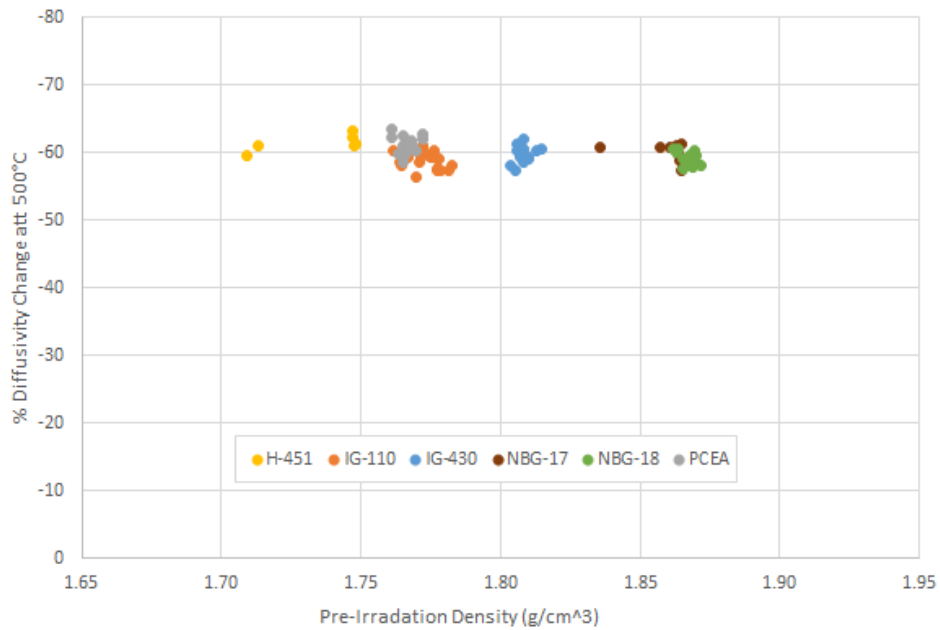


Figure 65. Percent diffusivity change versus specimen pre-irradiation density by graphite grade. Note the Y-axis is inverted.

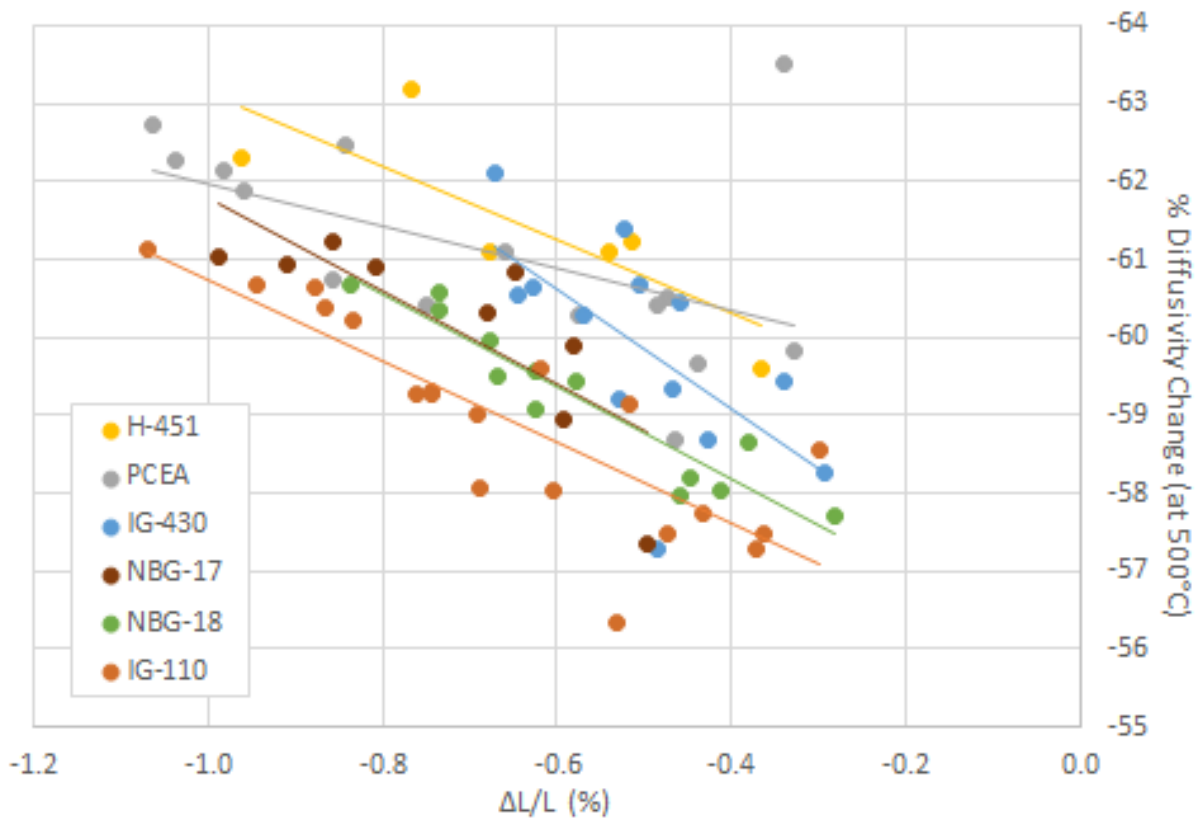


Figure 66. Percent diffusivity change at 500°C versus specimen strain by graphite grade. Note the Y-axis is inverted and negative strain increases from right to left (from 0.0 to -4.0%)

Finally, Figure 67 is an attempt to understand the influence irradiation temperature may have on the change in thermal diffusivity, because these diffusivity observations must recognize the data cover a range of irradiation temperatures that tend to correspond to dose. Figure 67 data are taken from the pool of data at the 500°C measurement temperature for the six major graphite grades. They are limited to a narrow dose range between 3.5 and 4.5 dpa. Graphite grades associated with the three different forming processes are broken out in three different plots for clarity. When data are filtered in this way, the number of specimens and temperature range is limited. However, it is clear that over this limited range that irradiation temperature has little to no effect on the post-irradiation diffusivity. Over an approximate 100°C range of irradiation temperatures, all graphite grades experienced a constant 60% change in diffusivity.

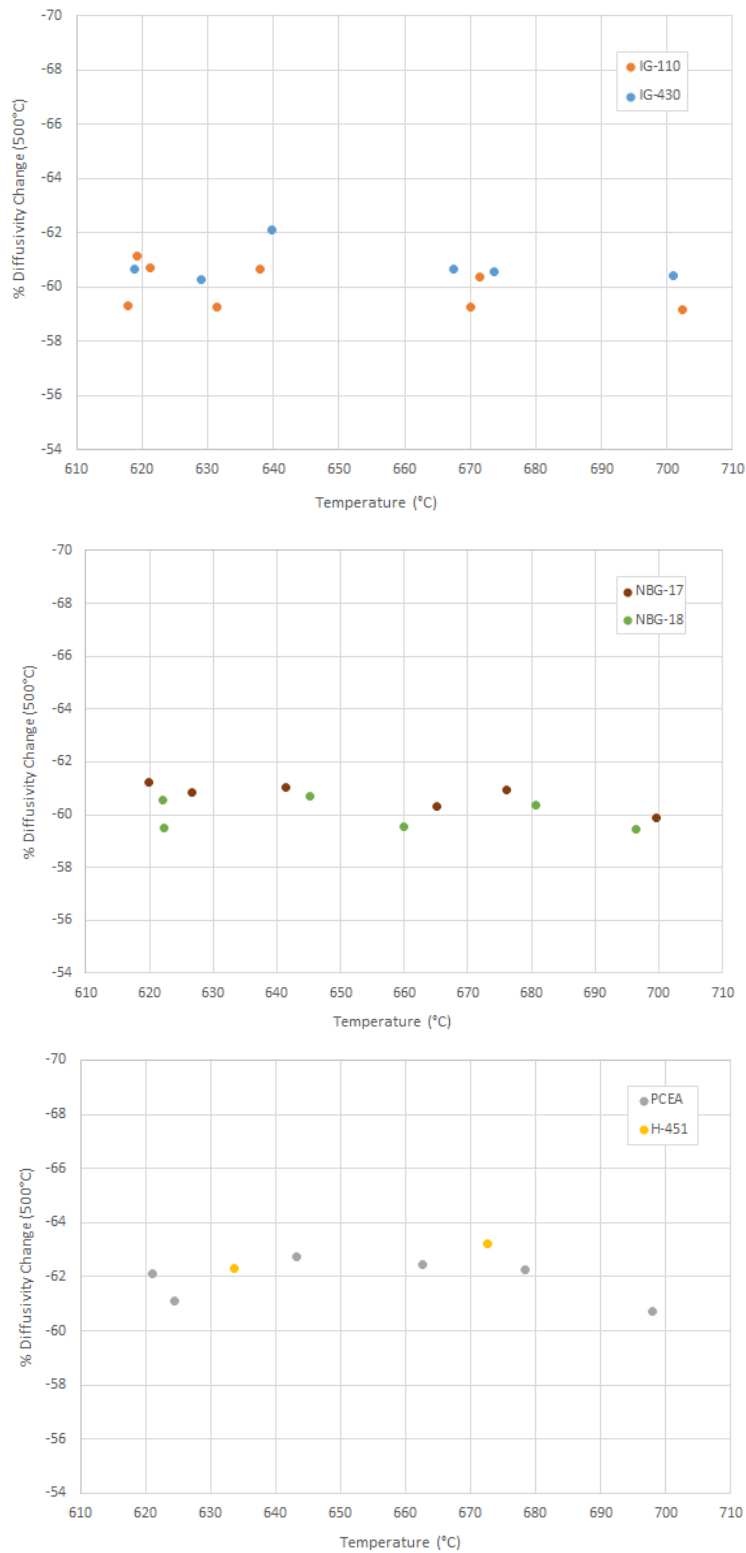


Figure 67. Percent change in thermal diffusivity (at a measurement temperature of 500°C) for unstressed specimens versus specimen irradiation temperature for a narrow dose range of 4.0 ± 0.5 dpa for different graphite grades. Note the Y-axis is inverted.

6. CONCLUSIONS

Comments from the AGC-2 irradiated material property analysis are provided as general comments common to all analyses and specific comments discussing specific issues for each individual material property analysis.

6.1 General Comments

In general, a number of common observations can be made for the irradiated material property data analyzed in this report:

1. All material properties change significantly and rapidly when exposed to neutron radiation.
2. For many material properties, the irradiated material property behavior appeared to achieve a constant value, after the initial change, over the dose range of about 1.25 to 4.7 dpa.
3. Irradiation-induced changes within each material property were remarkably similar for all tested specimens regardless of nuclear grade, grain size, stressed/unstressed condition, or grain orientation.
4. There is strong evidence that many of the changes are a result of both irradiation damage mechanisms and microstructural changes such as internal strain from dimensional change or irradiation-induced creep.
5. There was no apparent difference in material property changes due to grain orientation. The percentage change was very similar for with-grain and against-grain orientation for all irradiated material properties.
6. There was no apparent difference in material property changes due to a difference in density. Density differences up to 2 to 3% do not appear to create a noticeable change in material property.
7. The larger-than-designed AGC-2 irradiation temperature range appears to have had minimal effect on any material property changes.

Irradiation appeared to produce a significant change to all material properties analyzed, with an average change ranging from only about 25% to just under 160%. In nearly all cases, the maximum change appeared to occur at relatively low dose (i.e., less than 2.0 dpa), well before any significant microstructural changes could begin to affect the material property changes. This implies that irradiation damage to the graphite crystal structure may have been responsible for these rapid (< 2 dpa) and significant initial changes to the material properties. Density was the notable exception to this behavior, rising gradually and linearly as a function primarily of dimensional change (i.e., strain) within the microstructure. Because density change occurs from microstructural densification, this is logical because any irradiation damage-induced density change would have been largely masked by Mrozowski volume accommodation mechanisms.³⁸

Once this initial irradiation-induced change to the material property was achieved, the elastic and shear modulus, electrical resistivity, and CTE changes appeared to remain constant over the relatively short irradiation dose range of AGC-2 with over 50% of all tested specimens closer than ± 1 standard deviation. This has two implications: (1) irradiation response is relatively insensitive to increasing dose after the initial change in material property and (2) the nuclear graphite grades all responded similarly regardless of their differences (i.e., different grain size, fabrication method, coke source, etc.). Again, the AGC-2 dose range is relatively short (1.9 to 4.7 dpa) and provides data only on the initial behavior of graphite components to be used in high dose (20-25 dpa) reactor designs. However, this moderate dose range may be directly applicable for smaller graphite reactor designs with graphite component lifetimes of no more than 6 to 8 dpa. The similar irradiation response for all nuclear grades over this moderate dose

range may have significant impact on the graphite core component and licensing decisions for these reactor designs.

While the general irradiation response for all grades was very similar, the material property changes were significantly affected by grade type, fabrication method, and applied stress/strain levels in the tested specimens. Other than irradiation dose, the applied stress, which induced accelerated strain within the specimens, was the largest parameter to affect material property changes. Many times, it was possible to ascertain that continuing changes to the material property after the initial irradiation-induced change could be attributed to the strain experienced. These two mechanisms appeared to be responsible for nearly all material property changes.

These competing mechanisms (i.e., irradiation damage and microstructural strains) have historically been understood to be responsible for these changes. Notably, the changes in CTE have traditionally demonstrated an irradiation damage component and physical graphite crystalline change (strain) component to describe graphite behavior. The significance for both irradiation damage and irradiation-induced strain is demonstrated dramatically in the AGC-2 CTE analysis.

It was surprising that grain orientation and density variations had only minimal impact on irradiation-induced changes. Differences in material property values between with-grain and against-grain measurements can be significant, especially for extruded grades. However, as was demonstrated for all analyses the induced changes were extremely similar for both with and against-grain orientations. Similarly, density has an outsized influence on graphite material properties with even small changes to the density affecting the elastic moduli, strength, and thermal properties. While the density variations within AGC-2 graphite grades were not large (i.e., about 2%), it was expected there might be some differences. It was surprising to observe that specimens of the same grade with different densities had similar levels of material property change.

6.2 Specific Comments

Specific comments are provided for each of the analyses, noting material property-specific trends for dose, strain, and graphite grade differences.

6.2.1 Density

A graphite grade's density has a large effect on the measured graphite material property values. Even small variations between specimens of the same graphite grade have been shown to cause significant changes in the property values. Any irradiation-induced density changes to the graphite grades will be important to analysis of graphite behavior.

Nearly all material properties experience a significant change after receiving a dose less than 2 dpa. Density was the primary exception to this behavior, rising gradually and linearly as a function primarily of dimensional change (i.e., strain) within the microstructure. This behavior is expected because density change occurs from microstructural densification, and any irradiation damage-induced density change would have been largely masked by Mrozowski volume accommodation mechanisms. Thus, macroscopic density changes will closely follow microstructural strain.

Figure 10 clearly illustrates this strong dependency on density change to the observed strain. While the data scatter is fairly substantial, there is a clear difference in density change for stressed and unstressed specimens. This is an example of how a single direct measurement of the change in density may be used to predict an intrinsic property value such as internal strain (and stress). It is conceivable that real-time measurements of density could be made for reactor core blocks or sections of blocks that could indicate the irradiation or thermally induced internal stress levels of components. These stress values could then be used as property value input to a probabilistic fracture model of the reactor core components.

6.2.2 Electrical Resistivity

Electrical resistivity is used as a rapid, simple means for determining the isotropy, or grain orientation, of manufactured graphite. Changes in electrical resistivity can be used to ascertain irradiation-induced microstructure and crystallinity changes. When used in conjunction with optical microscopy, it can be used to determine the microstructural texture of graphite components with little sample preparation.

The rapid (i.e., less than 2 dpa) irradiation-induced electrical resistivity changes were the largest for any material property change; maximum of about 230% increase. However, once the initial change had been achieved, neither an increase in irradiation dose nor an increase in irradiation-induced strain affected the resistivity change. This indicates that changes to the resistivity of graphite specimens over this relatively moderate dose range (i.e., 1.9 to 4.7 dpa) is purely dependent on irradiation damage mechanisms within the graphitic crystallites; microstructural changes have minimal effect on isotropy changes. It should be noted that this effect on resistivity is greatest for the extruded grades (which have the lowest anisotropic behavior) while the IG-110 (an iso-molded grade with the highest isotropic behavior) has the least resistivity changes.

This behavior is somewhat expected because atomic and crystallite irradiation damage is expected to saturate at lower dose for irradiated graphite and to stay constant at moderate dose. However, some microstructural changes (such as pore structure, density changes, strain of material, or microstructural evolution) would seem to be important because they would affect the grain orientation within the microstructure, which provides the macroscopic isotropy to this naturally anisotropic material. Obviously, the true relationship between irradiation damage mechanisms and microstructural changes for isotropy changes requires additional study.

6.2.3 Elastic Modulus

A material's elastic moduli are a measure of how compliant (or stiff) the material behaves. In particular, differential temperature and radiation-induced strain will result in differential expansion in graphite components. The stress the component experiences from these conditions will be dictated by the elastic material modulus. It is useful for ascertaining a graphite grade's mechanical properties, irradiation creep response, and the structural strength and integrity of graphite components. The as-received elastic modulus and irradiation-induced changes to the elastic moduli will be required for accurate graphite behavior models, whole-core models, and eventual graphite reactor design.

After the initial irradiation-induced modulus increase (i.e., less than 2 dpa), the modulus behavior appears to be much more sensitive to graphite grade than for any other material property change. Figure 27 and Figure 30 illustrate the modulus behavior differences between individual grades and fabrication processes. Whereas the fine-grain, iso-molded grades show a small increase in modulus change, both the larger grain and vibrational-molded grades demonstrate a small decrease in modulus change. The behavior is further complicated from the data in Figure 28, Figure 29, and Figure 34, which demonstrate that applied stress (and induced strain) appear to produce a small, but steady decrease in the modulus changes for all grades. Of note is the small irradiation-induced strain in unstressed specimens that appear to be different than the changes seen in the stressed specimens (even for the same strain level), indicating that different microstructural changes are occurring in the specimens with an applied stress that affect the modulus differently.

This complicated behavior was anticipated because the modulus is sensitive to dislocation movement in the crystal structure (compliance), but it also can be sensitive to changes in the microstructure (i.e., pore sizes, grain orientation, and connected cracks). Consistently, unstressed control specimens for all grades demonstrate larger modulus change than the stressed creep specimens for similar strain levels. This implies that a microstructural change resulting from the increased strain on the material is competing with irradiation damage that tends to increase the stiffness of graphite. These microstructural changes in the creep specimens may exhibit increased microcracking from the large applied mechanical stresses, pore/grain structure realignment, or pore closure. Further fundamental studies will be necessary to assist in interpretation of these data trends.

6.2.4 Shear Modulus

Shear modulus (stiffness with shearing or torsion forces) is part of a material's elastic moduli and provides information for a graphite component mechanical strength, irradiation creep response, and the structural strength and integrity of graphite components similar to the Young's elastic modulus.

Shear modulus behavior is similar to the Young's modulus behavior with a large initial increase in modulus (at less than 2.0 dpa) with a relatively constant value over the entire received dose range of AGC-2 (1.9 to 4.7 dpa). However, shear modulus changes are much more consistent than observed for Young's modulus data. Figure 38 and Figure 41 show a very small increase with increasing dose and no significant change due to applied stress or induced strain for all grades (Figure 39, Figure 40, and Figure 45). This indicates shear modulus is only weakly sensitive to induced microstructural strains and increasing dose after the initial irradiation-induced modulus increase. Because all grades behave similarly, the fabrication process variables only weakly affect shear modulus changes.

This behavior is somewhat expected because the modulus is sensitive to dislocation movement in the crystal structure (i.e., compliance) and irradiation-induced damage will provide pinning sites to trap dislocations, leading to initial irradiation-induced increases. However, as was demonstrated for Young's modulus results, shear is also expected to be sensitive to changes in the microstructure (i.e., pore sizes, grain orientation, and connected cracks), which is not detected in the shear data. In addition, irradiation induced changes do not appear to be as sensitive to microstructural factors (such as grain size, pore size, fabrication process, or changes to the pore microstructure) over this relatively short irradiation dose range. Further fundamental studies will be necessary to assist in interpretation of these data trends.

6.2.5 Coefficient of Thermal Expansion

Understanding CTE for graphite components is critical for determining the dimensional changes that occur as a result of temperature cycles. Localized external stresses can be imposed on mechanically interlocked graphite core components because the individual pieces suffer differential thermal expansion. Internal stresses can occur within larger graphite components if there is a temperature gradient causing differential expansion within the piece (one side has a higher temperature than the other). Finally, thermal expansion is highly dependent on the graphite microstructure (such as orientation/anisotropy, pore size and distribution, and crystallinity). Irradiation damage can significantly alter graphite microstructure and CTE values. Determining the extent of the changes as a function of irradiation dose and temperature will be a key parameter for reliable calculation of stress states within graphite components, volumetric changes, and irradiation creep rates.

Other than density, CTE changes demonstrate the strongest sensitivity to induced strain than any other material property change. Strong correlation is demonstrated in Figure 51, Figure 52, Figure 54, and Figure 58, where applied stress and induced strain clearly increases CTE change for all grades across the entire test temperature range. The effects from irradiation clearly demonstrate a difference between the grades, indicating a difference between process variables such as grain size, forming methods, or coke sources (Figure 50 and Figure 53). However, Figure 58 illustrates that strong correlation between

microstructural change (strain) and CTE clearly overwhelms these fabrication differences, producing a consistent overall increase in CTE change as strain increases for all grades.

As discussed previously, stressed and unstressed specimens (i.e., matched pairs) experience similar neutron irradiation doses and temperatures; however, the stressed creep specimens showed much larger strains due to the added mechanical stresses. The unstressed control specimens also experience (lower) strain but CTE behavior is different between different grades. Further, for those creep and control specimens from the same grade that experience similar strain levels (where the creep and control data overlaps), there is a significant difference in CTE response. Because strain-induced changes to CTE cannot completely explain the behavior, neutron irradiation damage may still be altering the CTE change, even at dose greater than 2 dpa. However, current data are not enough to form firm conclusions on how microstructure strain and irradiation damage directly affect changes to CTE. Further fundamental studies will be required to assist in interpretation of these data trends.

6.2.6 Thermal Diffusivity

The ability to conduct heat through the graphite core is critical to the passive removal of decay heat in an off-normal event. Changes to thermal diffusivity/conductivity within the graphite components can have a significant effect on the passive heat removal rate and the peak temperature of the core (with potential excessive fuel particle temperatures). Furthermore, there will be thermal gradients in a graphite reactor core. Thermal stress is born from these temperature gradients resulting in differential thermal expansion within individual blocks and between blocks. Therefore, it is important that the influence of neutron radiation on thermal diffusivity be understood for the correct modeling, design, and safety analysis of an HTR.

Thermal diffusivity was the only material property that did not exhibit effects from an applied stress and irradiation-induced accelerated strain. Only irradiation effects from crystallographic damage and the resulting small dimensional changes were measured. Of interest is the behavior that thermal diffusivity initially decreases sharply at dose less than 2 dpa, but then continues to decrease at a much slower rate over the entire AGC-2 dose range (1.9 to 4.7 dpa) (Figure 63). The slow decrease in thermal diffusivity after 1 dpa was unexpected because it is assumed from previous studies that irradiation damage within the crystallites has saturated by 1 dpa, and thermal diffusivity will stay constant with increasing irradiation damage. This observation may show that simple defects such as Frenkel pair dislocations occur at very low dose but more complex atomic defects that continue to disrupt phonon transport may occur at higher neutron dose greater than 1 dpa.

This behavior may also be explained by the increase in irradiation-induced microstructural strain where the small Mrozowski cracks will be closing with increasing neutron dose. The nanometer-sized Mrozowski cracks have a length-scale that could affect the phonon transport and may continue to decrease the thermal diffusivity measurements. Other effects such as crystallite reorientation, larger pore closures, and increased microcracking may also be responsible. Further fundamental studies will be required to assist in interpretation of these data trends.

7. REFERENCES

1. P. E. Murray, "As-Run Thermal Analysis of the AGC-2 Experiment," ECAR-2322, Idaho National Laboratory, April 2014.
2. D. T. Rohrbaugh, W. D. Swank, and W. E. Windes, *AGC-2 Irradiation Report*, INL/EXT-16-38431, Idaho National Laboratory, June 2016.
3. T. D. Burchell, *AGC-1 Irradiation Creep Strain Data Analysis*, ORNL/TM-2014/255, Oak Ridge National Laboratory, September 2014.

4. T. D. Burchell, *AGC-1 Irradiation Induced Property Changes Analysis Report: Electrical Resistivity and Coefficient of Thermal Expansion*, ORNL/TM-2015/377, Oak Ridge National Laboratory, February 2016.
5. T. Burchell, R. Bratton, and W. Windes, *NGNP Graphite Selection and Acquisition Strategy*, ORNL/TM-2007/153, Oak Ridge National Laboratory, September 2007.
6. R. L. Bratton and T. D. Burchell, 2005, *NGNP Graphite Testing and Qualification Specimen Selection Strategy*, INL/EXT-05-00269, Idaho National Laboratory, May 2005.
7. PLN-2497, "Graphite Technology Development Plan," Revision 1, Idaho National Laboratory, October 2010.
8. W. E. Windes, D. T. Rohrbaugh, W. D. Swank, *AGC-2 Irradiation Creep Strain Data Analysis*, INL/EXT-16-39682, August 2016.
9. W. E. Windes, W. D. Swank, D. T. Rohrbaugh, and D. L. Cottle, *AGC-2 Specimen Post-Irradiation Data Package Report*, INL/EXT-15-36244, Idaho National Laboratory, August 2015.
10. TFR-645, "Advanced Graphite Capsule AGC-2 Experiment Test Train," Revision 0, Idaho National Laboratory, July 2010.
11. INL Drawing 600786, "ATR Advanced Graphite Capsule (AGC-2) Graphite Specimen Machining Details," Revision 1, Idaho National Laboratory, March 2009.
12. INL Drawing 600786, "ATR Advanced Graphite Capsule (AGC-2) Graphite Specimen Machining Details," Revision 2, Idaho National Laboratory, July 2012.
13. T. Burchell and R. Bratton, *Graphite Irradiation Creep Capsule AGC-1 Experimental Plan*, ORNL/TM-2005/505, Oak Ridge National Laboratory, May 2005.
14. INL Drawing 600787, "ATR Advanced Graphite Capsule (AGC-2) Experiment Graphite Specimen Cut-Out Diagrams," Revision 3, Idaho National Laboratory, July 2010.
15. INL Drawing 601266, "ATR Advanced Graphite Capsule Number 2 (AGC-2) Capsule Facility Assemblies," Revision 2, Idaho National Laboratory, July 2012.
16. INL Drawing 601258, "ATR Advanced Graphite Capsule 2 (AGC-2) Graphite Specimen Holder Assemblies and Details," Revision 1, Idaho National Laboratory, July 2012.
17. INL Drawing 600001, "ATR TMIST-1 Oxidation Experiment In-Vessel Installation," Revision 2, Idaho National Laboratory, March 2009.
18. J. R. Parry, 2010, "Engineering Calculations and Analysis Report: Reactor Physics Projections for the AGC-2 Experiment Irradiated in the ATR South Flux Trap," ECAR-1050, Revision 0, Idaho National Laboratory, October 13, 2010.
19. T. Burchell, 2009, *A Revised AGC-1 Creep Capsule Layout*, ORNL/TM-2009/009, Oak Ridge National Laboratory, January 2009.
20. T. Burchell, J. Strizak, and M. Williams, *AGC-1 Specimen Preirradiation Data Report*, ORNL/TM-2010/285, Oak Ridge National Laboratory, August 2011.
21. T. Reed, "AGC-1 Individual Fluence, Temperature, and Load Calculation and Tabulation," ECAR-1943, Idaho National Laboratory, September 2012.
22. T. Reed, "AGC-1 As Run Thermal Results," ECAR-1944, Idaho National Laboratory, September 2012.

23. L. Hull, *AGC-2 Irradiation Data Qualification Final Report*, INL/EXT-12-26248, Idaho National Laboratory, July 2012.
24. TFR-645, "Advanced Graphite Capsule AGC-2 Experiment Test Train," Revision 0, Idaho National Laboratory, July 2010.
25. D. Swank, *AGC-2 Graphite Preirradiation Data Package*, INL/EXT-10-19588, Revision 0, Idaho National Laboratory, August 2010.
26. R. G. Ambrosek, "Thermal Projections for AGC-2," ECAR-1161, Idaho National Laboratory.
27. W. Windes, *AGC-2 Disassembly Report*, INL/EXT-14-32060, Idaho National Laboratory, May 2014.
28. D. Swank, "AGC-2 Graphite Specimen Postirradiation Characterization Plan," PLN-4657, Rev. 0, Idaho National Laboratory.
29. J.R. Parry, "As-Run Physics Analysis for the AGC-2 Experiment Irradiated in the ATR," ECAR-2291, Idaho National Laboratory, March 2014.
30. D. Rohrbaugh, "AGC-2 Specimen Load Calculations by Stack," ECAR-2925, Idaho National Laboratory, January 2016.
31. P. E. Murray, "As-Run Thermal Analysis of the AGC-2 Experiment," ECAR-2322, Idaho National Laboratory, April 2014.
32. D. T. Rohrbaugh, W. D. Swank, and W. E. Windes, *AGC-2 Irradiation Report*, INL/EXT-16-38431, Idaho National Laboratory, June 2016.
33. T. D. Burchell, *AGC-1 Irradiation Creep Strain Data Analysis*, ORNL/TM-2014/255, Oak Ridge National Laboratory, September 2014.
34. T. D. Burchell, *AGC-1 Irradiation Induced Property Changes Analysis Report: Electrical Resistivity and Coefficient of Thermal Expansion*, ORNL/TM-2015/377, Oak Ridge National Laboratory, February 2016.
35. G. Brown et. al., "Approximation of AGC-1 and AGC-2 Specimen Temperatures," INL/MIS-16-40507, ECAR 3295, March 2012.
36. P. E. Murray, "Uncertainty Analysis of Temperature in the AGC-1 and AGC-2 Experiments," ECAR-3017, Idaho National Laboratory, April 2016.
37. W.D. Swank, "AGC Inter-laboratory Comparison of Graphite Testing Procedures", TEV-2530, Idaho National Laboratory, December 2015.
38. B. Kelly, *Physics of Graphite*, Applied Science Publishers Ltd, London and New Jersey, 1981.
39. L. L. Snead and T. D. Burchell, "Thermal conductivity degradation of graphites due to neutron irradiation at low temperature," *Journal of Nuclear Materials* 224 (1995), 222-229.

Appendix A

Data Plots for Dynamic Young's Modulus Measured by the Sonic Resonance Technique

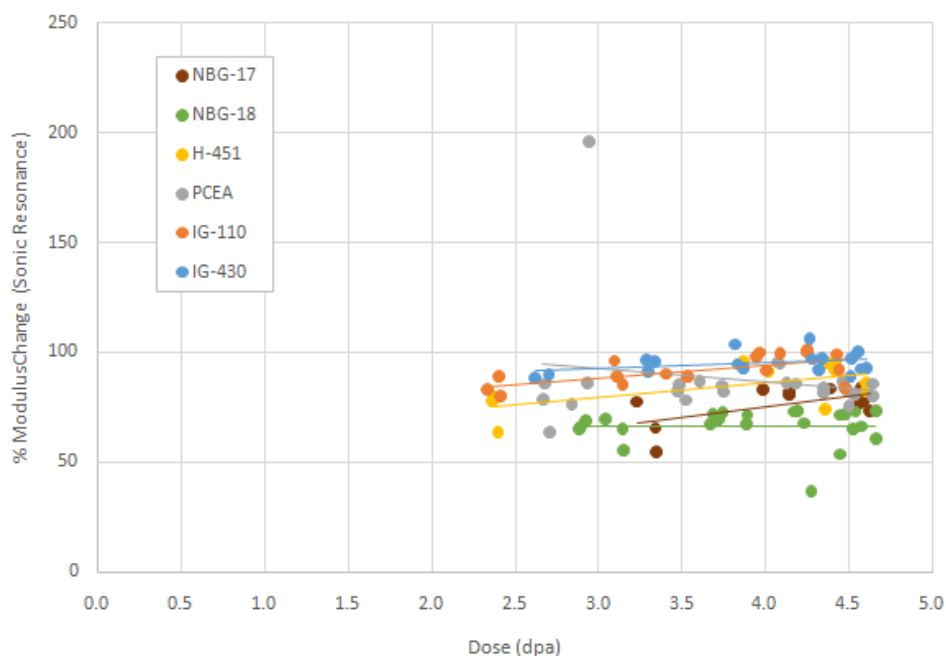


Figure A-1. Percent modulus change versus dose by graphite grade for control specimens only.

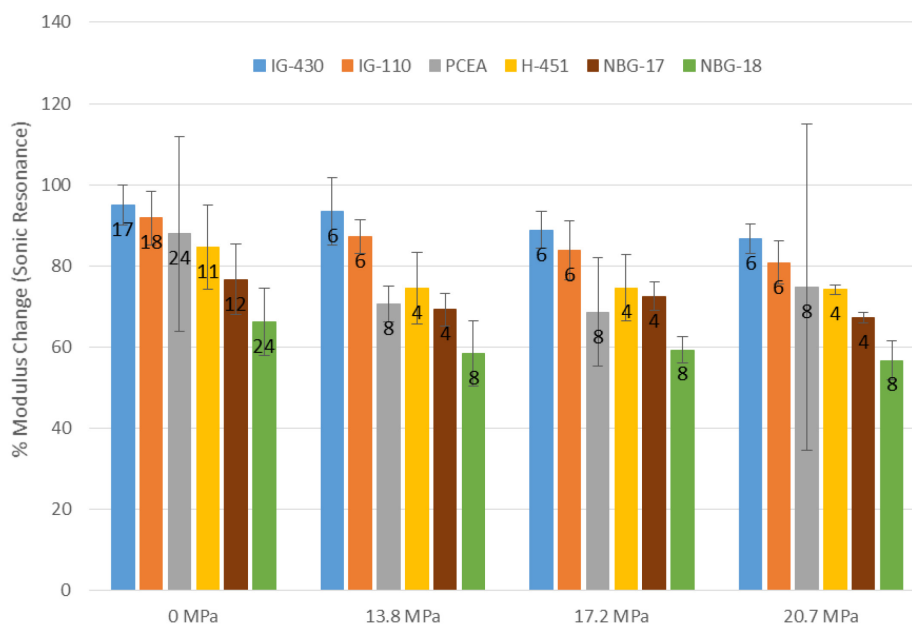


Figure A-2. Average percent modulus change by graphite grade and applied load. The error bars represent ± 1 standard deviation from the mean and the numbers in the bars represent the sample size.

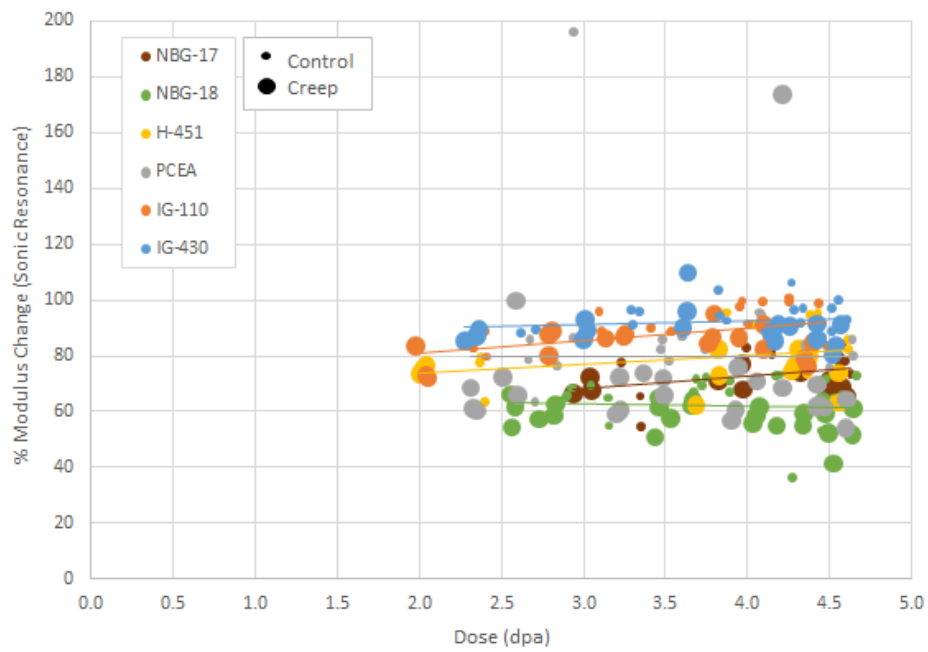


Figure A-3. Percent modulus change versus dose by graphite grade for control and creep specimens.

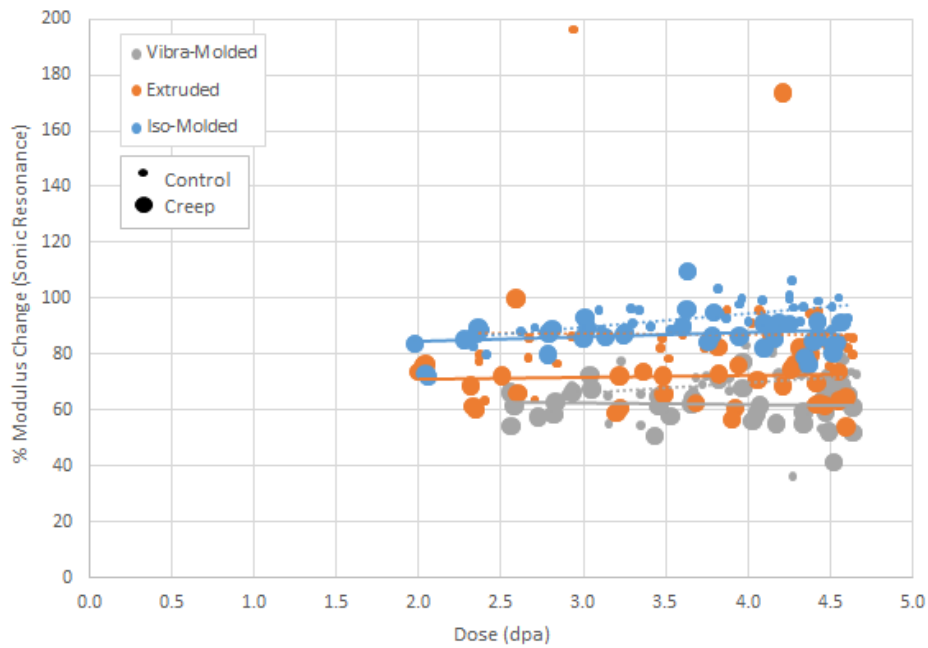


Figure A-4. Percent modulus change versus dose by fabrication process for control and creep specimens.

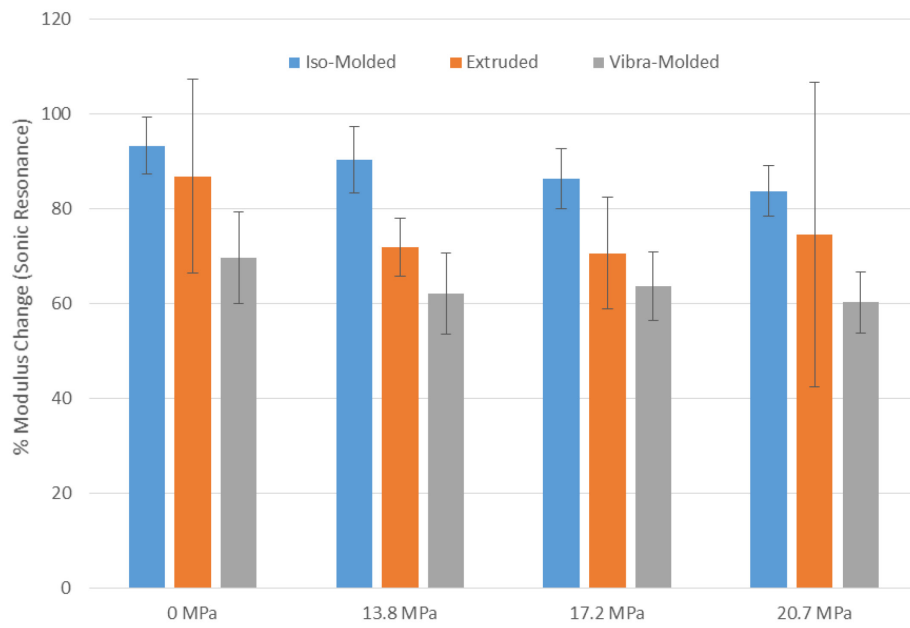


Figure A-5. Average percent modulus change by load and graphite forming process. The error bars represent ± 1 standard deviation from the mean.

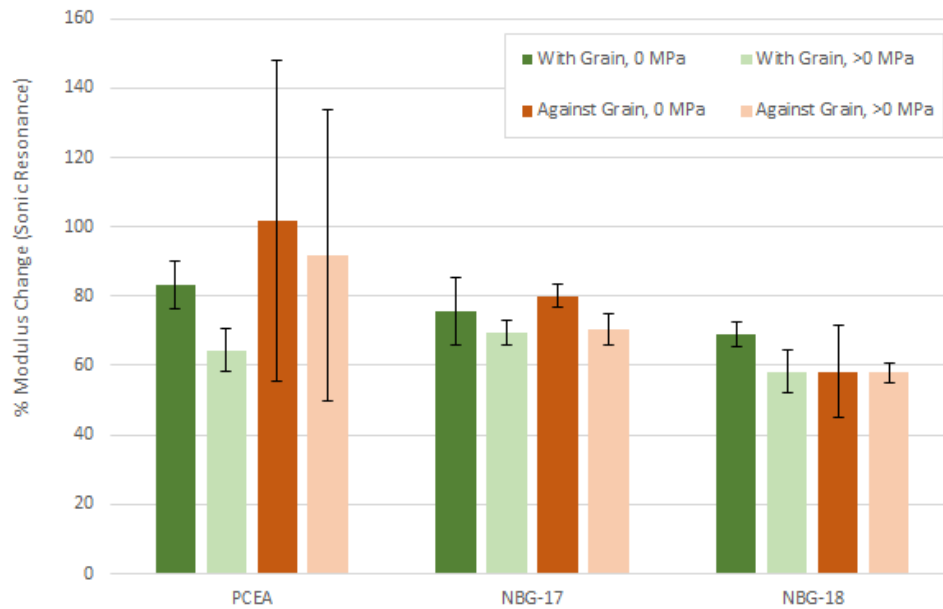


Figure A-6. Average percent modulus change by grain orientation and graphite grade.

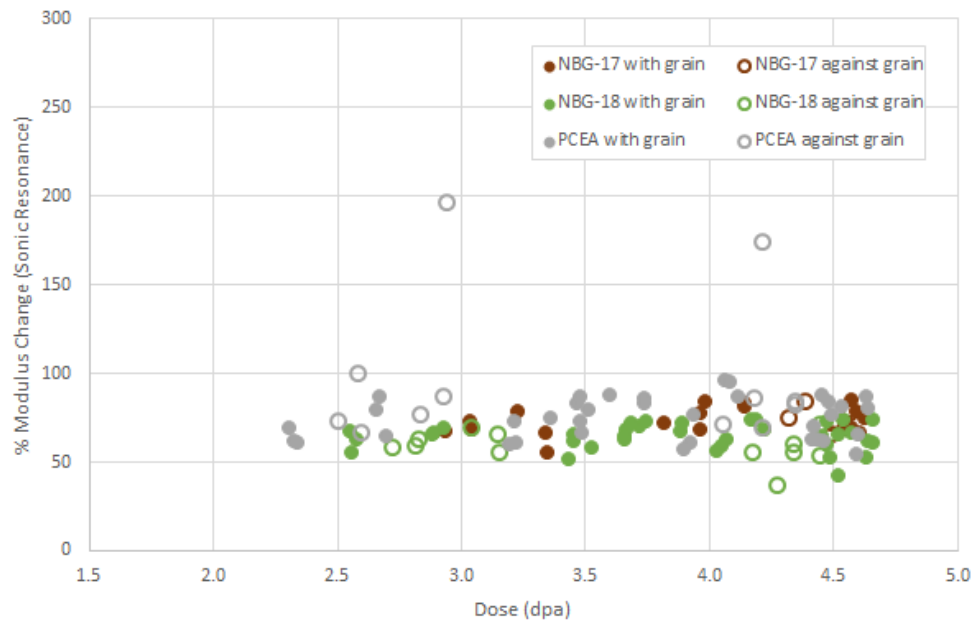


Figure A-7. Percent modulus change versus dose by graphite grade and specimen grain orientation.

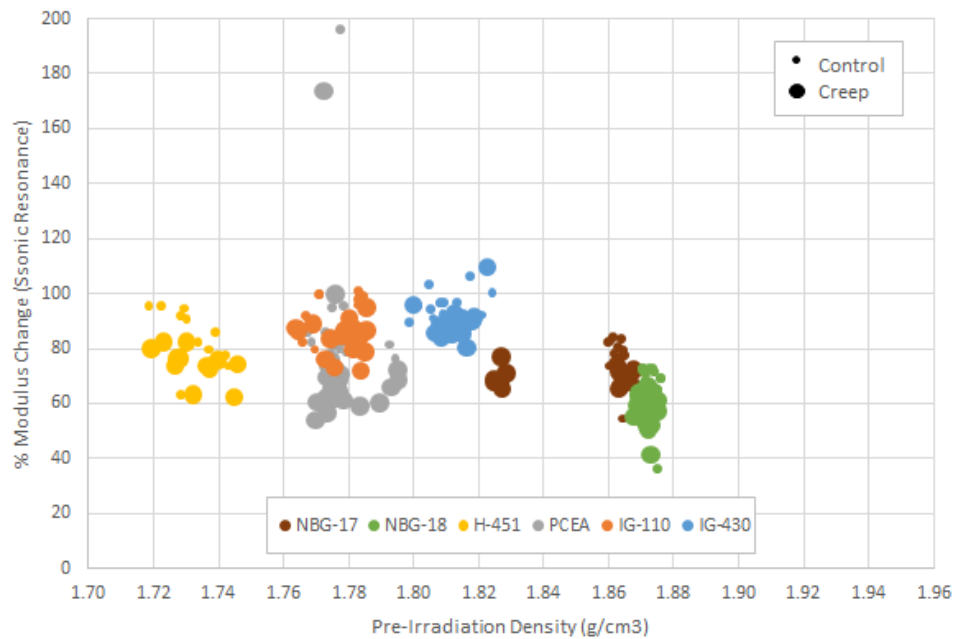


Figure A-8. Percent modulus change versus specimen pre-irradiation density by graphite grade for control and creep specimens.

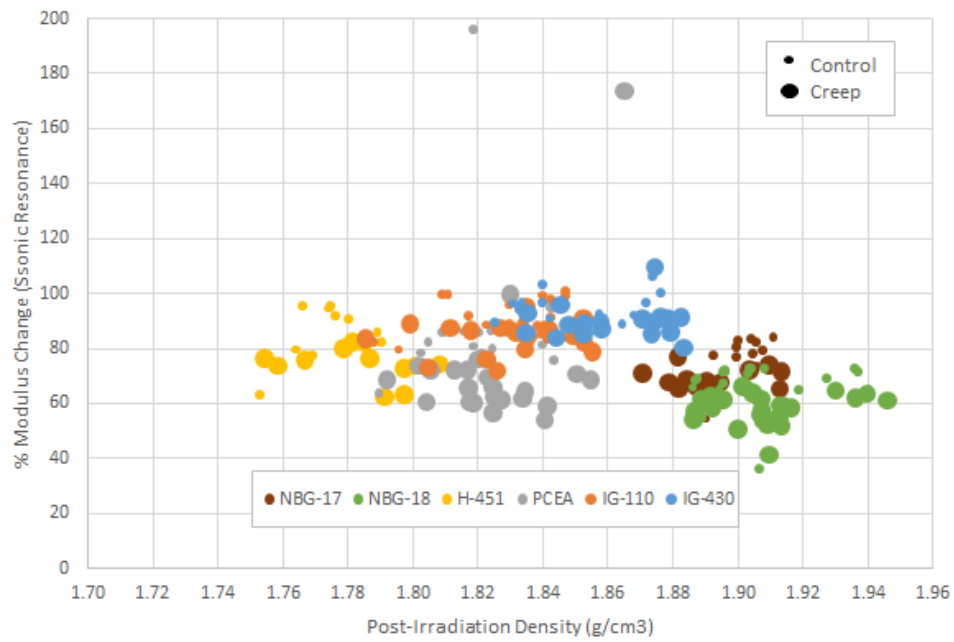


Figure A-9. Percent modulus change versus specimen post-irradiation density by graphite grade for stressed and unstressed specimens.

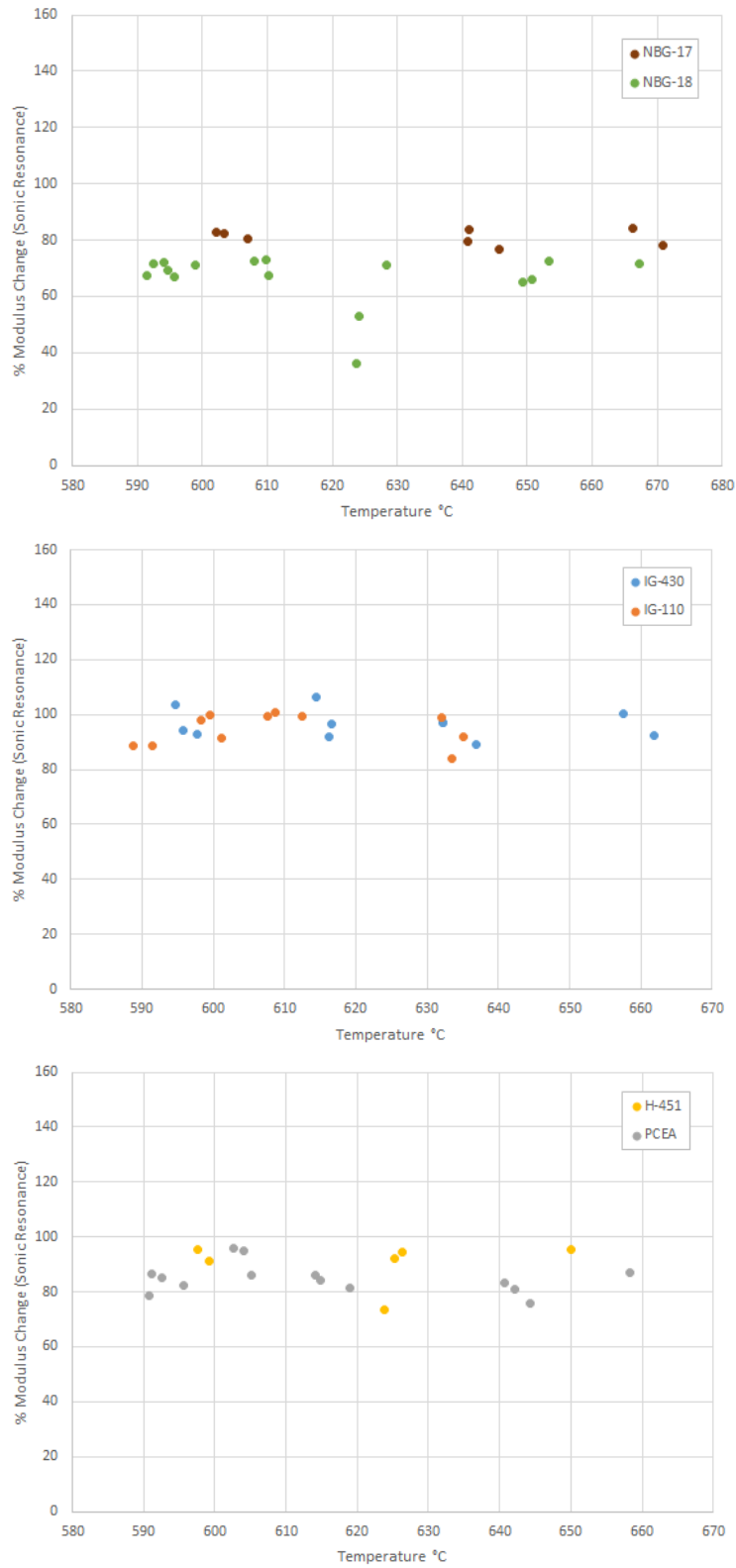


Figure A-10. Percent change in Young's modulus versus specimen irradiation temperature for a narrow dose range of 4.0 ± 0.5 dpa for different graphite grades.

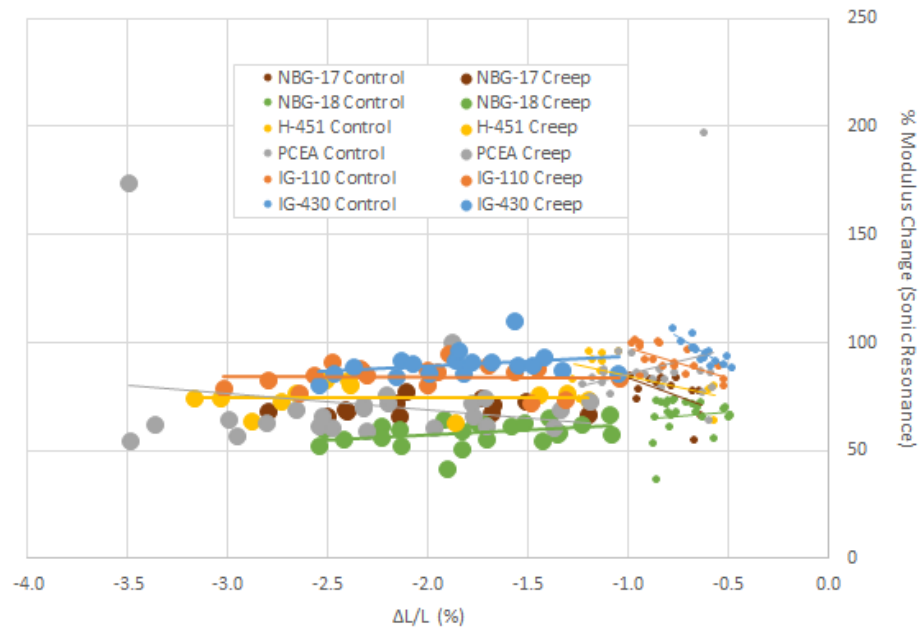


Figure A-11. Percent modulus change versus specimen strain by graphite grade for both control and creep specimens. Note negative strain increases from right to left (from 0.0 to -4.0%).